Doctoral Dissertation **Academic year 2015**

Substructural Damage Identification of Shear Structures Based on Autoregressive Models

Keio University

Graduate School of Science and Technology

School of Science for Open and Environmental Systems

Student ID Number 80947912 Name Mei, Liu

Thesis Advisor Professor Name Mita, Akira

Keio University
Graduate School of Science and Technology
September 2015

Abstract

Damage identification based on vibration data generated by SHM systems has been extensively studied for several decades and the literature on the subject is rather immense. However, most of them are not feasible or practical for large scale civil structures due to the challenges such as high equipment costs, long setup time, difficulties in cabling and the long computation time. This thesis is devoted to overcome these problems by proposing a decentralized damage identification strategy based on the combination of substructural approach and autoregressive models, which is especially effective and economic for large scale shear structures.

Firstly, an improved substructure-based damage detection approach is proposed to locate and quantify damages in a shear structure, which extends from a previously established substructure approach. To improve the noise immunity and damage detection robustness under different types of excitations and realistic conditions, this paper proposes an ARMAX model residual-based technique to correct the former damage indicator. The results of simulation and experimental verifications show that the improved procedure works much better and more robust than previous method especially when it is applied to realistic problems.

Secondly, to seek the balance between the number of substructures and the computation intensity inside each substructure, a more flexible substructural damage identification approach is proposed in this study to identify structural damage

including its location and severity, using changes in the first autoregressive coefficient matrix as the damage indicator.

Moreover, to simplify the above studied method, the diagonal elements from changes in the first autoregressive coefficient matrix (CFAR) are extracted to construct the damage indicating vector (DIV). Then simulations are conducted to investigate the potential of the DIV algorithm for implementation on wireless smart sensor networks (WSSN), where the issues of scalability of the DIV approach are undertaken by utilizing a decentralized, hierarchical and in-network processing strategy.

Finally, the conclusion is given. The proposed substructural damage identification approach can satisfactorily locate and quantify the damage in both simulation and laboratory experiment. As the damage identification process can be independently conducted on each substructure, by utilizing some decentralized and hierarchical processing strategy, this method is promising and efficient for application on wireless smart sensor networks (WSSN) to perform SHM systems for large scale shear structures.

Acknowledgements

My most sincere gratitude goes first and foremost to Professor Akira Mita, my supervisor, for his kind concern, endless support, constant encouragement and patient guidance throughout my time at Keio University. Without his consistent illuminating instruction and broad-ranging professional view through all the stages of my Ph.D. study, without his great encouragement and faith in me when difficulties and obstacles arose on my research, the completion of this thesis would not have been possible.

I would like to express my heartfelt gratitude to Professor Masayuki Kohiyama, Professor Masaki Takahashi and Professor Yasue Mitsukura for reviewing this thesis thoroughly and giving me instructive advice and useful suggestions.

Special thanks go to Professor Songtao Xue at Tongji University, for his unceasing concern and unwavering support.

In particular, I would like to thank all the members of Mita Laboratory and all my friends in Keio University for their warm friendship and memorial moments we shared.

I would like to thank to the Ministry of Education, Culture, Sports, Science and Technology in Japan (Monbukagakusho), the Global COE (Center of Excellence) Program, Keio Leading-edge Laboratory of Science and Technology and Amano Institute of Technology for the financial support and the research facilities they provided during my graduate study.

Finally, my thanks would go to my parents, my brother and my girl friend, Baolin Xia, for their love, faith and support.

Contents

Abstract ii

Acknowledgements iv

Contents v

Figures viii

Tables xi

1 Introduction 1

1.1 Structural Health Monitoring 1

1.2 Definition of Damage 2

1.3 Damage Detection Methods 4

1.4 Objectives 13

1.5 Organization of Thesis 14

2 Substructural Damage Identification Based on ARMAX Model Residual 18

2.1 Introduction 18

2.2 Autoregressive Models 19

2.3 Substructure Division Method 21

2.4 Correction of Damage Indicator 24

2.4.1 Empirical Cumulative Distribution Function of ARMAX Model Residual....26

2.4.2 K-S Test on ARMAX Model Residual....28

2.5 Performance Verification by Simulation....31

2.6 Experimental Verification....42

2.6.1 Experimental Setup....43

2.6.2 Procedure....44

2.7 Conclusions....48

3 Substructural Damage Identification Using Changes in the First Autoregressive Coefficient Matrix....51

3.1 Introduction....51

3.2 Proposed Method....52

3.3 Performance Verification by Simulation....61

3.4 Experimental Verification....69

3.5 Decentralized Damage Identification Strategy for Shear Structures....74

3.5.1 Damage Indicating Vector (DIV)....77

3.5.2 Decentralized Damage Identification Strategy (DDIS)....78

3.5.3 Performance Verification by Simulation....84

3.6 Conclusions....92

4 Conclusions and Future Studies....94

4.1 Conclusions....94

4.2 Future Studies 96

References 98

Author’s biography 106

List of publications 107

Figures

Figure 1.1. Organization of thesis 17

Figure 2.1. Divided substructural model 23

Figure 2.2. Flowchart for obtaining the corrected damage indicator 25

Figure 2.3. Five-story shear building 32

Figure 2.4. Structural division 32

Figure 2.5. ECDF of dimensionless residual error (white noise excitation, 5% noise, ARMAX model, data length=2000, na=2, nb=3, nc=3, nk=1) 35

Figure 2.6. ECDF of dimensionless residual error (El Centro earthquake excitation, 5% noise, ARMAX model, data length=4000, na=2, nb=3, nc=3, nk=1) 36

Figure 2.7. Damage indicator without correction coefficient D_{ks} (white noise excitation, 5% noise, ARMAX model, data length=2000, na=2, nb=3, nc=3, nk=1) 39

Figure 2.8. Damage indicator with correction coefficient D_{ks} (white noise excitation, 5% noise, ARMAX model, data length=2000, na=2, nb=3, nc=3, nk=1) 40

Figure 2.9. Damage indicator without correction coefficient D_{ks} (El Centro

earthquake excitation, 5% noise, ARMAX model, data length=4000, na=2, nb=3, nc=3, nk=1).....41

Figure 2.10. Damage indicator with correction coefficient D_{ks} (El Centro earthquake excitation, 5% noise, ARMAX model, data length=4000, na=2, nb=3, nc=3, nk=1).....42

Figure 2.11. Experimental setup of five-story building model 44

Figure 2.12. Input excitation.....45

Figure 2.13. Damage indicator without correction coefficient D_{ks} (Experimental measured data, ARMAX model, data length=4000, na=2, nb=3, nc=3, nk=1) 47

Figure 2.14. Damage indicator with correction coefficient D_{ks} (Experimental measured data, ARMAX model, data length=4000, na=2, nb=3, nc=3, nk=1) 48

Figure 3.1. Complete and sub-structural dynamic system.....54

Figure 3.2. 12-story shear building 63

Figure 3.3. Structure division for 12-story shear building.....64

Figure 3.4. Changes in the first AR model coefficient matrix for Substructure II (10% damage) 66

Figure 3.5. Changes in the first AR model coefficient matrix for Substructure II 67

Figure 3.6. Linear relationship between CFAR and damage intensity 68

Figure 3.7. Structure division for 5-story experimental building model 70

Figure 3.8. Changes in the first AR model coefficient matrix for Substructure I (10% damage) 72

Figure 3.9. Changes in the first AR model coefficient matrix for Substructure I 73

Figure 3.10. Linear relationship between CFAR and damage intensity 74

Figure 3.11. Network topologies (Nagayama and Spencer 2007) 79

Figure 3.12. Sketch of hierarchical organization 80

Figure 3.13. 15-story shear building 83

Figure 3.14. Structure division and community formation for 15-story shear building 86

Figure 3.15. Data aggregation and decision making 87

Figure 3.16. DIV values for substructure 4: damage at column 10 89

Figure 3.17. DIV values for substructure 5: damage at column 10 89

Figure 3.18. DIV values for substructure 1: damage at columns 4 and 14 90

Figure 3.19. DIV values for substructure 2: damage at columns 4 and 14 90

Figure 3.20. DIV values for substructure 6: damage at columns 4 and 14 91

Figure 3.21. DIV values for substructure 7: damage at columns 4 and 14 91

Tables

Table 2.1. Correction coefficient D_{ks} (normalized K-S test statistical distance) (white noise excitation, 5% noise, ARMAX model, data length=2000, na=2, nb=3, nc=3, nk=1).....37

Table 2.2. Correction coefficient D_{ks} (normalized K-S test statistical distance) (El Centro earthquake excitation, 5% noise, ARMAX model, data length=4000, na=2, nb=3, nc=3, nk=1).....38

Table 2.3. Parameters of five-story building model.....43

Table 2.4. Correction coefficient D_{ks} (normalized K-S test statistical distance) (Experimental measured data, ARMAX model, data length=4000, na=2, nb=3, nc=3, nk=1).....46

Table 3.1. Changes in the first AR model coefficient matrix for Substructure I (10% damage).....68

Table 3.2. Changes in the first AR model coefficient matrix for Substructure III (10% damage).....69

Table 3.3. Changes in the first AR model coefficient matrix for Substructure II (10% damage).....71

CHAPTER 1
Introduction

1.1 Structural Health Monitoring

Research and development of SHM are getting strong attention for evaluating and maintaining structural integrity of an aging building or a suffering structure against natural hazards such as large earthquakes and strong winds. The process of implementing a damage detection and characterization strategy for engineering structures is referred to as Structural Health Monitoring (SHM). As an analogy, the concept of SHM is similar to routine checkups of human bodies to make sure their health and fix the disease if needed (Mita 2003).

There three main components involved in the typical process of SHM: ① the constant monitoring of a structure over time using periodically measured responses from an array of sensors, ② the damage-sensitive features extraction from these measured responses, and ③ the statistical analysis of these features to evaluate the current condition of structural health. SHM system performed during a long period periodically updates and reports the information regarding the timely condition of the structure in order to keep them performing their intended functions upon the

inevitable aging and degradation resulting from operational environments. After extreme events, such as large earthquakes, strong winds or blast loading, SHM system is implemented to conduct the rapid condition evaluation and then provide the real time and reliable information regarding the integrity of the structure (Cempel 1980; Hou et al. 2000; Auweraer and Peeters 2003; Farrar and Worden 2007).

Basically, the SHM problem can be considered as one of a statistical pattern recognition paradigm, which can then be categorized into four fields as follows (Sohn et al. 2004; Hayton et al. 2007):

1) Operational Evaluation,

2) Data Acquisition, Fusion, and Cleansing,

3) Feature Extraction and Information Condensation, and

4) Statistical Model Development for Feature Discrimination.

To reveal the damage information hidden in the outward appearance, SHM adopts a deep pool of mixed knowledge and interdisciplinary branches of science, as follows: ①operational evaluation methods (such as economic analysis, statistical theory, intelligent optimization, etc.); ② data acquisition and signal processing techniques (such as excitation methods, MEMS technology, material science and technology, data transmission, etc.); ③ feature extraction approaches (such as structural mechanics, control theories, system identification, etc.); and ④ statistical discrimination algorithms of features for damage detection (such as information condensation, pattern classification, intelligence diagnosis, statistical learning theories, etc.)

1.2 Definition of Damage

Damage can be generally defined as changes taking place at a system that adversely

have influence on its behavior (Farrar and Cone 1995). Specifically considering civil engineering structures, damage can be defined as changes occurring in materials, connections, boundary conditions, etc., which can cause deterioration of the structure. Usually there are various reasons for causing damage, such as corrosion, aging, daily activities, etc. Many different ways such as traffic, wind loads and collisions by boats can all have the possibility to cause damage to bridges. These loads can also give extreme distress to offshore structures, associated with wave loading and corrosion due to seawater. Additionally, some damage sources emerge not so frequently. However, they can cause terrible consequences. For instance, earthquakes, tornados, and hurricanes can potentially cause catastrophic damage in civil engineering structures.

The final goal of SHM is to estimate the remaining life of structures. This purpose is still an open question, and faces many obstacles to get a good answer in the current stage. Rytter (1993) categorized the damage identification into four different levels based on giving answers to these four questions as following listed in order to represent the increasing knowledge and difficulty of the damage identification state:

Level 1: Damage Existence. Is there damage in the system?

Level 2: Location. Where is the damage in the system?

Level 3: Extent. How severe is the damage?

Level 4: Prognosis. How much useful life remains?

Statistical models are usually adopted to answer questions regarding the existence and location of damage when they are used in an unsupervised learning mode, while the statistical procedures can be applied to better detect the type of damage, evaluate the extent of damage and estimate the remaining useful life of the structure when they are adopted in a supervised learning mode and coupled with analytical models. The

statistical models are also utilized to minimize spurious alarms of damage (Farrar and Worden 2007).

Spurious alarms of damage can be classified into two main categories:

1) False-positive damage alarms (indication of damage when actually there is none damage existing in the structure),

2) False-negative damage alarms (no indication of damage when actually there is some damage which took place in the structure).

It is undesirable for the first type of faults, because they will cause unnecessary downtime and consequently result in loss of revenue together with loss of confidence in the SHM system. More importantly, if the second type of errors happened, it maybe will lead to catastrophic consequences. Many damage identification algorithms allow one to weigh one type of fault above the other. Normally this weighting may be one of the factors to be determined at the operational evaluation stage of SHM (Hayton et al. 2007; Sohn 2007).

1.3 Damage Detection Methods

The main parts of the SHM in civil engineering are damage detection, localization and quantification, which are essential monitoring zones for structures after major events such as large earthquakes, tsunami, strong winds, etc. (Ljung 1999; Mita 2003). Damage identification based on vibration data generated by SHM systems has been extensively studied for several decades and the literature on the subject is rather immense.

One of the earliest damage indicators studied is the estimated modal property from system identification (Alvin et al. 2003; Ljung 1999), as it is directly related to

structural physics according to classical dynamics theory. The basic idea is that modal parameters, such as frequencies, mode shapes and modal damping, are functions of the physical properties of the structure (mass, stiffness and damping). Therefore changes in the physical properties will cause changes in the modal properties. Thus they are often referred to as mode-based methods.

Using Natural Frequency There are a large amount of literatures related to damage detection based on the shifts in natural frequencies. Salawu (1997) and He and Zhu(2011) provided a review on structural damage detection using changes in natural frequency. Generally speaking, there are two categories of frequency analysis, the forward identification and the inverse identification that can be adopted for damage identification (Hearn and Testa 1991; Ljung 1999; Vestroni and Capecchi 2000; Peeters et al. 2001; Kessler et al. 2002; Kim et al. 2003). Both approaches assume that existence of damage will result in changes in natural frequency. Cawley and Adams (1979) proposed frequency shifts as a damage indicator to detect damage in composite materials. It assumes that natural frequency alters when the physical properties change. A vibration test of a full-scale four-story reinforced concrete building was conducted by Rytter and Kirkegaard (1997) at the European Laboratory for Structural Assessment (ELSA). The relative changes in the modal parameters are adopted as inputs of the networks to detect the bending stiffness changes of the system at the output layer. A correlation coefficient comparing changes in a structure's resonant frequencies with predictions was derived by Williams and Messina (1999), which was based on a frequency-sensitivity model derived from a finite element model. Wong et al. (2004) proposed an iterative damage detection method which can locate and quantify the damage in a simple structure by using the changes in the natural frequencies of the first several modes.

Using Mode Shape Doebling and Farrar (1997) considered the changes in the frequencies and mode shapes as the damage indicator of a bridge. The application of

the modal assurance criterion (MAC) was recommended by West (1986) and Wolff and Richardson (1989) to detect the existence and the location of structural damage. MAC represents that the degree of correlation between two sets of modal vectors is uncorrelated at all or perfectly correlated respectively, which is a scale quantity ranging from 0 to 1.0. The basic assumption of this approach is that changes in modal vectors at the degrees of freedom near the damage are relatively higher than others remotely located from the damage. As the MAC only uses one pair of modes for damage localization, the problem of choosing appropriate modes for MAC calculation induces the similar COMAC methods for damage localization, which stands for Coordinate Modal Assurance (Lieven and Ewins 1988). The location where a COMAC value is close to zero is the possible damage location. Modal tests of a full-scale bridge before and after rehabilitation were conducted by Salawu and Williams (1995). They drew a conclusion that the natural frequencies of the bridge did not change much as a result of structural repairs whilst both MAC and COMAC performed good to indicate the location of the repairs. However, this method can work well only when the measurement point is close to node points for a particular mode, which is a limitation of this approach. A comprehensive summarization of damage identification techniques using changes in the vibration characteristics was presented by Doebling et al. (1996).

Using Curvature/Strain Mode Compared with the method based on mode shape, the method using curvature or strain mode is feasible for locating the damage and higher order derivatives of mode shapes are considered to be more sensitive to damage. Pandey et al. (1991) proposed a damage detection approach adopting mode shape curvature as the damage indicator and it is proved that this approach can obtain satisfactory damage detection results for beam structures. Chance et al. (1994) conducted the study on the measured strain mode shape and showed that it could be adopted for damage localization. The changes of the mode shape curvatures was

adopted as the damage indicator by Wang et al. (2000) in a numerical study of damage detection of Tsing Ma Bridge in Hong Kong SAR and this method worked quite well in the simulation case. Qiao et al. (2007) adopted the experimental and numerical curvature mode shapes to detect, locate, and quantify the delamination in structures.

Using Modal Strain Energy Stubbs et al. (1992) are considered to be the pioneer to conduct the research on damage detection and localization based on Modal Strain Energy (MSE). Stubbs and Kim (1996) and Shi et al. (1998) made improvement to this approach by adopting modal strain energy to identify the location of the damage and quantify the damage size without baseline modal properties.

Using Dynamic Flexibility Because higher modes are considered to contribute more to the system stiffness matrix than lower modes (Berman and Flannelly 1971), it is required to obtain a large number of dynamic modes in order to accurately estimate stiffness matrix or its changes. However, usually it is very difficult to obtain the higher frequency response due to the practical limitations. To avoid this difficulty, an approach based on dynamically measured flexibility matrix is developed to estimate the changes in structural stiffness. Bernal (2002) conducted a numerical simulation of a 39-DOF truss and accurately identified the modes of it. He drew a conclusion that it is desirable to estimate and monitor the changes in the flexibility matrix than the changes in stiffness matrix. Gao and Spencer (2006) investigated the issues relating to the comprehensiveness of modal flexibility matrix from ambient and forced vibration data and proposed a damage locating vector (DLV) method based on modal flexibility matrix for online damage localization.

Artificial Neural Network Artificial neural network (ANN) learning methods help us to develop a robust approach to approximating real-valued, discrete-valued, and vector-valued target functions for certain types of problems, such as learning to interpret complex real-world sensor data. The artificial neural networks are considered

to be the most effective among various learning methods currently known. The research of artificial neural network has been inspired partly by the phenomenon that biological learning systems are constructed with very complicated networks of neurons interconnected with each other. A neural network is constituted by a group of artificial neurons interconnected with each other, and it adopt a connectionist approach to perform the computation and information processing. ANNs learning is suitable to problems in which the training data comes from noisy and complex sensor data, such as inputs from cameras and microphones. It is also appropriate to problems for which more symbolic representations are often used. The most commonly used ANN learning technique is the back-propagation algorithm. In the field of SHM, the advantage of ANN learning technique is that it is not required to know the physical relationships between the structural properties and damage occurrence. This approach depends on the utility of vibration measurements from a undamaged state to train a neural network for damage identification aims. Subsequently, the trained network is fed comparable vibration responses from the same structure under different states in order to monitor the health of the structure (Berman and Flannelly 1971; Cawley and Adams 1979; Cempel 1980; Qian and Mita 2008). However, the limitation of this method is that large training samples are necessary for accurate detection.

Wavelet Method Any signal can be decomposed by the Wavelets, and it is shown that the signals transformed by Wavelets method are more sensitive to local changes in structural properties. It can be also viewed as an extension of the traditional Fourier transform with adjustable window location and size. Hou et al. (2000) proposed a structural damage detection methodology based on wavelets, which was applied to simulation data generated from a simple structural model subjected to a harmonic excitation. The damage detection results showed the wavelet approach is promising for damage detection and structural health monitoring.

Time-series-based Method The modal parameters are proved to be insensitive to local

damage for they are global properties of the structure while damage is a local phenomenon. Additionally, traditional mode-based methods, especially those that operate in time domain, are usually computationally intensive to implement and physical or finite-element models are necessarily required for those methods. In order to overcome these obstacles, time-series-based methods become another important category within the broader family of vibration-based methods for damage identification purposes. Comparing with the traditional mode-based methods, although time-series-based methods are also concerned with numerical modeling, they are more flexible because they are data-based rather than physics-based, which can use various damage features that do not necessarily have an explicit physical meaning (Fassois and Sakellariou 2007).

Autoregressive Models Among the time-series-based methods, the autoregressive (AR) model, the autoregressive with exogenous input (ARX) model or the autoregressive moving average with exogenous input (ARMAX) model are mathematical structures that can be used to formulate various data-driven damage features. By adopting one of the standard algorithms, AR/ARX/ARMAX model parameters can be estimated from input-output datasets very efficiently. According to the specific feature extraction process, the damage features generated from these models can be classified into two categories: model coefficients based and model residual based. There are a lot of model coefficients based techniques that have been investigated during the past decades. Sohn and Farrar (2001) proposed statistical pattern recognition methodology in which the recorded dynamic signals were modeled by adopting the AR time-series models and then classified from either undamaged or damaged systems by statistically examining changes in AR coefficients. Nair et al. (2006) proposed a sensitive damage feature by only using the first three AR coefficients of the ARMA model. By looking into various changes in coefficients of the vector seasonal autoregressive integrated moving average (ARIMA) model,

Omenzetter and Brownjohn (2006) proposed a health monitoring algorithm for bridge structure by analyzing the time histories of static strain data. de Lautour and Omenzetter (2006) adopted an artificial neural network (ANN) to detect the extent of the damage by feeding the AR coefficients as input features into it. Harikrishnan et al. (2014) proposed a combined approach for damage characterization involving the fundamental mode shape and its derivatives as well as the first ARX model coefficients. On the other hand, model residual based methods have also been receiving attention and a large amount of related research has been documented and published. Fanning and Carden (2001) proposed a statistical process control approach to detect damage by using the mean and variance of the residuals of the AR model to form the statistical process control charts. Mattson and Pandit (2006) chose the standard deviation of the residual of the vector AR (VAR) model as the damage-sensitive index.

Distance Measures of AR Models Distance measures are widely used tools in the field of speech recognition (Tohkura 1987; Itakura and Umezaki 1987). Basseville (1989) developed some general tools for measuring distances either between two statistical models or between a parametric model and a signal. The autoregressive (AR) models and autoregressive moving average (ARMA) models are always used to infer the spectral distances between different processes. Martin (2000) defined and discussed a metric based on ARMA models, and provided a natural measurement of the "distance" between two ARMA processes. Kalpakis (2001) proposed a distance measure using the dissimilarity and the similarity between different autoregressive integrated moving average (ARIMA) models. Zheng and Mita (2007; 2008; 2009) introduced the distance measures of AR models into civil structural damage detection by proposing a novel damage indicator based on the cepstral distance measure between AR models. Xing and Mita (2011) conducted a subsequent study to clarify how to determine the optimal order for distance measures and reduce the noise effect on this approach.

Substructure Method Though numerous damage detection methods are already developed for SHM systems, most of them are not feasible or practical for large-scale civil structures due to the challenges such as high equipment costs, long setup time, difficulties in cabling and the long computation time. To overcome these problems, some researchers have been using the substructure method for local damage detection of the large-scale structures. Koh et al. (1991) are considered to be the first to present the concept of substructure identification. In their approach, the Extended Kalman Filter (EKF) (Hoshiya and Saito 1984; Ljung 2002) was used as the numerical tool to identify unknown structural parameters. Yun and Lee (1997) applied the sequential prediction error method to estimate unknown parameters of each substructure with noisy measurements. Park et al. (1998) proposed structural damage detection methods based on the relative changes in localized flexibility properties, which are obtained either by applying a decomposition procedure to an experimentally determined global flexibility matrix or by processing the output signals of a vibration test in a substructure-by-substructure manner. Tee et al. (2005) proposed a substructure identification method considering both first-order and second-order models. Koh and Shankar (2003) proposed a substructure identification approach in frequency-domain without the need of interface measurement. The special techniques such as sub-structuring and "model order reduction" (MOR) become quite useful in the practical SHM systems for large-scale civil structures. Sara and Lucia (2014) contributed the deep discussion about the consequences on the achieved accuracy of adopting different model order reduction technique patterns. Several new substructure methods have been developed in recent years. Hou et al. (2010, 2012) proposed and experimentally studied a substructure isolation method which can be applied for local structural health monitoring and damage identification by virtually isolating the substructure from a large and complex global structure into a simple, small and independent structure. Kuwabara et al. (2013) proposed a damage detection method

for high-rise buildings which is devised to find the story shear and bending stiffnesses of a specific story from the floor accelerations just above and below the specific story. Zhang et al. (2014) presented a loop substructure identification method to estimate the parameters of any story in a shear structure using the cross power spectral densities (CPSD) of structural responses. Lee and Eun (2014) presented a model-based substructuring method in which the damaged substructure is detected by tracing the distribution of the constraint forces at the nodes between the partitioned substructures and the local damage is found by the displacement curvature of the isolated substructure. However, there are several problems in the existing methods. These methods are either too complicated to require long computation time or require the construction of complex structure models. And for some approaches of system identification and damage detection, noise problems in the case of practical application may cause some difficulties.

Xing and Mita (2011) proposed a substructure approach to divide a complete structure into several substructures in order to significantly reduce the number of unknown parameters for each substructure so that damage identification processes can be independently conducted on each substructure. Difference between squared original frequency and squared damaged frequency was adopted as damage indicator in the substructure damage detection approach. The approach can work well in the simulation scenarios in which the target structure is subjected to white noise excitation and no noise is added to the vibration signals. However, when the approach is applied to noise-contaminated vibration signals of a structure subjected to real earthquake excitation, the damage detection algorithm will become unrobust and it is difficult to obtain a satisfactory result. An improvement to this method based on the combined use of residual errors and the squared frequencies will be proposed in Chapter 2.

A new algorithm which can locate and quantify the damage inside a substructure

without requiring the information from adjacent substructures will be proposed in Chapter 3. The application of the proposed algorithm for decentralized damage identification system will also be discussed in Chapter 3. Finally contributions of this thesis will be summarized in Chapter 4.

1.4 Objectives

Structural damage identification approaches based on vibration data generated by SHM systems have been extensively studied and applied for engineering practice for several decades. Because of the structural complexity and the local phenomenon property of damage, complete information are always required for accurately evaluating the structural condition for large scale structures, which means a large number of sensors densely distributed over the entire structure are considered necessary to effectively detect arbitrary deterioration in a large scale structure. However, the traditional way to collect data centrally from a large number of sensors faces many troubles and obstacles for conducting SHM system either adopting wired or wireless sensors. Using of traditional wired sensors has the troubles and difficulties such as high equipment costs, long deploying time, difficulties in cabling and the constant maintenance for a large wiring plant. On the other hand, it is a huge difficulty to send all the measured data to a certain central station using wireless sensors because of the power requirements and bandwidth limitations. In both cases of wired and wireless sensors, the SHM measurement system will generate a tremendous amount of data and all of them would need to be transferred to such a central station. It is challenging and time-consuming to manage and deal with this huge amount of data. Thus, the main objective of this thesis is to develop a more effective damage identification algorithm which can get rid of the redundant information before transferring data back to the central station so that the efficiency of the SHM network

can be raised. The damage identification algorithm proposed in this thesis aims to make the SHM system works more efficiently and solve the problems and difficulties caused by large scale structures such as high equipment costs, long deploying time, difficulties in cabling, and etc.

1.5 Organization of Thesis

This thesis is divided into five chapters as illustrated in Figure 1.1.

Chapter 1 gives a brief introduction of SHM and damage detection.

To deal with the unrobust problem when the approach is applied to noise-contaminated vibration signals of a structure subjected to real earthquake excitation, Chapter 2 proposes an improvement to the previous substructure approach based on the combined use of residual errors and the squared frequencies. The improved substructure approach adopts a corrected damage indicator involving a model coefficients-based as well as model residual-based technique for local damage detection in shear structures. Firstly, a substructure algorithm is used to divide a complete structure into substructures, each of which is confined to one DOF with overlaps. Thus the accelerations are fed into autoregressive-moving average with exogenous inputs (ARMAX) models to determine the model coefficients, based on which the modal information of each substructure is obtained afterwards (Xing and Mita 2012). In what follows the normalized K-S test statistical distance between ARMAX model residual is adopted as a correction coefficient D_{ks} to correct the former damage indicator (difference between squared original frequency and squared damaged frequency). After presenting the proposed approach, simulation and experimental verifications were conducted and the results were presented and compared with the previous approach. Finally, conclusions and expectations were

discussed.

Chapter 3 proposes a substructural approach based on changes in the first autoregressive coefficient matrix for local damage identification in shear structures. Firstly, a substructure algorithm is used to divide a complete structure into several substructures, each of which shares a common form of the equation of motion. Then the equation of motion for each substructure is rewritten in terms of ARX model with different inputs and outputs. In what follows, it is derived theoretically that the elements of changes in the first AR model coefficient matrix (hereafter will be termed as CFAR) corresponding to the output DOFs adjacent to the damaged location are proportional to the stiffness reduction in the structure, indicating the damage location and severity. Thus the accelerations are fed into autoregressive-moving average with exogenous inputs (ARMAX) models to determine the AR model coefficients for each substructure under undamaged and various damaged conditions, based on which the CFAR is obtained and adopted as the damage indicator for the proposed substructure damage identification approach afterwards. After presenting the proposed approach, a numerical simulation and an experimental verification were conducted and the results were presented to show the feasibility and robustness of the proposed methodology. Finally, conclusions and expectations were discussed.

Next, Chapter 3 also presents a decentralized damage identification strategy (DDIS) that is suitable for implementation on a smart sensor network applied on shear structures. In this proposed strategy, the entire structure is divided into several substructures with some overlaps, the smart sensors inside and at the interface of the substructure are grouped together and only the locally measured information is used to evaluate the condition of local substructures; the associated damage identification algorithm is done in a decentralized manner. Damage identification results for these local substructures can then be reported back to the central station. In the sequel, to simplify the damage indicator (CFAR), the diagonal elements from changes in the

first autoregressive coefficient matrix (CFAR) are extracted to construct a vector in their original order and the vector is designated here as damage indicating vector (DIV). In each substructure, DIV can reveal the location and severity of the damage, which forms the basis for the decentralized damage identification strategy. Finally, simulations are conducted to investigate the potential of the DIV algorithm for implementation on wireless smart sensor networks (WSSN), where the issues of scalability of the DIV approach are undertaken by utilizing a decentralized, hierarchical and in-network processing strategy.

Chapter 4 summarizes contributions of this thesis, and points out the direction for future works.

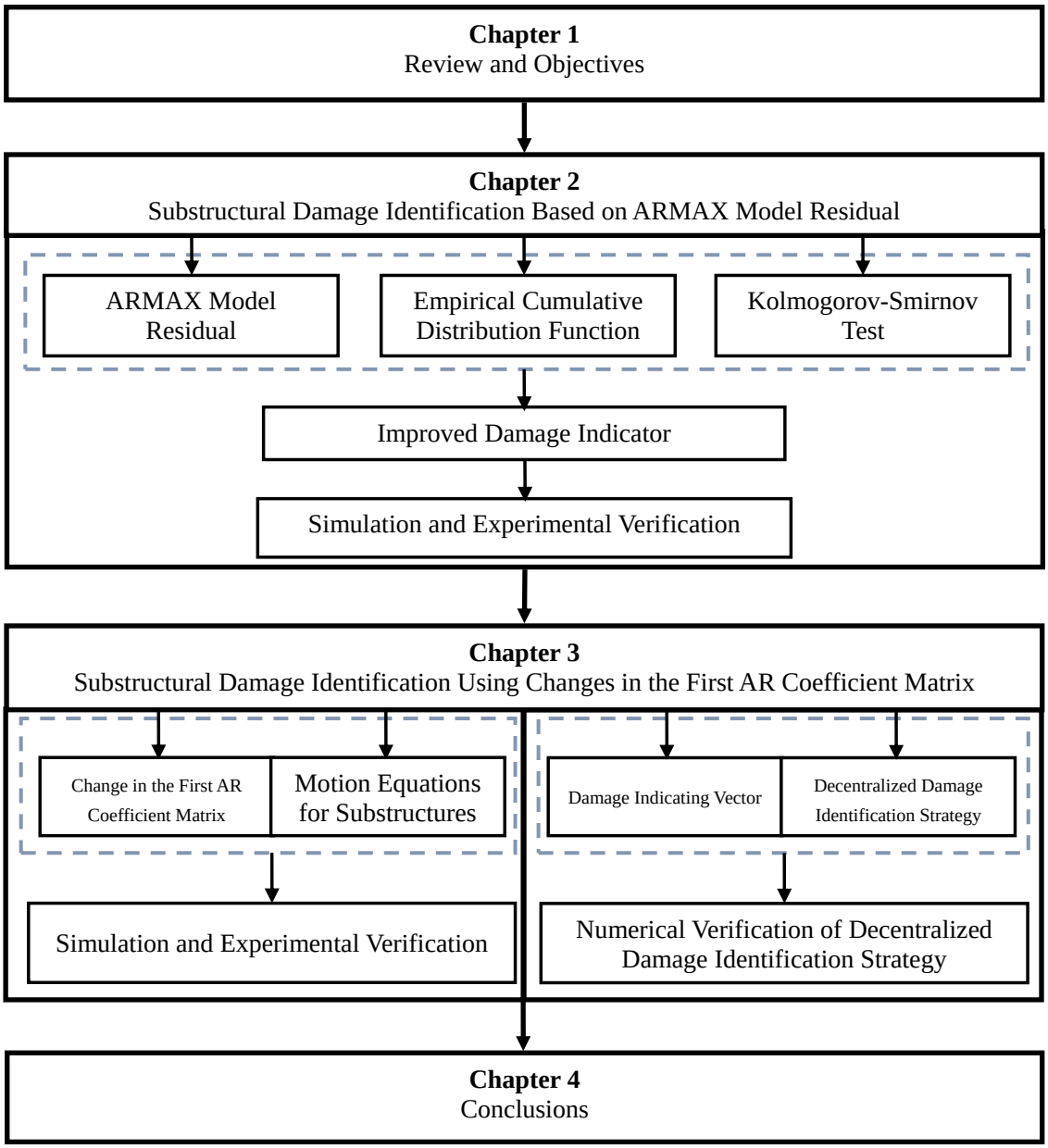

Figure 1.1. Organization of thesis

CHAPTER 2

Substructural Damage Identification Based on ARMAX Model Residual

2.1 Introduction

As mentioned in Chapter 1, there are a large number of damage detection approaches being researched and published singly based on model coefficients or model residual. However, the damage feature both considering model coefficients and model residual has been little investigated. Much as it appears as a simple concept, damage feature based on both model coefficients and model residual may contain more complete structural damage information than those only singly considering model coefficients or model residual. Thus in this chapter, a new combined substructure approach involving a model coefficients-based as well as model residual-based technique has been proposed for local damage detection in shear structures. Firstly, a substructure algorithm is used to divide a complete structure into substructures, each of which is confined to one DOF with overlaps. Thus the accelerations are fed into autoregressive-moving average with exogenous inputs (ARMAX) models to determine the model coefficients, based on which the modal information of each

substructure is obtained afterwards (Xing and Mita 2012). In what follows the normalized K-S test statistical distance between ARMAX model residual is adopted as a correction coefficient D_{ks} to correct the former damage indicator (difference between squared original frequency and squared damaged frequency). After presenting the proposed approach, simulation and experimental verifications were conducted and the results were presented and compared with the previous approach. Finally, conclusions and expectations were discussed.

2.2 Autoregressive Models

There are various autoregressive models existing to simulate the behavior of a linear, time-invariant (LTI) system. AR model is a type of random process which is often used to model and predict various types of time series. It is suited for describing a model with no input, i.e. a free vibration, with arbitrary initial conditions. The form of AR model is given as following (Ljung 1999; Soderstrom and Stoica 1989; Mita 2003):

$$w(t) + \sum_{k=1}^{na} a_k w(t-k) = e(t) \tag{2.1}$$

where $w(t)$ is the output of the structure at sample index t, a_k are the coefficients to be estimated, na is the order of the AR model, and $e(t)$ are the residuals of the estimation process up to time t.

The ARMA model is similar to the AR model except that it is capable to model a noise as following (Ljung 1999; Soderstrom and Stoica 1989; Mita 2003):

$$w(t) + \sum_{k=1}^{na} a_k w(t-k) = \sum_{k=1}^{nc} c_k\, e(t-k) + e(t) \tag{2.2}$$

where $w(t)$ is the output of the structure at sample index t, a_k and c_k are the coefficients to be estimated, na and nc are the orders of the ARMA model, and $e(t)$ are the residuals of the estimation process up to time t.

The ARX model is an AR model with an extra input as described below (Ljung 1999; Soderstrom and Stoica 1989; Mita 2003):

$$w(t) + \sum_{k=1}^{na} a_k w(t-k) = \sum_{k=1}^{nb} b_k u(t-nk-k+1) + e(t) \qquad (2.3)$$

where $w(t)$ and $u(t)$ are the output and input of the structure at sample index t, respectively, a_k and b_k are the coefficients to be estimated, na, nb, and nk are the orders of the ARX model, and $e(t)$ are the residuals of the estimation process up to time t.

The ARMAX model is a generalization of ARX model. The form of ARMAX model can be written as following (Ljung 1999; Soderstrom and Stoica 1989; Mita 2003):

$$w(t) + \sum_{k=1}^{na} a_k w(t-k) = \sum_{k=1}^{nb} b_k u(t-nk-k+1) + \sum_{k=1}^{nc} c_k\, e(t-k) + e(t) \qquad (2.4)$$

where $w(t)$ and $u(t)$ are the output and input of the structure at sample index t, respectively, a_k, b_k, and c_k are the coefficients to be estimated, na, nb, nc, and nk are the orders of the ARMAX model, and $e(t)$ are the residuals of the estimation process up to time t.

When you have dominating disturbances that enter early in the process, such as at the input, the ARMAX model proves to be an appropriate model as it has strong flexibility for handling the disturbance modeling and gives results which are satisfying and better than those of AR, ARX, and ARMA models (Ljung 1999; Soderstrom and Stoica 1989; Mita 2003; Stoffels et al. 2012). Xing and Mita (2012) show that the substructure method based on the ARX model almost does not work when it is applied to 5% noise contaminated data. Since the ARMAX model structure includes disturbance dynamics, the method based on this model has more flexibility in handling the disturbance modeling than the method based on the ARX model. Thus in this study the ARMAX model is chosen instead of ARX model to fit the input-output data sets.

Akaike Information Criterion (AIC) proposed by Akaike (1974) is adopted to

determine the order of ARMAX model. When a model involving p independently adjusted parameters is fitted to data, the AIC is defined by $AIC(p) = Nln\hat{\sigma}_p^2 + 2p$.

where N is the number of observations to which the model is fitted, and $\hat{\sigma}_p^2$ the estimated variance of the linear prediction error.

Note that the term $\hat{\sigma}_p^2$ decreases and therefore $\hat{\sigma}_p^2$ also decreases as the order of the ARMAX model is increased. However, $2p$ increases with an increase of order p. Hence, a minimum value can be obtained. If we plot $AIC(p)$ against p the graph will, in general, show a definite minimum value, and the appropriate order of the model is determined by that value of p at which $AIC(p)$ attains its minimum value.

2.3 Substructure Division Method

Similarly as in the previous paper by Xing and Mita (2012), a substructure algorithm is adopted to divide a complete structure into substructures. In this substructure approach, firstly a complete structure is divided into several substructures, which have a considerably smaller number of degrees of freedom (DOFs) when compared with the entire structure, as shown in Figure 2.1. Considering strong flexibility for handling the disturbance modeling, ARMAX model is adopted to extract the modal information of each substructure. Each substructure can be treated independently.

To illustrate the concept of substructuring, consider a shear building which is represented by a lumped mass system as shown in Figure 2.1. The dynamic equations of motion for the complete structure is:

$$\boldsymbol{M}\ddot{\boldsymbol{y}}(t) + \boldsymbol{C}\dot{\boldsymbol{y}}(t) + \boldsymbol{K}\boldsymbol{y}(t) = -\boldsymbol{M}\boldsymbol{r}\ddot{z}_{\mathrm{g}}(t) \tag{2.5}$$

where $\boldsymbol{M}$, $\boldsymbol{C}$ and $\boldsymbol{K}$ are the mass, damping, and stiffness matrices, respectively, $\boldsymbol{y}(t)$, $\dot{\boldsymbol{y}}(t)$, and $\ddot{\boldsymbol{y}}(t)$ are the dynamic response vectors of displacement, velocity, and acceleration relative to the ground, respectively, $\boldsymbol{r}$ is an $n \times 1$ unit vector ($\boldsymbol{r} = [1 \cdots 1]^{\mathrm{T}}$),

and $\ddot{z}_{\mathrm{g}}(t)$ is the ground acceleration.

$$\boldsymbol{y} = [y_1 \ y_2 \ \cdots \ y_{n-1} \ y_n]^{\mathrm{T}}$$

$$\boldsymbol{M} = \begin{bmatrix} m_1 & & & & & & 0 \\ & m_2 & & & & & \\ & & \ddots & & & & \\ & & & m_i & & & \\ & & & & \ddots & & \\ & & & & & m_{n-1} & \\ 0 & & & & & & m_n \end{bmatrix}$$

$$\boldsymbol{K} = \begin{bmatrix} k_1+k_2 & -k_2 & & & & & 0 \\ -k_2 & k_2+k_3 & -k_3 & & & & \\ & \ddots & \ddots & \ddots & & & \\ & & -k_{i-1} & k_{i-1}+k_i & -k_i & & \\ & & & \ddots & \ddots & \ddots & \\ & & & & -k_{n-1} & k_{n-1}+k_n & -k_n \\ 0 & & & & & -k_n & k_n \end{bmatrix}$$

$$\boldsymbol{C} = \begin{bmatrix} c_1+c_2 & -c_2 & & & & & 0 \\ -c_2 & c_2+c_3 & -c_3 & & & & \\ & \ddots & \ddots & \ddots & & & \\ & & -c_{i-1} & c_{i-1}+c_i & -c_i & & \\ & & & \ddots & \ddots & \ddots & \\ & & & & -c_{n-1} & c_{n-1}+c_n & -c_n \\ 0 & & & & & -c_n & c_n \end{bmatrix}$$

By considering the equilibrium of the m_i cut out of the whole structure, the motion equation of substructure #*i* ($1 \leqslant i \leqslant n$-1) can be formulated as

$$m_i\ddot{y}_i^r + (c_i + c_{i+1})\dot{y}_i^r + (k_i + k_{i+1})y_i^r = -m_i\ddot{z}_{i-1} + c_{i+1}\dot{y}_{i+1}^r + k_{i+1}y_{i+1}^r \quad (2.6)$$

where $\ddot{z}_{i-1}$ is the absolute acceleration of $m_{i\text{-}1}$, while y_i^r and y_{i+1}^r are the displacement of m_i and m_{i+1} relative to $m_{i\text{-}1}$, respectively, and when i=1, $\ddot{z}_{i-1}$ is the ground acceleration $\ddot{z}_{\mathrm{g}}$.

Similarly, for the particular case substructure #*n* (the top DOF), the motion equation of substructure #*n* is obtained as

$$m_n\ddot{y}_n^r + c_n\dot{y}_n^r + k_n y_n^r = -m_n\ddot{z}_{n-1} \tag{2.7}$$

where $\ddot{z}_{n-1}$ is the absolute acceleration of $m_{n\text{-}1}$, and y_n^r is the displacement of m_n relative to $m_{n\text{-}1}$.

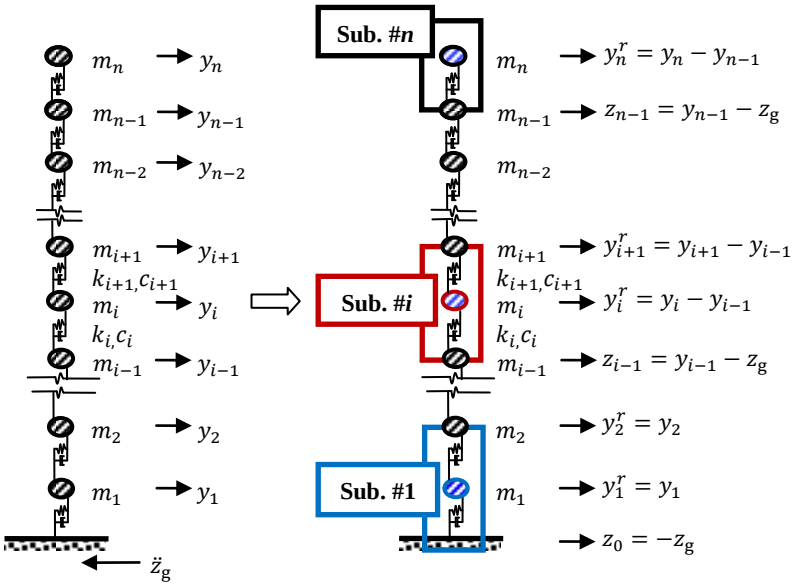

Figure 2.1. Divided substructural model

Introducing the difference expression

$$\dot{y}_i^r(t) = \frac{y_i^r(t+T) - y_i^r(t-T)}{2T} \tag{2.8}$$

$$\ddot{y}_i^r(t) = \frac{y_i^r(t+T) - 2y_i^r(t) + y_i^r(t-T)}{T^2} \tag{2.9}$$

where T is the sampling interval, assuming T=1 and substituting Equations 2.8 and 2.9 into the motion equation of substructure #i, Equation 2.6 can be reformulated in the form of

$$\begin{aligned}\ddot{y}_i^r(t) + a_1\ddot{y}_i^r(t-1) + a_2\ddot{y}_i^r(t-2) = b_{11}\ddot{z}_{i-1}(t-1) + b_{12}\ddot{z}_{i-1}(t-2) \\ + b_{21}\ddot{y}_{i+1}^r(t-1) + b_{22}\ddot{y}_{i+1}^r(t-2) + c_1 e(t-1) + c_2 e(t-2)\end{aligned} \tag{2.10}$$

where $e(t\text{-}1)$ and $e(t\text{-}2)$ are the prediction error terms or residuals.

Equation 2.10 can be regarded as a two-input ($\ddot{z}_{i-1}$ and $\ddot{y}_{i+1}^r$) and single-output ($\ddot{y}_i^r$) ARMAX model. The similar equation can be obtained by substituting Equations 2.8 and 2.9 into the motion equation of substructures #*n*, then Equation 2.7 can be rewritten in the form of

$$\ddot{y}_n^r(t) + a_1\ddot{y}_n^r(t-1) + a_2\ddot{y}_n^r(t-2) = b_1\ddot{z}_{n-1}(t-1) + b_2\ddot{z}_{n-1}(t-2) + c_1e(t-1) + c_2e(t-2) \quad (2.11)$$

Equation 2.11 can be regarded as a single-input ($\ddot{z}_{n-1}$) and single-output ($\ddot{y}_n^r$) ARMAX model.

The divided substructure model with corresponding input and output for constructing ARMAX model is shown in Figure 2.1.

2.4 Correction of Damage Indicator

Xing and Mita (2012) adopted difference between squared original frequency and squared damaged frequency as damage indicator in the substructure damage detection approach. The approach can work well in the simulation scenarios in which the target structure is subjected to white noise excitation and no noise is added to the vibration signals. However, when the approach is applied to noise-contaminated vibration signals of a structure subjected to real earthquake excitation, the damage detection algorithm will become unrobust and it is difficult to obtain a satisfactory result. As an improvement to this method, a scheme is proposed to correct the previous damage indicator in order to obtain more accurate and robust damage detection results.

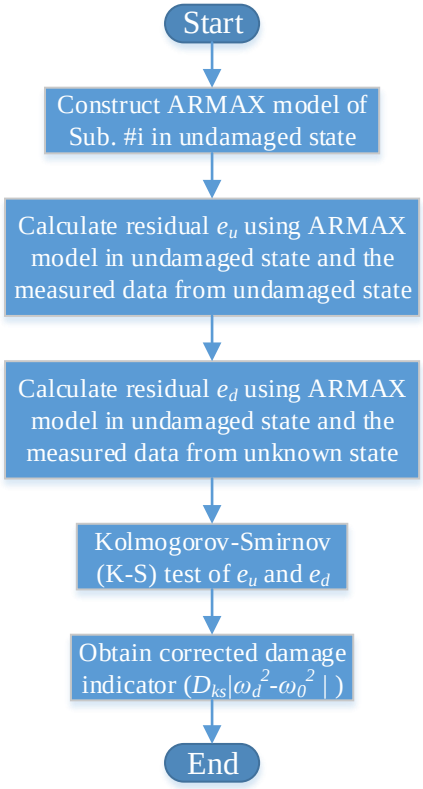

Figure 2.2. Flowchart for obtaining the corrected damage indicator

As mentioned previously in the introduction session, the model coefficients and model residual both contain the information of structure damage and the information contained in the two has close correlation and overlap with each other, however, they certainly do not equate. Obviously it is impossible to include all the essential information necessary for damage detection based on only one aspect of the two. In other words, it appears as a simple and clear idea that damage features based on both model coefficients and model residual may contains more complete essential structural damage information than those only singly considering model coefficients or model residual. Thus, the normalized Kolmogorov-Smirnov (K-S) test statistical distance between ARMAX model residual error is adopted as a correction coefficient D_{ks} to correct the previous damage indicator only based on the model coefficients

(difference between squared original frequency and squared damaged frequency). The corrected damage indicator will combine the information from the model coefficients as well as model residual by the proposed correction procedure. The flowchart for obtaining the corrected damage indicator is shown in Figure 2.2.

2.4.1 Empirical Cumulative Distribution Function of ARMAX Model Residual

The Burg's (maximum entropy) method (BM) (Marple 1987) can be used to identify the model parameters from data $\{\boldsymbol{u}(t), \boldsymbol{w}(t)\}_{t\in[t_1,t_2]}$ acquired on an appropriate time interval $t \in [t_1, t_2]$. Once the model is constructed from the baseline signal, for both undamaged and damaged cases, a residual $\boldsymbol{e}$ can be generated between the measurement output $\boldsymbol{w}$ and the predicted output $\widehat{\boldsymbol{w}}$ through the reference ARMAX model, which is ideally a Gaussian process for a stationary signal (Lee 1997).

$$\boldsymbol{e}_u(t) = \boldsymbol{w}_u(t) - \widehat{\boldsymbol{w}}_u^u(t) \tag{2.12}$$

$$\boldsymbol{e}_d(t) = \boldsymbol{w}_d(t) - \widehat{\boldsymbol{w}}_d^u(t) \tag{2.13}$$

where $\boldsymbol{w}_u(t)$ and $\boldsymbol{w}_d(t)$ are the undamaged and damaged measurement output from the target structure, respectively, and $\widehat{\boldsymbol{w}}_u^u(t)$ and $\widehat{\boldsymbol{w}}_d^u(t)$ are the undamaged and damaged predicted output based on the ARMAX model constructed from the undamaged (reference) signal, respectively, which can be expressed as follows according to Equations 2.4, 2.12 and 2.13:

$$\widehat{w}_u^u(t) = -\sum_{k=1}^{na} a_k^u w_u(t-k) + \sum_{k=1}^{nb} b_k^u u_u(t-nk-k+1) + \sum_{k=1}^{nc} c_k^u\, e_u(t-k) \tag{2.14}$$

$$\widehat{w}_d^u(t) = -\sum_{k=1}^{na} a_k^u w_d(t-k) + \sum_{k=1}^{nb} b_k^u u_d(t-nk-k+1) + \sum_{k=1}^{nc} c_k^u\, e_d(t-k) \tag{2.15}$$

where $u_u(t)$ and $u_d(t)$ are the input of the undamaged and damaged structure at sample index *t*, respectively, a_k^u, b_k^u, and c_k^u are the ARMAX model coefficients estimated from the undamaged (reference) signal, *na*, *nb*, *nc*, and *nk* are the orders of the ARMAX model, and $e_u(t)$ and $e_d(t)$ are the residuals of the estimation process

of the undamaged and damaged state up to time *t*, respectively.

As a general understanding, the damaged system response alters from the undamaged state due to the story stiffness degradation. If ARMAX model is used for time series modeling of the data, ARMAX model residual error will carry vital information of the data. In this study, an ARMAX model is constructed from the reference signal and model residuals can then be generated by fitting the baseline model to the signals collected from the undamaged case. Thereafter, for a damaged case, the reference model cannot produce a good fit of the damaged response data anymore. That means the gap between predicted response data from reference model and measurement response data will get bigger. From Equations 2.12 and 2.13, it also shows clearly that the residual error generated from the damaged response data is different from that of the undamaged one.

In order to eliminate the influence of different response amplitude, the model residual vector are normalized to a dimensionless vector through dividing it by the norm of output response vector as follows:

$$\bar{\boldsymbol{e}}_u = \frac{\boldsymbol{e}_u}{\|\boldsymbol{w}_u\|} \tag{2.16}$$

$$\bar{\boldsymbol{e}}_d = \frac{\boldsymbol{e}_d}{\|\boldsymbol{w}_d\|} \tag{2.17}$$

where $\boldsymbol{e}_u$ and $\boldsymbol{e}_d$ are the ARMAX model residual vector generated from the undamaged and damaged state, respectively, $\bar{\boldsymbol{e}}_u$ and $\bar{\boldsymbol{e}}_d$ are the normalized dimensionless residual vector correspondingly, $\|\boldsymbol{w}_u\|$ and $\|\boldsymbol{w}_d\|$ are the norm of output response vector of the undamaged and damaged state, respectively.

In what follows the difference in the normalized dimensionless residuals between damaged state and undamaged state will be analyzed through an appropriate statistical test. In this study, a graphical visualization of empirical cumulative distribution function (ECDF) is adopted to check the similarity between the two distinguished data

sets of residual error generated from undamaged and damaged state.

An empirical cumulative distribution function (ECDF) of the normalized dimensionless residuals $\bar{e}$ is defined by

$$F(\bar{e}) = \frac{1}{n}\sum_{i=1}^{n} I(\bar{e}_i \leq \bar{e}) \tag{2.18}$$

where *n* is the number of data points, and *I* is the event indicator and it can be expressed as

$$I = \begin{cases} 1: & \bar{e}_i \leq \bar{e} \\ 0: & \text{otherwise} \end{cases} \tag{2.19}$$

The procedure to obtain ECDF can be mainly divided into three steps (Equations 2.18 and 2.19): (i) rearrangement of data in ascending order; (ii) evaluation of event indicator; and (iii) calculate and plot the ECDF.

2.4.2 K-S Test on ARMAX Model Residual

As mentioned above, it is known that the ARMAX model residual error of the damaged data is different from that of the undamaged one and the ECDF can help us to tell the difference between the two distinguished residuals in a graphical and visualized way.

Furthermore, in statistics the Kolmogorov-Smirnov (K-S) test (Wang and Makis 2009; Kar and Mohanty 2004) is a nonparametric test that can be used to determine whether two underlying probability distributions differ or not based on the properties of the ECDF. There is no prior assumption towards the distribution pattern required for K-S test as it is a kind of nonparametric test; In addition, K-S test is sensitive to differences in both location and shape of the ECDF of two samples. It was shown that the K-S test has many advantages when compared with the conventional statistics such as mean, variance, kurtosis and skewness (Wang and Makis 2009; Kar and

Mohanty 2004). Furthermore, the K-S test is more sensitive at points near the median of the distribution while the Anderson-Darling test better captures the discrepancy for the tails. In this study, the residual discrepancy between damaged and undamaged state around the median is bigger that the tails, thus K-S test is more optimal for quantifying the residual discrepancy. Because of these advantages, K-S test has been considered to be one of the most preferred and extremely powerful statistical signal processing tool in time domain signal analysis. The K-S test based signal processing technique compares two samples and tests the hypothesis that the two samples have the same probability distribution. The K-S statistic quantifies a distance between the ECDF of two samples. The null distribution of this statistic is calculated under the hypothesis that both samples are drawn from the same underlying distribution for a particular significance level. Using this technique, it is possible to quantitatively determine the difference between the two samples. Therefore, by comparing a given vibration signature to a baseline signature (i.e. the signature from known undamaged state), it is possible to detect, locate and quantify damage existing in the structure from the given vibration signal.

The K-S test considers the null hypothesis *H* that the ECDF of the target distribution is the same as the ECDF of the reference distribution. Hence, it is possible to compare two vibration signatures, and assess if both have the same ECDFs (Wang and Makis 2009; Dilena and Morassi 2004). Note that the application of this test for damage detection assumes that the damage existing in the structure is strong enough to vary the ECDF of the original vibration signature, which will be shown in the following numerical studies section. In this paper, the proposed algorithm adopt two-sample K-S test to check the similarity and quantify the distance between the ARMAX model residual errors of the undamaged and damaged data sets. First of all, an ARMAX model is constructed from the known reference signal and the residual error, denoted by $\bar{e}_u(t)$, is calculated for the undamaged state, which is chosen to represent the

reference distribution. Thereafter, for a damaged state, the residual error is calculated utilizing the deviation of the damaged response data from the reference ARMAX model data and it is denoted by $\bar{e}_d(t)$, chosen to represent the target distribution. Thus, the ECDF of the reference distribution and the target distribution are denoted by $F_u(\bar{e})$ and $F_d(\bar{e})$, respectively. In this nonparametric hypothesis test, the K-S test statistical distance plays a vital role, which decides whether the null hypothesis *H* is to be rejected for a given confidence interval. Accordingly, when applying a two-sample K-S test, the null hypothesis *H* can be shown as the following form:

$$H = \begin{cases} 1: \bar{e}_u \neq \bar{e}_d \\ 0: \bar{e}_u \equiv \bar{e}_d \end{cases} \tag{2.20}$$

The K-S test statistical distance, which means the distance between two ECDFs $F_u(\bar{e})$ and $F_d(\bar{e})$, is calculated as:

$$D_{ks} = \sup_{-\infty<e<\infty} \left| F_u^{N_1}(\bar{e}) - F_d^{N_2}(\bar{e}) \right| \tag{2.21}$$

where N_1 and N_2 are the data length of the first and second sample, respectively. Let

$$N = \frac{N_1 N_2}{N_1 + N_2} \tag{2.22}$$

The null hypothesis *H* that the two distributions are equal is rejected, at significance level α, if $D_{ks}^* = \sqrt{N} D_{ks}$ is greater than the corresponding critical value K_α,

where K_α is found from

$$Pr(K \leq K_\alpha) = 1 - \alpha \tag{2.23}$$

where *K* is a random variable obeying the Kolmogorov distribution as following:

$$K = sup_{t\in[0,1]} |B(t)| \tag{2.24}$$

where $B(t)$ is the Brownian bridge. The cumulative distribution function of *K* is given by

$$Pr(K \le x) = 1 - 2\sum_{k=1}^{\infty}(-1)^{k-1}e^{-2k^2x^2} = \frac{\sqrt{2\pi}}{x}\sum_{k=1}^{\infty}e^{-(2k-1)^2\pi^2/(8x^2)} \quad (2.25)$$

Xing and Mita's paper (2012) adopted difference between squared original frequency and squared damaged frequency as the damage indicator in the substructure damage detection approach. As an improvement to this method, the normalized K-S test statistical distance is established and adopted as a correction coefficient D_{ks} to correct the previous damage indicator. Consequently, the corrected damage indicator (DI) can be expressed as:

$$\mathrm{DI} = D_{ks}\left|\omega_d^2 - \omega_0^2\right| \quad (2.26)$$

where, ω_d and ω_0 are the damaged and undamaged natural frequency respectively. The correction coefficient D_{ks} is the normalized K-S test statistical distance between two ECDFs of the ARMAX model residual errors in the baseline undamaged condition and the unknown condition.

2.5 Performance Verification by Simulation

A simulation of a five-story shear building model was performed to show the feasibility and advantage of the proposed scheme for damage detection. The building is simplified into a 5-DOF structural system as shown in Figure 2.3.

The mass of every floor and the lateral stiffness were assumed to be 100 kg and 1 MN/m, respectively. The damping ratio of all modes was chosen as 3%. The data sampling frequency was 200 Hz. The undamaged natural frequencies of the structure were 4.5, 13.2, 20.8, 28.6, and 30.5 Hz for the 1st, 2nd, 3rd, 4th, and 5th modes, respectively. The 5-DOF system was simulated to be subjected to two types of excitations, including white noise excitation and the 1940 El Centro ground motion (N-S acceleration at the Imperial Valley Irrigation District substation in El Centro, CA, during the 1940 Imperial Valley earthquake), and the noise contributing to 5% of the

signal RMS value was added to the acceleration responses of the structure. The story stiffness reduction was regarded to be damage to the structure. Five damage cases (damage in the 1st, 2nd, 3rd, 4th, or 5th story) with five different damage severities (10%, 20%, 30%, 40%, and 50% lateral stiffness reduction) were studied. Hence, there were 25 different damage scenarios in total.

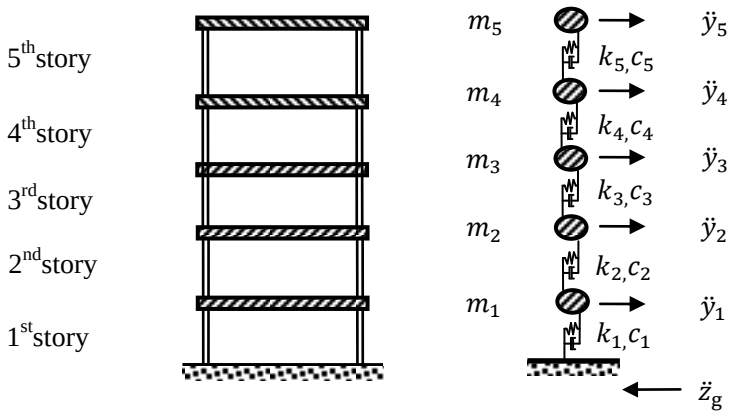

Figure 2.3. Five-story shear building

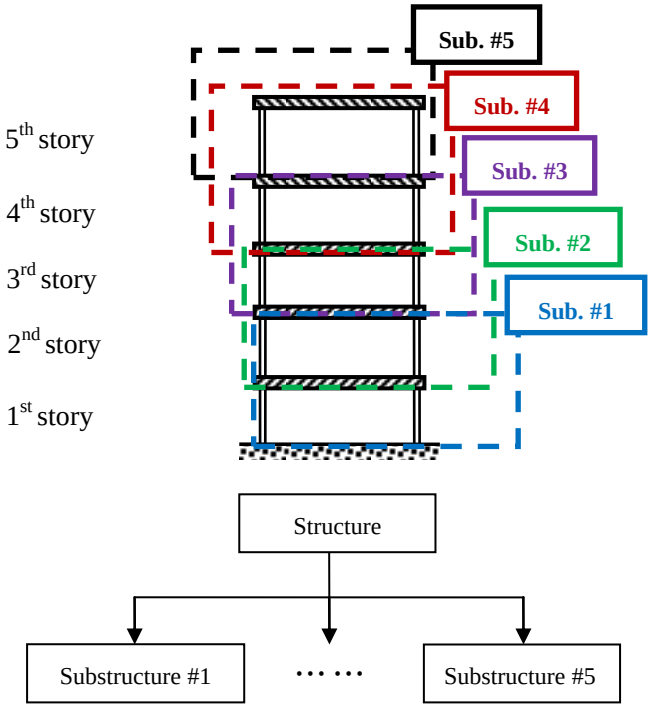

Figure 2.4. Structural division

Firstly, according to the substructure division method described in section 2.3, the whole structure was divided into substructures, as shown in Figure 2.4. Then, ARMAX model is developed to model each substructure for the undamaged state and unknown state. The i^{th} substructure (except the 5^{th} substructure) can be modeled as a two-input one-output ARMAX model. The relative acceleration of m_{i+1} to m_{i-1} ($\ddot{y}_{i+1}^{r}$) and the absolute acceleration of m_{i-1} ($\ddot{z}_{i-1}$) are used as the input, and the relative acceleration of m_i to m_{i-1} ($\ddot{y}_{i}^{r}$) is used as the output.

The 5^{th} substructure can be modeled as a one-input one-output ARMAX model. The absolute acceleration of m_4 ($\ddot{z}_4$) are used as the input, and the relative acceleration of m_5 to m_4 ($\ddot{y}_5^r$) is used as the output.

The Burg's (maximum entropy) method (BM) were used to identify the ARMAX model coefficients from input-output data sets for each substructure and each damage scenario. It is easy to obtain the natural frequency of each substructure based on the estimated ARMAX model coefficients. Then model residuals were generated by fitting the baseline model to the signals collected from the undamaged and damaged cases.

The ECDF of ARMAX model residual errors for the undamaged and damaged states were calculated and plotted to indicate the damage existing in the structure. Figures 2.5 and 2.6 provide plots of ECDF for each substructure in undamaged state and 25 different damaged scenarios subjected to white noise excitation and El Centro earthquake excitation, respectively.

From Figures 2.5 and 2.6, it is shown that the undamaged state is associated with a steepest curve and the curve becomes more and more gentle with the increase of the damage intensity, which indicates the damage existence and damage extent. Additionally, it can also be observed from Figures 2.5 and 2.6 that only the ECDF plots of ARMAX model residual errors for the substructures containing the damaged floors alter considerably, while those for the substructures without the damaged floors remain

unchanged, which indicates the damage location.

However, it is difficult to exactly quantify the gap between the ECDF curves of different damaged scenarios without the help of some statistical tools. That is the reason why it is necessary to introduce the K-S statistic D_{ks}, a powerful statistical signal processing tool which quantifies a distance between the ECDF of two samples. Then in the next step the K-S statistic D_{ks} is combined with the difference between squared original frequency and squared damaged frequency to form the new damage indicator which can exactly locate and quantify the damage.

Tables 2.1 and 2.2 show the values of normalized K-S test statistical distance D_{ks} for each substructure with various damage severities subjected to white noise excitation and El Centro earthquake excitation, respectively. From Tables 2.1 and 2.2, it can be clearly observed that the D_{ks} value tends to 1 when the substructure contains the damaged floor. On the other hand, the D_{ks} value tends to 0 for the substructure without the damaged floor. It means that the D_{ks} value shows a quite good capability in damage localization.

And even more important, it is shown in Tables 2.1 and 2.2 that the D_{ks} value is sensitive to damage, immune to noise and robust under different types of excitations. Even when it is applied to noise-contaminated vibration signals of a structure subjected to real earthquake excitation, the D_{ks} value can still indicate perfect damage localization results, with the spurious damage detection results at a very low level. Therefore, the normalized K-S test statistical distance D_{ks} is adopted as a correction coefficient to correct the previous damage indicator (difference between squared original frequency and squared damaged frequency). The corrected damage indicator combines the information from the model coefficients as well as model residual, possessing both robustness in damage localization from D_{ks} and high efficiency in accurate damage quantification from the natural frequency shift.

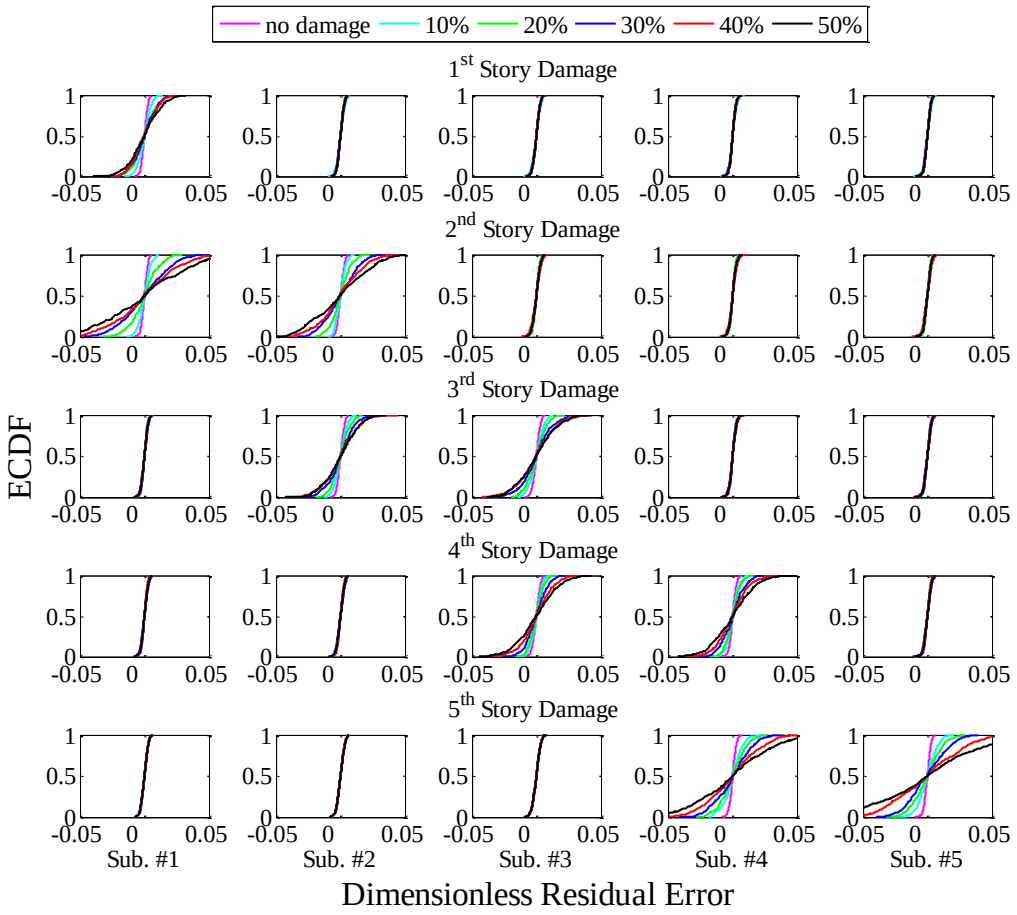

Figure 2.5. ECDF of dimensionless residual error (white noise excitation, 5% noise, ARMAX model, data length=2000, na=2, nb=3, nc=3, nk=1)

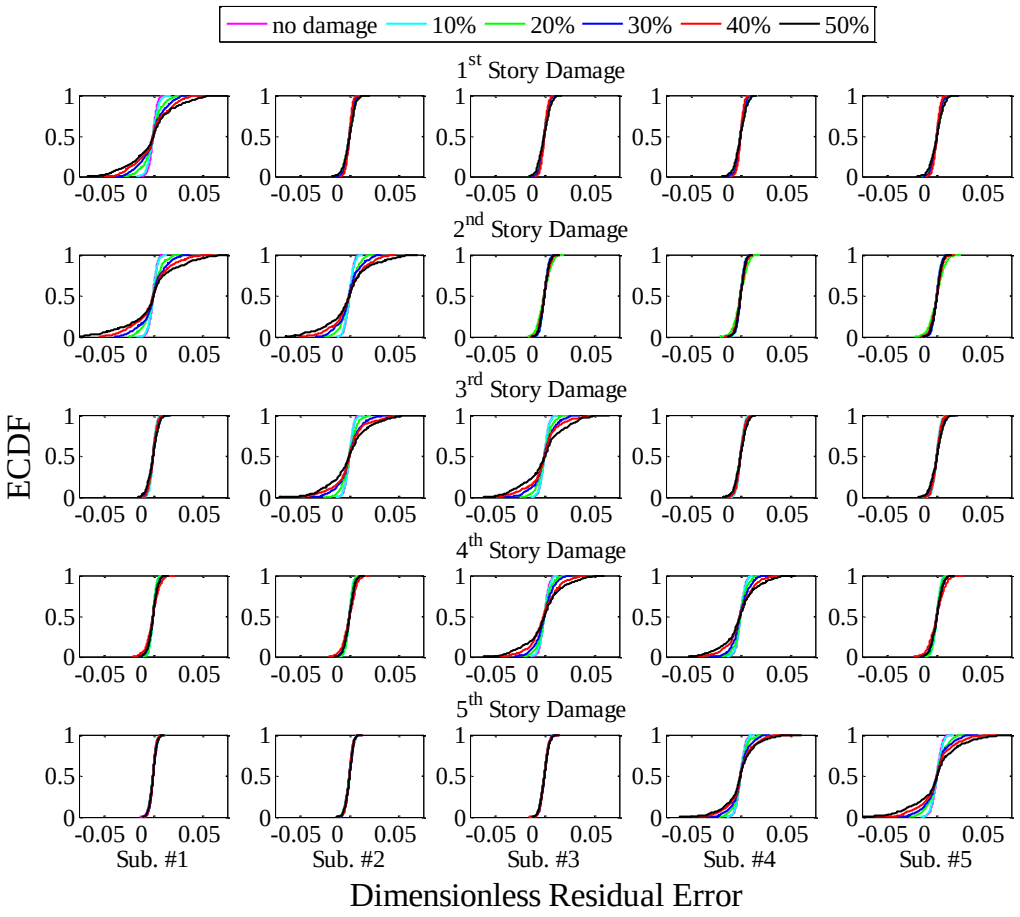

Figure 2.6. ECDF of dimensionless residual error (El Centro earthquake excitation, 5% noise, ARMAX model, data length=4000, na=2, nb=3, nc=3, nk=1)

Table 2.1. Correction coefficient D_{ks} (normalized K-S test statistical distance) (white noise excitation, 5% noise, ARMAX model, data length=2000, na=2, nb=3, nc=3, nk=1)

Damage(%)		Sub. #1	Sub. #2	Sub. #3	Sub. #4	Sub. #5
1st Story	10	1.0000	0.0162	0.0000	0.0365	0.0243
	20	1.0000	0.0124	0.0131	0.0267	0.0000
	30	1.0000	0.0082	0.0043	0.0016	0.0000
	40	1.0000	0.0060	0.0000	0.0120	0.0014
	50	1.0000	0.0049	0.0014	0.0066	0.0000
2nd Story	10	1.0000	0.9492	0.0000	0.0197	0.0066
	20	1.0000	0.8965	0.0007	0.0215	0.0000
	30	1.0000	0.9128	0.0003	0.0024	0.0000
	40	1.0000	0.9646	0.0000	0.0074	0.0003
	50	1.0000	0.9201	0.0000	0.0026	0.0022
3rd Story	10	0.0071	1.0000	0.9929	0.0000	0.0142
	20	0.0089	1.0000	0.9618	0.0150	0.0000
	30	0.0135	1.0000	0.9883	0.0211	0.0000
	40	0.0036	1.0000	1.0000	0.0000	0.0078
	50	0.0084	0.9943	1.0000	0.0031	0.0000
4th Story	10	0.0150	0.0234	0.9363	1.0000	0.0000
	20	0.0000	0.0005	0.9224	1.0000	0.0077
	30	0.0060	0.0000	0.9288	1.0000	0.0144
	40	0.0074	0.0052	0.9961	1.0000	0.0000
	50	0.0066	0.0000	0.9941	1.0000	0.0052
5th Story	10	0.0104	0.0000	0.0032	0.9352	1.0000
	20	0.0054	0.0000	0.0018	0.9831	1.0000
	30	0.0021	0.0000	0.0026	0.9393	1.0000
	40	0.0032	0.0000	0.0030	0.9136	1.0000
	50	0.0000	0.0019	0.0031	0.9026	1.0000

Table 2.2. Correction coefficient D_{ks} (normalized K-S test statistical distance) (El Centro earthquake excitation, 5% noise, ARMAX model, data length=4000, na=2, nb=3, nc=3, nk=1)

Damage(%)		Sub. #1	Sub. #2	Sub. #3	Sub. #4	Sub. #5
1st Story	10	1.0000	0.0304	0.0000	0.0679	0.0515
	20	1.0000	0.0449	0.0275	0.0487	0.0000
	30	1.0000	0.0173	0.0006	0.0035	0.0000
	40	1.0000	0.0135	0.0094	0.0249	0.0000
	50	1.0000	0.0090	0.0049	0.0116	0.0000
2nd Story	10	1.0000	0.8703	0.0000	0.0574	0.0436
	20	1.0000	0.8814	0.0624	0.0083	0.0550
	30	1.0000	0.8641	0.0000	0.0079	0.0058
	40	1.0000	0.8331	0.0000	0.0145	0.0066
	50	1.0000	0.8833	0.0000	0.0033	0.0010
3rd Story	10	0.0238	0.9762	1.0000	0.0102	0.0000
	20	0.0277	1.0000	0.8616	0.0626	0.0000
	30	0.0169	1.0000	0.9574	0.0272	0.0000
	40	0.0024	1.0000	0.9972	0.0000	0.0055
	50	0.0075	1.0000	0.9901	0.0012	0.0000
4th Story	10	0.0000	0.0302	0.8798	1.0000	0.0211
	20	0.0000	0.0096	0.8920	1.0000	0.0056
	30	0.0051	0.0000	0.8830	1.0000	0.0125
	40	0.0163	0.0000	0.9543	1.0000	0.0070
	50	0.0061	0.0000	0.9939	1.0000	0.0052
5th Story	10	0.0333	0.0000	0.0240	0.9427	1.0000
	20	0.0097	0.0020	0.0000	0.9949	1.0000
	30	0.0023	0.0000	0.0089	0.9230	1.0000
	40	0.0028	0.0000	0.0084	0.8910	1.0000
	50	0.0000	0.0004	0.0067	0.8711	1.0000

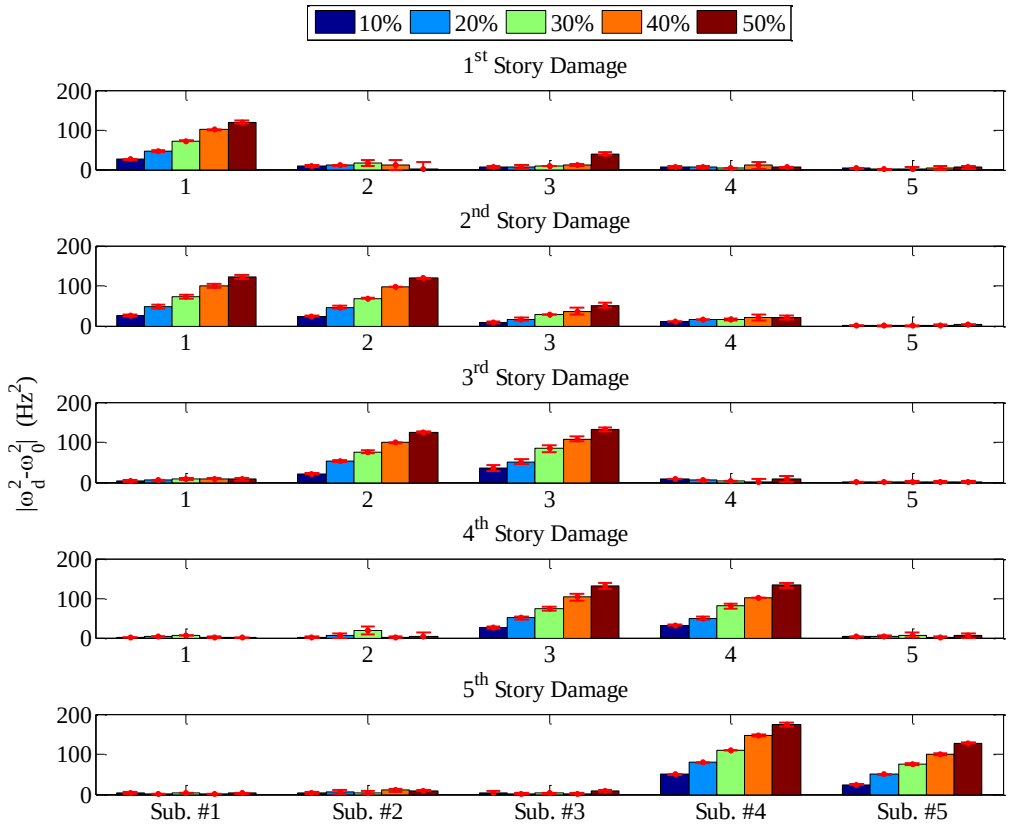

Figure 2.7. Damage indicator without correction coefficient D_{ks} (white noise excitation, 5% noise, ARMAX model, data length=2000, na=2, nb=3, nc=3, nk=1)

Figures 2.7 and 2.8 are bar charts of the damage indicator for each substructure before and after correction with D_{ks}, respectively, in 25 different damaged scenarios subjected to white noise excitation. As mentioned beforehand, the vertical axis stands for the damage indicator. And the damage indicator before correction is the difference between squared original frequency and squared damaged frequency, while the corrected damage indicator is adopted as the product of the correction coefficient D_{ks} and the difference between squared original frequency and squared damaged frequency. The error bars show the standard deviation of the damage indicator under 95% confidence interval. The results in Figure 2.7 show that when the noise contributing to 5% of the signal RMS value was added, the method based on the former damage indicator

without correction can get a satisfactory result, however, some spurious damage detection results occur on undamaged story, which shows the unrobustness of this method when it is applied to noise contaminated data. On the other hand, it is shown in Figure 2.8 that the method based on the corrected damage indicator after correction with D_{ks} can obtain excellent results, with the spurious damage detection results almost close to zero. The standard deviation under 95% confidence interval is quite small, which proves the robustness of this corrected damage indicator.

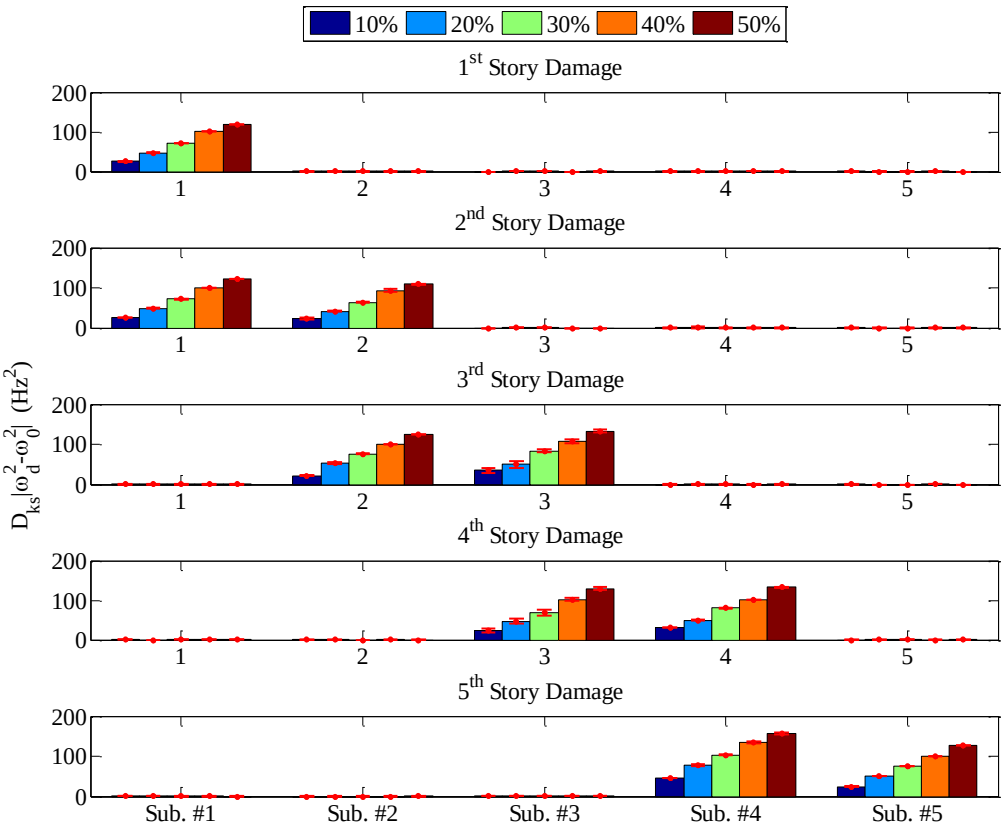

Figure 2.8. Damage indicator with correction coefficient D_{ks} (white noise excitation, 5% noise, ARMAX model, data length=2000, na=2, nb=3, nc=3, nk=1)

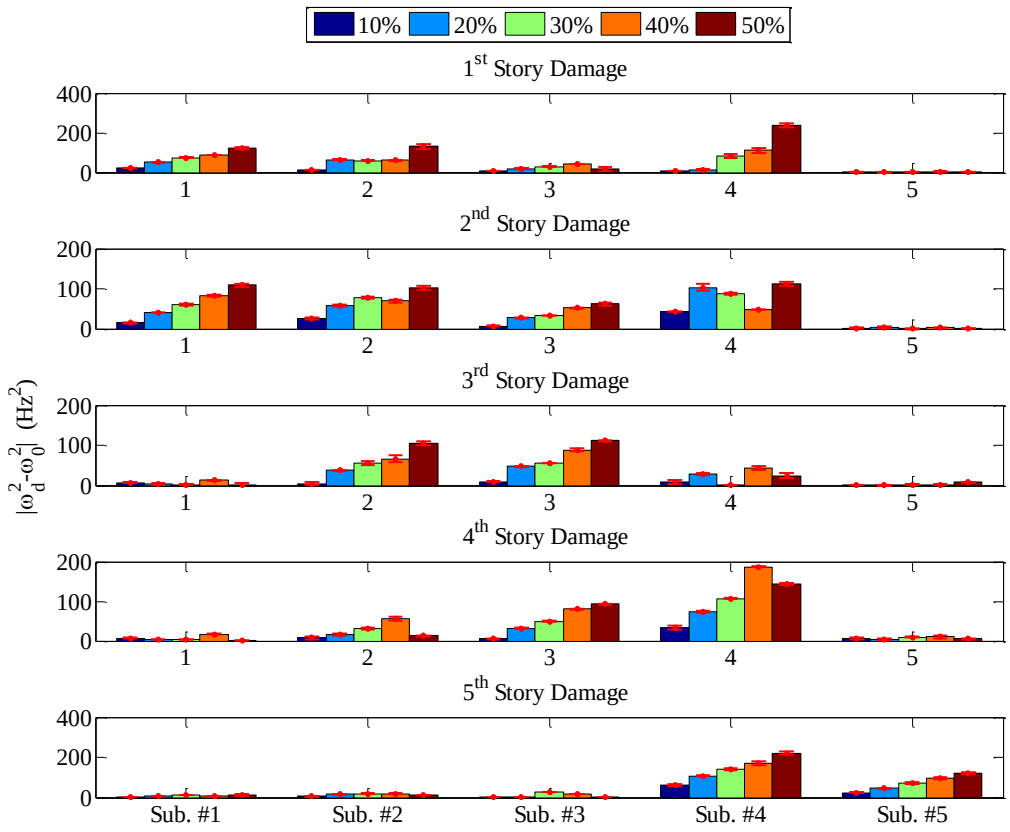

Figure 2.9. Damage indicator without correction coefficient D_{ks} (El Centro earthquake excitation, 5% noise, ARMAX model, data length=4000, na=2, nb=3, nc=3, nk=1)

Next let's take a look at the results of the 25 different damaged scenarios subjected to El Centro earthquake excitation, which are shown in Figures 2.9 and 2.10. It can be observed from Figure 2.9 that the method based on the former damage indicator without correction almost doesn't work at all, with very high level spurious damage detection results occur on undamaged story, which will confusing the practical damage detection task. On the contrary, Figure 2.10 shows that the method based on the corrected damage indicator after correction with D_{ks} still can get a satisfactory result and only some very low lever spuriously damage identification results happen, which shows the false detection can be circumvented by correcting the damage indicator with D_{ks}. It means the corrected damage indicator is robust even when it is applied to

noise-contaminated vibration signals of a structure subjected to real earthquake excitation. The low values of standard deviation under 95% confidence interval also show the robustness of the corrected damage indicator.

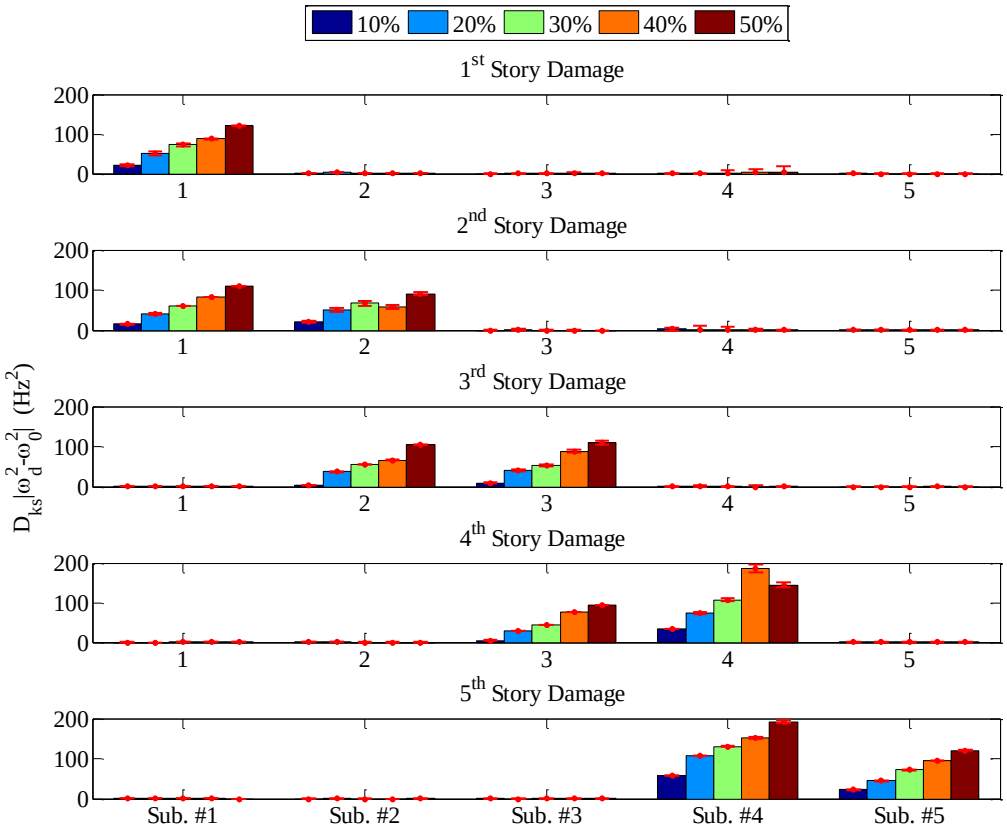

Figure 2.10. Damage indicator with correction coefficient D_{ks} (El Centro earthquake excitation, 5% noise, ARMAX model, data length=4000, na=2, nb=3, nc=3, nk=1)

2.6 Experimental Verification

In this section, the measured data from a shake table experiment of a five-story frame structure was utilized to verify the advantage of the proposed methodology. To show the advantages of the proposed method, the results based on the previous method are used for comparison.

2.6.1 Experimental Setup

The model structure is depicted in Figure 2.11(a). This experimental setup imitates a five-story shear frame building. The story mass was provided by the weight of aluminium floor slabs, bronze columns and sensors, which is 4.360 kg for the $1^{st}\sim4^{th}$ story and 3.544 kg for the 5^{th} story. The interfloor stiffness was decided by the bronze plate springs which are shown in Figure 2.11(b). The Young's modulus of bronze is 1.0×10^{11} N/m^2. The cross section size and the theoretical stiffness in the weak-axis of each column are shown in Table 2.3 and Figure 2.11(c). The structure was initially healthy with all original columns intact (Column type 0). The damage was introduced in the experiment by replacing two original columns in the diagonal position of one story with two weak ones. Three types of weaker columns were used in the experiment as shown in Figure 2.11(b) and Table 2.3. The undamaged natural frequencies of the specimen were 2.2, 7.0, 10.8, 12.6, and 14.6 Hz for the 1^{st}, 2^{nd}, 3^{rd}, 4^{th}, and 5^{th} modes, respectively.

Table 2.3. Parameters of five-story building model

	Column size $h\times b\times l$ (m)	Theoretical stiffness (N/m)
Column type 0	0.0025×0.03×0.24	3.4×10^3
Column type 1	0.003×0.014×0.24	2.7×10^3
Column type 2	0.003×0.010×0.24	2.0×10^3
Column type 3	0.003×0.006×0.24	1.2×10^3

The building model was placed on a shake table, as shown in Figure 2.11(a). The basement of the structure was set on bearings so that the structure could experience input motion. The force input to the structure was provided with an electrodynamic shaker. Accelerometers were installed on each floor plate to measure the acceleration

response, and one was installed on the basement to measure the input motion.

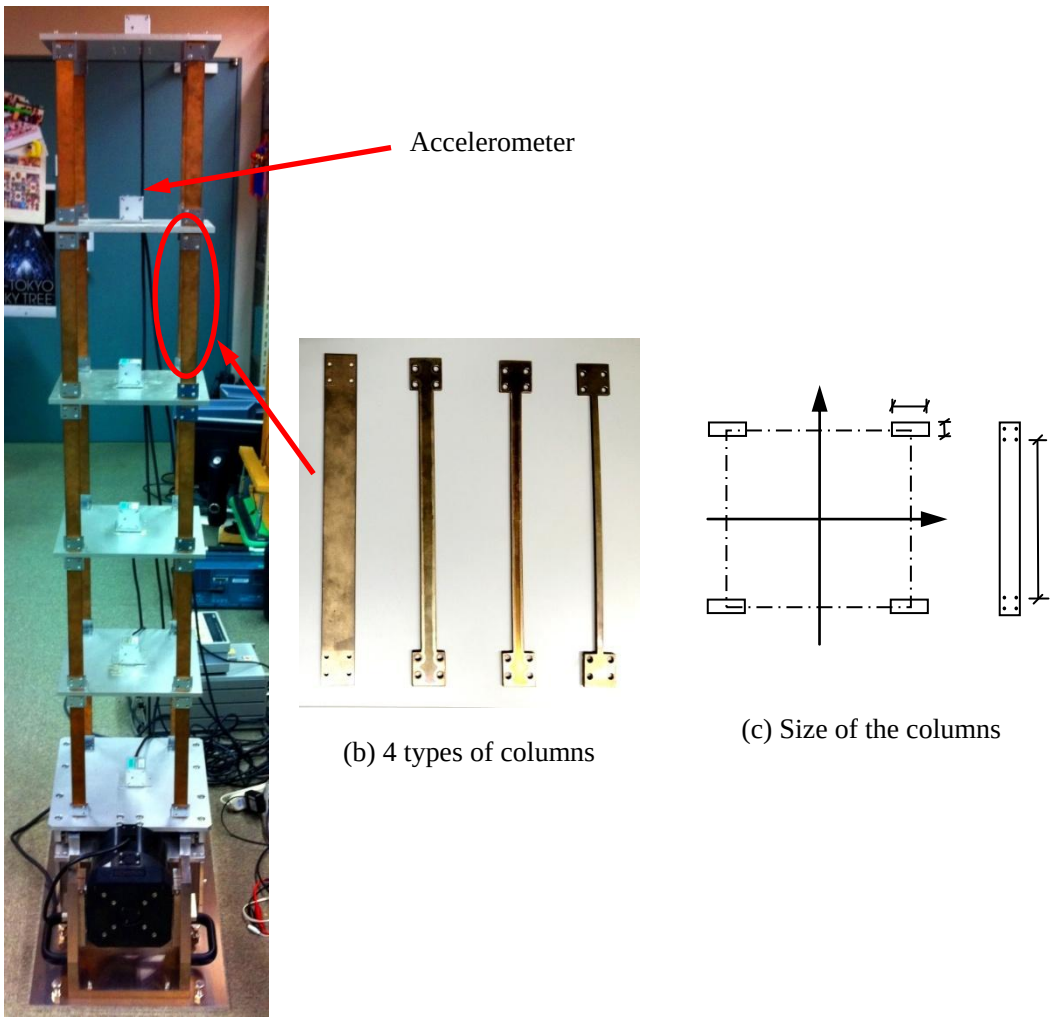

(a) Building model

(b) 4 types of columns

(c) Size of the columns

Figure 2.11. Experimental setup of five-story building model

2.6.2 Procedure

A sinusoidal wave with frequencies sweeping from 1.0 to 18.0 Hz was used as the input signal. The acceleration time histories were recorded for 180 s at a sampling

frequency of 200 Hz. Then they were decimated into 100 Hz. A part of one typical acceleration time history measured is shown in Figure 2.12. An 8-order low-pass Butterworth filter with cut-frequency 40 Hz was applied to the measured responses in order to remove the effects of noise.

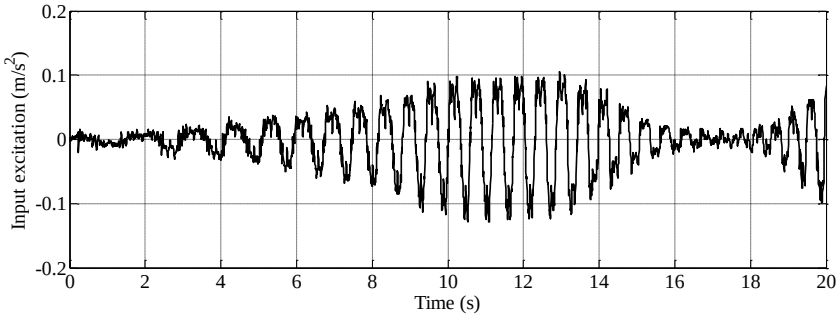

Figure 2.12. Input excitation

The five-story structure was firstly tested under the healthy state with all original columns. The force input to the structure was provided by the shaker to obtain the acceleration data of the healthy structure.

Then, two columns of one story were replaced by weaker columns to simulate the damage case. By replacing two original columns (Column type 0) in one story with three types of weaker ones (Column type 1, 2, and 3), the interfloor stiffness was reduced by around 10%, 20%, and 30%, respectively. The shaker provided excitation again in order to generate the acceleration data of the damaged structure, which were measured and recorded by the accelerometers. In total, data were collected for the undamaged state and fifteen (10%, 20%, and 30% damage in the 1^{st}, 2^{nd}, 3^{rd}, 4^{th}, and 5^{th} story: $3\times5=15$) damaged cases.

The same procedures as the simulation cases were performed on the experimental

measured data to detect both location and severity of damages in the test building model. Table 2.4 shows the values of normalized K-S test statistical distance D_{ks} of each substructure for all 15 damaged scenarios. The results in Table 2.4 show that the D_{ks} value is still robust to locate the damage when applied to the realistic experimental data. Figures 2.13 and 2.14 show bar plots of the damage indicator of each substructure before and after correction with D_{ks}, respectively. By comparing the two results, it shows that the spurious damage detection results were significantly circumvented and the damage detection performance was highly improved after correction with D_{ks}, which experimentally verifies and confirms the strong robustness and advantage of the improved methodology. Therefore, it is concluded that the improved method is applicable to realistic problems.

Table 2.4. Correction coefficient D_{ks} (normalized K-S test statistical distance) (Experimental measured data, ARMAX model, data length=4000, na=2, nb=3, nc=3, nk=1)

Damage(%)		Sub. #1	Sub. #2	Sub. #3	Sub. #4	Sub. #5
1st Story	10	1.0000	0.0134	0.0000	0.0496	0.0031
	20	1.0000	0.0188	0.0031	0.0859	0.0000
	30	1.0000	0.0214	0.0086	0.0426	0.0000
2nd Story	10	1.0000	0.9638	0.0000	0.0362	0.0217
	20	1.0000	0.9775	0.0051	0.0288	0.0000
	30	0.9989	1.0000	0.0000	0.0279	0.0000
3rd Story	10	0.0626	0.9903	1.0000	0.0644	0.0000
	20	0.0762	1.0000	0.9958	0.0095	0.0000
	30	0.0951	1.0000	1.0000	0.0845	0.0000
4th Story	10	0.0237	0.0073	0.9740	1.0000	0.0000
	20	0.0155	0.0166	0.9876	1.0000	0.0000
	30	0.0298	0.0000	0.9979	1.0000	0.0168
5th Story	10	0.0290	0.0000	0.0184	1.0000	0.9939
	20	0.0844	0.0000	0.0133	1.0000	0.9764
	30	0.0248	0.0000	0.0092	0.9867	1.0000

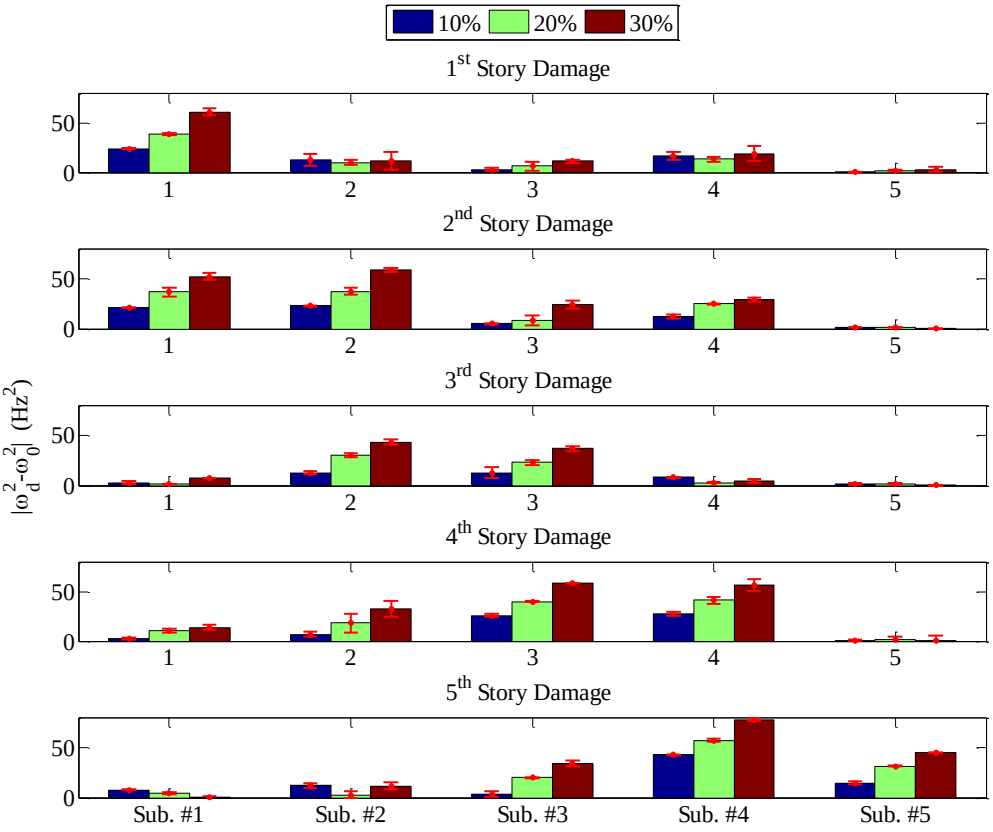

Figure 2.13. Damage indicator without correction coefficient D_{ks} (Experimental measured data, ARMAX model, data length=4000, na=2, nb=3, nc=3, nk=1)

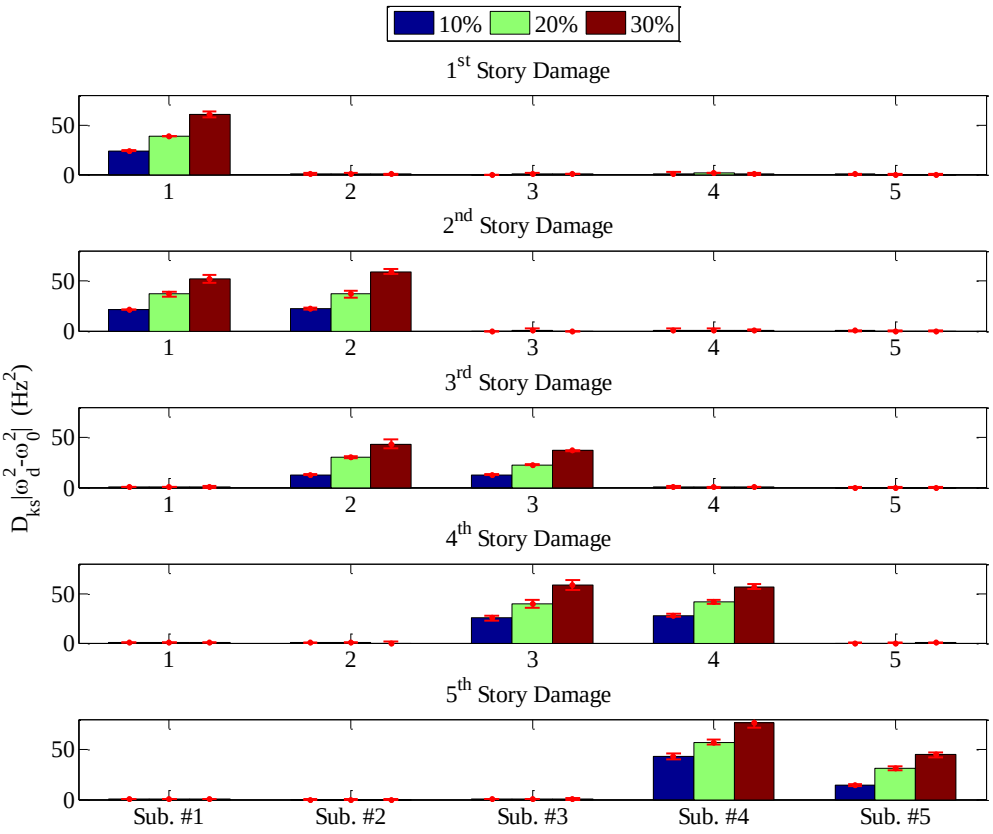

Figure 2.14. Damage indicator with correction coefficient D_{ks} (Experimental measured data, ARMAX model, data length=4000, na=2, nb=3, nc=3, nk=1)

2.7 Conclusions

To circumvent the false detection and unrobust problem existing in the former method, a new combined substructure approach involving a model coefficients-based as well as model residual-based technique has been proposed for local damage detection in shear structures. The improved technique realizes the combination of damage information contained in model coefficients and model residuals by correcting the previous damage indicator (difference between squared original frequency and squared damaged frequency). The correction coefficient is defined as the normalized Kolmogorov-Smirnov (K-S) test statistical distance between the two distinguished

data sets of ARMAX model residual generalized from undamaged and damaged states. A numerical simulation of a five-story shear building model has been conducted to verify the performance of the improved approach. The results are compared with the previous method, which show that the improved approach works much better and more robust than the previous method especially when it is applied to noise-contaminated vibration signals of a structure subjected to real earthquake excitation. In advance, the strong robustness and advantage of the improved methodology have been verified and confirmed with realistic shake table experimental data. As the structure is divided into substructures, which have a considerably smaller number of degrees of freedom (DOFs), thus the analysis on each substructure needs fewer data and less computation time. It may also be noted that evaluation of the correction coefficients involves only statistical calculation, which is not significant additional computation. These means that the improved approach is easy, efficient and robust for local substructure damage detection of shear structures. Moreover, as the damage detection process can be independently conducted on each substructure, this method is promising for application in a parallel and decentralized damage detection system.

Following can be expected as some limitations of the proposed substructural damage identification approach based on ARMAX model residual. Figure 2.1 shows that this method requires the targeted n-DOF structure to be divided into n separated one DOF substructures. This means that the total number of the substructures will be very large when this method applied to a complex structure with a large number of DOFs. Thus it is required to develop a more flexible substructural damage identification algorithm in advance for the sake of seeking the balance between the number of substructures and the computation intensity inside each substructure. The second limitation of the approach based on ARMAX model residual can be seen from damage identification results shown in Figures 2.7 to 2.10, Figures 2.13 and 2.14, Tables 2.1, 2.2 and 2.4.

The results show that it requires the damage identification information from two adjacent substructures to locate the damage. For instant, if the damage indicator attains large value in substructure #3, the damage might occur in the 3rd story or 4th story, which depends on the damage indicator of substructure #2 or #4 attaining large value.

CHAPTER 3

Substructural Damage Identification Using Changes in the First Autoregressive Coefficient Matrix

3.1 Introduction

To break through the limitations of the proposed substructural damage identification approach based on ARMAX model residual as previously mentioned in Chapter 2, it is in need of developing a more flexible substructural damage identification algorithm in advance for the sake of seeking the balance between the number of substructures and the computation intensity inside each substructure. It is also needed to develop an algorithm which can locate and quantify the damage inside a substructure without requiring the information from adjacent substructures, which will minimize the communication traffic in the sensor network. Thus in this chapter, a substructural approach based on changes in the first autoregressive coefficient matrix has been proposed for local damage identification in shear structures. Firstly, a substructure algorithm is used to divide a complete structure into several substructures, each of which shares a common form of the equation of motion. Then the equation of motion

for each substructure is rewritten in terms of ARX model with different inputs and outputs. In what follows, it is derived theoretically that the elements of changes in the first AR model coefficient matrix (hereafter will be termed as CFAR) corresponding to the output DOFs adjacent to the damaged location are proportional to the stiffness reduction in the structure, indicating the damage location and severity. Thus the accelerations are fed into autoregressive-moving average with exogenous inputs (ARMAX) models to determine the AR model coefficients for each substructure under undamaged and various damaged conditions, based on which the CFAR is obtained and adopted as the damage indicator for the proposed substructure damage identification approach afterwards. After presenting the proposed approach, a numerical simulation and an experimental verification were conducted and the results were presented to show the feasibility and robustness of the proposed methodology. Finally, conclusions and expectations were discussed.

3.2 Proposed Method

To illustrate the concept of substructuring, consider a shear building which is represented by a lumped mass system as shown in Figure 3.1(a). The dynamic equation of motion for the complete structure is shown as Equation 2.1 in Chapter 2.

Without loss of generality, considering the complete structure divided into three parts such as the substructure I (the lower DOFs), the substructure II (the middle DOFs) and the substructure III (the upper DOFs), as shown in Figure 3.1(b), the dynamic equation of motion (Equation 2.1) can be written in the following partition form:

$$\begin{bmatrix} \boldsymbol{M}_{l,l} & & & & 0 \\ & m_i & & & \\ & & \boldsymbol{M}_{m,m} & & \\ & & & m_j & \\ 0 & & & & \boldsymbol{M}_{u,u} \end{bmatrix} \begin{Bmatrix} \ddot{\boldsymbol{y}}_l \\ \ddot{y}_i \\ \ddot{\boldsymbol{y}}_m \\ \ddot{y}_j \\ \ddot{\boldsymbol{y}}_u \end{Bmatrix}$$

$$+ \begin{bmatrix} \boldsymbol{C}_{l,l} & \boldsymbol{C}_{l,i} & & & 0 \\ \boldsymbol{C}_{i,l} & c_i + c_{i+1} & \boldsymbol{C}_{i,m} & & \\ & \boldsymbol{C}_{m,i} & \boldsymbol{C}_{m,m} & \boldsymbol{C}_{m,j} & \\ & & \boldsymbol{C}_{j,m} & c_j + c_{j+1} & \boldsymbol{C}_{j,u} \\ 0 & & & \boldsymbol{C}_{u,j} & \boldsymbol{C}_{u,u} \end{bmatrix} \begin{Bmatrix} \dot{\boldsymbol{y}}_l \\ \dot{y}_i \\ \dot{\boldsymbol{y}}_m \\ \dot{y}_j \\ \dot{\boldsymbol{y}}_u \end{Bmatrix}$$

$$+ \begin{bmatrix} \boldsymbol{K}_{l,l} & \boldsymbol{K}_{l,i} & & & 0 \\ \boldsymbol{K}_{i,l} & k_i + k_{i+1} & \boldsymbol{K}_{i,m} & & \\ & \boldsymbol{K}_{m,i} & \boldsymbol{K}_{m,m} & \boldsymbol{K}_{m,j} & \\ & & \boldsymbol{K}_{j,m} & k_j + k_{j+1} & \boldsymbol{K}_{j,u} \\ 0 & & & \boldsymbol{K}_{u,j} & \boldsymbol{K}_{u,u} \end{bmatrix} \begin{Bmatrix} \boldsymbol{y}_l \\ y_i \\ \boldsymbol{y}_m \\ y_j \\ \boldsymbol{y}_u \end{Bmatrix} =$$

$$- \begin{bmatrix} \boldsymbol{M}_{l,l} & & & & 0 \\ & m_i & & & \\ & & \boldsymbol{M}_{m,m} & & \\ & & & m_j & \\ 0 & & & & \boldsymbol{M}_{u,u} \end{bmatrix} \begin{Bmatrix} \boldsymbol{r}_l \\ 1 \\ \boldsymbol{r}_m \\ 1 \\ \boldsymbol{r}_u \end{Bmatrix} \ddot{z}_{\mathrm{g}} \qquad (3.1)$$

where the subscripts, *l*, *m* and *u*, denote inner DOFs of the divided substructures corresponding to the lower, the middle and the upper parts. And the subscripts, *i* and *j*, denote interface DOFs of the substructures.

Extracting the row *m* from Equation 3.1 and moving the interaction force between the interface and the middle substructure to the right-hand side, the dynamic equations of motion for the middle substructure can be rewritten as follows:

$$\boldsymbol{M}_{m,m}\ddot{\boldsymbol{y}}_m(t) + \boldsymbol{C}_{m,m}\dot{\boldsymbol{y}}_m(t) + \boldsymbol{K}_{m,m}\boldsymbol{y}_m(t) =$$

$$-\boldsymbol{M}_{m,m}\boldsymbol{r}_m\ddot{z}_g(t) - \boldsymbol{C}_{m,i}\dot{y}_i(t) - \boldsymbol{C}_{m,j}\dot{y}_j(t) - \boldsymbol{K}_{m,i}y_i(t) - \boldsymbol{K}_{m,j}y_j(t) \qquad (3.2)$$

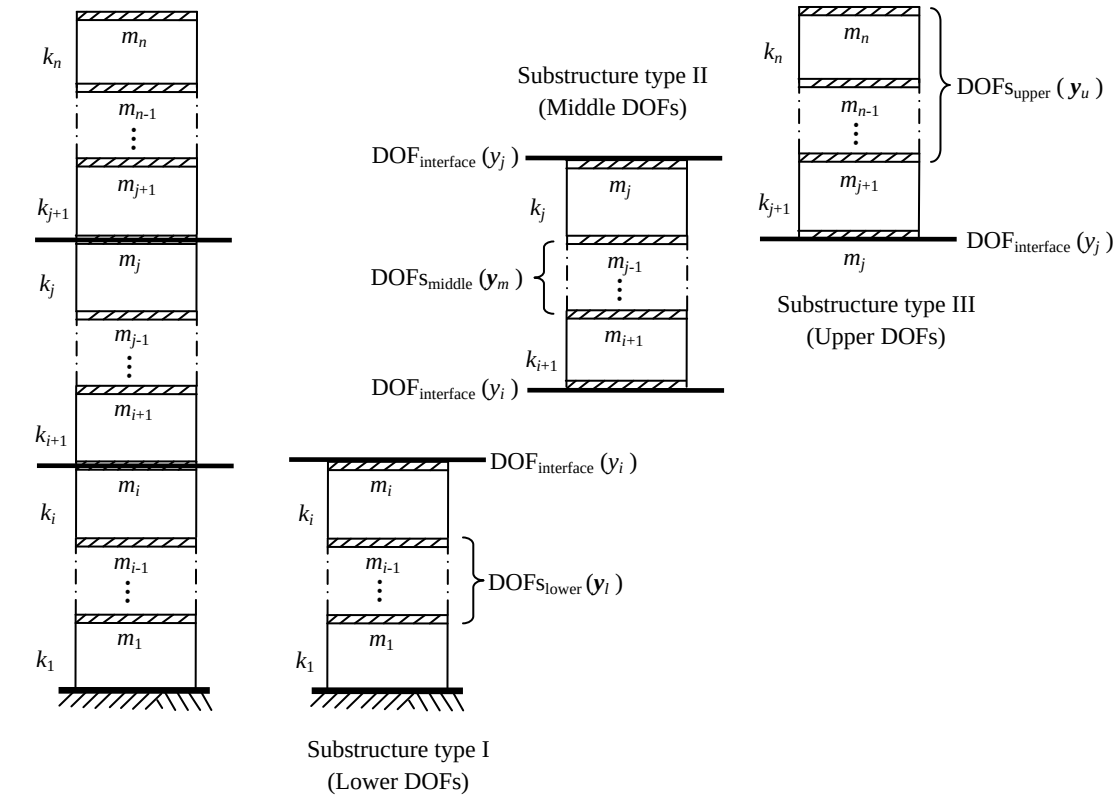

Figure 3.1. Complete and sub-structural dynamic system

From the terms in the right-hand side, it can be found that the interaction effects at the interface ends can be treated as "input" so the new input to the substructure includes two parts: the system input and the interface force input. And the computation of the interface force input requires the measurements of velocities and displacements at the interface DOFs. However, in reality it is usually much easier and preferred to measure accelerations (by accelerometers) than velocities and displacements. Therefore, for practicability, to eliminate the requirement of velocities and displacements, the idea of "quasi-static displacement" vector proposed by Koh et al. (2003) is adopted. The displacement relative to the ground DOF is split into a quasi-static displacement term, $\boldsymbol{y}_m^s(t)$, and a displacement term relative to the interface ends, $\boldsymbol{y}_m^r(t)$, i.e.

$$\boldsymbol{y}_m(t) = \boldsymbol{y}_m^s(t) + \boldsymbol{y}_m^r(t) \tag{3.3}$$

The former term can be obtained by solving Equation 3.2 while ignoring all time-derivative terms and the dynamic excitation:

$$\boldsymbol{y}_m^s(t) = -\boldsymbol{K}_{m,m}^{-1}\boldsymbol{K}_{m,i}y_i(t) - \boldsymbol{K}_{m,m}^{-1}\boldsymbol{K}_{m,j}y_j(t) \tag{3.4}$$

Substituting Equations 3.3 and 3.4 into Equation 3.2 leads to the dynamic equations of motion for the middle substructure:

$$\boldsymbol{M}_{m,m}\ddot{\boldsymbol{y}}_m^r(t) + \boldsymbol{C}_{m,m}\dot{\boldsymbol{y}}_m^r(t) + \boldsymbol{K}_{m,m}\boldsymbol{y}_m^r(t) = -\boldsymbol{M}_{m,m}\boldsymbol{r}_m\ddot{z}_g(t) + \boldsymbol{M}_{m,m}\boldsymbol{K}_{m,m}^{-1}\boldsymbol{K}_{m,i}\ddot{y}_i(t) +$$

$$\boldsymbol{M}_{m,m}\boldsymbol{K}_{m,m}^{-1}\boldsymbol{K}_{m,j}\ddot{y}_j(t) - \left(\boldsymbol{C}_{m,i} - \boldsymbol{C}_{m,m}\boldsymbol{K}_{m,m}^{-1}\boldsymbol{K}_{m,i}\right)\dot{y}_i(t) - (\boldsymbol{C}_{m,j} - \boldsymbol{C}_{m,m}\boldsymbol{K}_{m,m}^{-1}\boldsymbol{K}_{m,j})\dot{y}_j(t) \tag{3.5}$$

Similarly for the lower and upper substructures, the dynamic equations of motion can be obtained as follows:

$$\boldsymbol{M}_{l,l}\ddot{\boldsymbol{y}}_l^r(t) + \boldsymbol{C}_{l,l}\dot{\boldsymbol{y}}_l^r(t) + \boldsymbol{K}_{l,l}\boldsymbol{y}_l^r(t) =$$

$$-\boldsymbol{M}_{l,l}\boldsymbol{r}_l\ddot{z}_g(t) + \boldsymbol{M}_{l,l}\boldsymbol{K}_{l,l}^{-1}\boldsymbol{K}_{l,i}\ddot{y}_i(t) - (\boldsymbol{C}_{l,i} - \boldsymbol{C}_{l,l}\boldsymbol{K}_{l,l}^{-1}\boldsymbol{K}_{l,i})\dot{y}_i(t) \tag{3.6}$$

$$\boldsymbol{M}_{u,u}\ddot{\boldsymbol{y}}_u^r(t) + \boldsymbol{C}_{u,u}\dot{\boldsymbol{y}}_u^r(t) + \boldsymbol{K}_{u,u}\boldsymbol{y}_u^r(t) =$$

$$-\boldsymbol{M}_{u,u}\boldsymbol{r}_u\ddot{z}_g(t) + \boldsymbol{M}_{u,u}\boldsymbol{K}_{u,u}^{-1}\boldsymbol{K}_{u,j}\ddot{y}_j(t) - (\boldsymbol{C}_{u,j} - \boldsymbol{C}_{u,u}\boldsymbol{K}_{u,u}^{-1}\boldsymbol{K}_{u,j})\dot{y}_j(t) \tag{3.7}$$

where the dynamic response terms with the superscript *r*, $\boldsymbol{y}^r$, $\dot{\boldsymbol{y}}^r$ and $\ddot{\boldsymbol{y}}^r$, denote the dynamic responses relative to the interface ends. The subscripts, *m*, *l* and *u*, denote the DOFs corresponding to the middle, the lower and the upper substructure.

Since damping force is usually much smaller compared to inertia force in typical civil engineering structures, the velocity-dependent components in the interface motion forces are assumed to be negligible (Koh et al. 2003). Hence, Equations 3.5 to 3.7 can be simplified as following:

$$\boldsymbol{M}_{m,m}\ddot{\boldsymbol{y}}_m^r(t) + \boldsymbol{C}_{m,m}\dot{\boldsymbol{y}}_m^r(t) + \boldsymbol{K}_{m,m}\boldsymbol{y}_m^r(t) = \boldsymbol{L}_m\boldsymbol{u}_m(t) \tag{3.8}$$

$$\boldsymbol{M}_{l,l}\ddot{\boldsymbol{y}}_l^r(t) + \boldsymbol{C}_{l,l}\dot{\boldsymbol{y}}_l^r(t) + \boldsymbol{K}_{l,l}\boldsymbol{y}_l^r(t) = \boldsymbol{L}_l\boldsymbol{u}_l(t) \tag{3.9}$$

$$\boldsymbol{M}_{u,u}\ddot{\boldsymbol{y}}_u^r(t) + \boldsymbol{C}_{u,u}\dot{\boldsymbol{y}}_u^r(t) + \boldsymbol{K}_{u,u}\boldsymbol{y}_u^r(t) = \boldsymbol{L}_u\boldsymbol{u}_u(t) \tag{3.10}$$

where $\boldsymbol{u}_m(t)$, $\boldsymbol{u}_l(t)$ and $\boldsymbol{u}_u(t)$ are the input vectors for the middle, lower and upper substructures, respectively, and $\boldsymbol{u}_m(t) = [\ddot{z}_{\mathrm{g}}(t) \;\; \ddot{y}_i(t) \;\; \ddot{y}_j(t)]^{\mathrm{T}}$, $\boldsymbol{u}_l(t) = [\ddot{z}_{\mathrm{g}}(t) \;\; \ddot{y}_i(t)]^{\mathrm{T}}$, $\boldsymbol{u}_u(t) = [\ddot{z}_{\mathrm{g}}(t) \;\; \ddot{y}_j(t)]^{\mathrm{T}}$, it can be seen that there are 3 inputs for the middle substructure and 2 inputs for the lower and upper substructures; $\boldsymbol{L}_m$, $\boldsymbol{L}_l$ and $\boldsymbol{L}_u$ are the input coefficient matrices for the middle, lower and upper substructures, respectively, and $\boldsymbol{L}_m = [-\boldsymbol{M}_{m,m}\boldsymbol{r}_m \quad \boldsymbol{M}_{m,m}\boldsymbol{K}_{m,m}^{-1}\boldsymbol{K}_{m,i} \quad \boldsymbol{M}_{m,m}\boldsymbol{K}_{m,m}^{-1}\boldsymbol{K}_{m,j}]$, $\boldsymbol{L}_l = [-\boldsymbol{M}_{l,l}\boldsymbol{r}_l \quad \boldsymbol{M}_{l,l}\boldsymbol{K}_{l,l}^{-1}\boldsymbol{K}_{l,i}]$, $\boldsymbol{L}_u = [-\boldsymbol{M}_{u,u}\boldsymbol{r}_u \quad \boldsymbol{M}_{u,u}\boldsymbol{K}_{u,u}^{-1}\boldsymbol{K}_{u,j}]$.

Equations 3.8 to 3.10 show that the equations of motion for the middle, lower and upper substructures take the same form as following:

$$\boldsymbol{M}_{s,s}\ddot{\boldsymbol{y}}_s^r(t) + \boldsymbol{C}_{s,s}\dot{\boldsymbol{y}}_s^r(t) + \boldsymbol{K}_{s,s}\boldsymbol{y}_s^r(t) = \boldsymbol{L}_s\boldsymbol{u}_s(t) \tag{3.11}$$

where the subscript *s* can be replaced with *m*, *l* and *u*, denoting all the three types of substructures.

Equation 3.11 can be rewritten as

$$\ddot{\boldsymbol{y}}_s^r(t) + \widetilde{\boldsymbol{C}}_{s,s}\dot{\boldsymbol{y}}_s^r(t) + \widetilde{\boldsymbol{K}}_{s,s}\boldsymbol{y}_s^r(t) = \tilde{\boldsymbol{L}}_s\boldsymbol{u}_s(t) \tag{3.12}$$

where $\widetilde{\boldsymbol{C}}_{s,s} = \boldsymbol{M}_{s,s}^{-1}\boldsymbol{C}_{s,s}$, $\widetilde{\boldsymbol{K}}_{s,s} = \boldsymbol{M}_{s,s}^{-1}\boldsymbol{K}_{s,s}$, and $\tilde{\boldsymbol{L}}_s = \boldsymbol{M}_{s,s}^{-1}\boldsymbol{L}_s$.

The knowledge of dynamics tells us that the mass normalized stiffness $\widetilde{\boldsymbol{K}}_{s,s}$ can be expressed as $\boldsymbol{\Phi}_s\boldsymbol{\Lambda}_s\boldsymbol{\Phi}_s^{\mathrm{T}}$, where $\boldsymbol{\Phi}_s$ and $\boldsymbol{\Lambda}_s$ are the mass normalized mode shape and natural (circular) frequency matrices for the corresponding substructure, respectively. Lu and Gao (2005) proves that Equation 3.12 can be written in terms of ARX model as following:

$$\hat{\boldsymbol{y}}_s^r(t) = \sum_{i=1}^{2} \boldsymbol{A}_i\, \boldsymbol{y}_s^r(t-i) + \sum_{j=1}^{3} \boldsymbol{B}_j\, \boldsymbol{u}_s(t-j) \tag{3.13}$$

where $\hat{\boldsymbol{y}}_s^r(t)$ is the predicted signal, $\boldsymbol{A}_1 = 2\boldsymbol{\Phi}_s cos\,(\boldsymbol{\Lambda}_s^{\frac{1}{2}}\Delta t)\boldsymbol{\Phi}_s^{\mathrm{T}}$, $\boldsymbol{A}_2 = -\boldsymbol{I}$, $\boldsymbol{B}_1 = \tilde{\boldsymbol{L}}_s$, $\boldsymbol{B}_2 = -\boldsymbol{\Phi}_s[\boldsymbol{I} + cos\,(\boldsymbol{\Lambda}_s^{\frac{1}{2}}\Delta t)]\boldsymbol{\Phi}_s^{\mathrm{T}}\tilde{\boldsymbol{L}}_s$, and $\boldsymbol{B}_3 = \boldsymbol{\Phi}_s cos\,(\boldsymbol{\Lambda}_s^{\frac{1}{2}}\Delta t)\boldsymbol{\Phi}_s^{\mathrm{T}}\tilde{\boldsymbol{L}}_s$ with Δt being the sampling period of the dynamic response measurement and $\boldsymbol{I}$ being the identity matrix.

Obviously, the ARX model coefficients are governed by the structural parameters (i.e., mass, stiffness etc.) as shown by Lu and Gao (2005). Hence any sorts of deterioration in structural properties will lead to a change in the ARX model coefficients. Now, let us consider a shear structure which has undergone some damage. Thus, the first AR model coefficient matrices corresponding to the undamaged and damaged states can be termed as $\boldsymbol{A}_1^u$ and $\boldsymbol{A}_1^d$, respectively.

We have $\tilde{\boldsymbol{K}}_{s,s} = \boldsymbol{\Phi}_s\boldsymbol{\Lambda}_s\boldsymbol{\Phi}_s^T = \boldsymbol{\Phi}_s\boldsymbol{\Lambda}_s^{\frac{1}{2}}\boldsymbol{\Lambda}_s^{\frac{1}{2}}\boldsymbol{\Phi}_s^T = \boldsymbol{\Phi}_s\boldsymbol{\Lambda}_s^{\frac{1}{2}}\boldsymbol{\Phi}_s^T\boldsymbol{\Phi}_s\boldsymbol{\Lambda}_s^{\frac{1}{2}}\boldsymbol{\Phi}_s^T = (\boldsymbol{\Phi}_s\boldsymbol{\Lambda}_s^{\frac{1}{2}}\boldsymbol{\Phi}_s^T)^2$. It follows that $\boldsymbol{\Phi}_s\boldsymbol{\Lambda}_s^{\frac{1}{2}}\boldsymbol{\Phi}_s^T = \tilde{\boldsymbol{K}}_{s,s}^{\frac{1}{2}}$. Now the first AR model coefficient matrix can be expressed as follows:

$$\boldsymbol{A}_1 = 2\boldsymbol{\Phi}_s cos\,(\boldsymbol{\Lambda}_s^{\frac{1}{2}}\Delta t)\boldsymbol{\Phi}_s^{\mathrm{T}} = 2\,cos\left(\tilde{\boldsymbol{K}}_{s,s}^{\frac{1}{2}}\Delta t\right)$$

$$= 2\boldsymbol{I} - \frac{2}{2!}\tilde{\boldsymbol{K}}_{s,s}\Delta t^2 + \frac{2}{4!}\tilde{\boldsymbol{K}}_{s,s}^2\Delta t^4 - \frac{2}{6!}\tilde{\boldsymbol{K}}_{s,s}^3\Delta t^6 + \cdots\cdots\infty \tag{3.14}$$

Thus the change in the first AR model coefficient matrix from the undamaged state to the damaged state can be expressed as

$$\Delta\boldsymbol{A}_1 = \boldsymbol{A}_1^d - \boldsymbol{A}_1^u$$

$$= -\frac{2}{2!}(\tilde{\boldsymbol{K}}_{s,s}^d - \tilde{\boldsymbol{K}}_{s,s}^u)\Delta t^2 + \frac{2}{4!}[(\tilde{\boldsymbol{K}}_{s,s}^d)^2 - (\tilde{\boldsymbol{K}}_{s,s}^u)^2]\Delta t^4 - \frac{2}{6!}[(\tilde{\boldsymbol{K}}_{s,s}^d)^3 - (\tilde{\boldsymbol{K}}_{s,s}^u)^3]\Delta t^6 + \cdots\cdots\infty$$

$$= \sum_{p=1}^{\infty}(-1)^p\frac{2}{(2p)!}[(\tilde{\boldsymbol{K}}_{s,s}^d)^p - (\tilde{\boldsymbol{K}}_{s,s}^u)^p]\Delta t^{2p} \tag{3.15}$$

Now, assuming that the damage occurred on the f[th] story of the shear structure building, it can be simulated as a stiffness reduction of that story by an amount of δk_f from its original stiffness, k_f. Considering the damaged story locating in three different substructures, the modified stiffness matrix of the damaged substructure takes the forms in three different cases as following:

1) $1 \leqslant f \leqslant i$, in case of damaged story in lower substructure

$$\widetilde{\boldsymbol{K}}_{l,l}^{d} = \begin{bmatrix} k_1 + k_2 & -k_2 & & & & & & & & 0 \\ -k_2 & k_2 + k_3 & -k_3 & & & & & & & \\ & \ddots & \ddots & \ddots & & & & & & \\ & & -k_{f-1} & k_{f-1} + (k_f - \delta k_f) & -(k_f - \delta k_f) & & & & & \\ & & & -(k_f - \delta k_f) & (k_f - \delta k_f) + k_{f+1} & -k_{f+1} & & & & \\ & & & & \ddots & \ddots & \ddots & & & \\ & & & & & -k_{i-2} & k_{i-2} + k_{i-1} & -k_{i-1} & & \\ & & & & & & -k_{i-1} & k_{i-1} + k_i & & \\ 0 & & & & & & & & & \end{bmatrix} \tag{3.16}$$

2) $i+1 \leqslant f \leqslant j$, in case of damaged story in middle substructure

$$\widetilde{\boldsymbol{K}}_{m,m}^{d} = \begin{bmatrix} k_{i+1} + k_{i+2} & -k_{i+2} & & & & & & & & 0 \\ -k_{i+2} & k_{i+2} + k_{i+3} & -k_{i+3} & & & & & & & \\ & \ddots & \ddots & \ddots & & & & & & \\ & & -k_{f-1} & k_{f-1} + (k_f - \delta k_f) & -(k_f - \delta k_f) & & & & & \\ & & & -(k_f - \delta k_f) & (k_f - \delta k_f) + k_{f+1} & -k_{f+1} & & & & \\ & & & & \ddots & \ddots & \ddots & & & \\ & & & & & -k_{j-2} & k_{j-2} + k_{j-1} & -k_{j-1} & & \\ & & & & & & -k_{j-1} & k_{j-1} + k_j & & \\ 0 & & & & & & & & & \end{bmatrix} \tag{3.17}$$

3) $j+1 \leqslant f \leqslant n$, in case of damaged story in upper substructure

$$\widetilde{\boldsymbol{K}}_{u,u}^{d} = \begin{bmatrix} k_{j+1} + k_{j+2} & -k_{j+2} & & & & & & & & 0 \\ -k_{j+2} & k_{j+2} + k_{j+3} & -k_{j+3} & & & & & & & \\ & \ddots & \ddots & \ddots & & & & & & \\ & & -k_{f-1} & k_{f-1} + (k_f - \delta k_f) & -(k_f - \delta k_f) & & & & & \\ & & & -(k_f - \delta k_f) & (k_f - \delta k_f) + k_{f+1} & -k_{f+1} & & & & \\ & & & & \ddots & \ddots & \ddots & & & \\ & & & & & -k_{n-1} & k_{n-1} + k_n & -k_n & & \\ & & & & & & -k_n & k_n & & \\ 0 & & & & & & & & & \end{bmatrix} \tag{3.18}$$

In a uniform way, the stiffness matrix of the damaged substructure in all three cases above can be expressed as, $\widetilde{\boldsymbol{K}}_{s,s}^{d} = \widetilde{\boldsymbol{K}}_{s,s}^{u} + \Delta \boldsymbol{K}_f$ with $\Delta \boldsymbol{K}_f = \boldsymbol{I}_f \delta k_f$, and $\boldsymbol{I}_f$ can be written in matrix form in three different cases as following:

1) in case of damaged story nonadjacent to the interface end

$$\boldsymbol{I}_f = \begin{bmatrix} 0 & 0 & & & & & & 0 \\ 0 & 0 & 0 & & & & & \\ & \ddots & \ddots & \ddots & & & & \\ & & 0 & -1 & 1 & & & \\ & & & 1 & -1 & 0 & & \\ & & & & \ddots & \ddots & \ddots & \\ & & & & & 0 & 0 & 0 \\ 0 & & & & & & 0 & 0 \end{bmatrix} \tag{3.19}$$

2) in case of damaged story adjacent to the bottom interface end

$$\boldsymbol{I}_f = \begin{bmatrix} -1 & 0 & & & & & & 0 \\ 0 & 0 & 0 & & & & & \\ & \ddots & \ddots & \ddots & & & & \\ & & 0 & 0 & 0 & & & \\ & & & 0 & 0 & 0 & & \\ & & & & \ddots & \ddots & \ddots & \\ & & & & & 0 & 0 & 0 \\ 0 & & & & & & 0 & 0 \end{bmatrix} \tag{3.20}$$

3) in case of damaged story adjacent to the top interface end

$$\boldsymbol{I}_f = \begin{bmatrix} 0 & 0 & & & & & & 0 \\ 0 & 0 & 0 & & & & & \\ & \ddots & \ddots & \ddots & & & & \\ & & 0 & 0 & 0 & & & \\ & & & 0 & 0 & 0 & & \\ & & & & \ddots & \ddots & \ddots & \\ & & & & & 0 & 0 & 0 \\ 0 & & & & & & 0 & -1 \end{bmatrix} \tag{3.21}$$

By representing $\widetilde{\boldsymbol{K}}_{s,s}^{d}$ with $\widetilde{\boldsymbol{K}}_{s,s}^{u}$, $\boldsymbol{I}_f$ and δk_f, the term $[(\widetilde{\boldsymbol{K}}_{s,s}^{d})^p - (\widetilde{\boldsymbol{K}}_{s,s}^{u})^p]$ of Equation 3.15 can be rewritten as follows:

$$(\widetilde{\boldsymbol{K}}_{s,s}^{d})^p - (\widetilde{\boldsymbol{K}}_{s,s}^{u})^p = (\widetilde{\boldsymbol{K}}_{s,s}^{u} + \boldsymbol{I}_f \delta k_f)^p - (\widetilde{\boldsymbol{K}}_{s,s}^{u})^p = \sum_{q=1}^{\infty} C_q^p [(\widetilde{\boldsymbol{K}}_{s,s}^{u})^{-1} \boldsymbol{I}_f]^q \left(\widetilde{\boldsymbol{K}}_{s,s}^{u}\right)^q (\delta k_f)^q \tag{3.22}$$

where C_q^p denotes the usual binomial coefficient and $C_q^p = \frac{p!}{q!(p-q)!}$.

Substituting Equation 3.22 into Equation 3.15 leads to:

$$\Delta \boldsymbol{A}_1 = \sum_{p=1}^{\infty}(-1)^p \frac{2}{(2p)!}\sum_{q=1}^{\infty} C_q^p [(\widetilde{\boldsymbol{K}}_{s,s}^u)^{-1}\boldsymbol{I}_f]^q \left(\widetilde{\boldsymbol{K}}_{s,s}^u\right)^q (\delta k_f)^q \Delta t^{2p} \quad (3.23)$$

For small value of story stiffness degradation on the f[th] story (δk_f), the higher order terms of δk_f can be neglected, i.e., only the term with q=1 is retained leading Equation 3.23 into the following form:

$$\Delta \boldsymbol{A}_1 = \sum_{p=1}^{\infty}(-1)^p \frac{2}{(2p)!} p(\widetilde{\boldsymbol{K}}_{s,s}^u)^{-1}\boldsymbol{I}_f \widetilde{\boldsymbol{K}}_{s,s}^u \delta k_f \Delta t^{2p} \quad (3.24)$$

Similarly, for small time step, Δt^{2p} turns to be negligible as p increases. Thus, only the term with p=1 is kept and one can write:

$$\Delta \boldsymbol{A}_1 = -(\widetilde{\boldsymbol{K}}_{s,s}^u)^{-1}\boldsymbol{I}_f \widetilde{\boldsymbol{K}}_{s,s}^u \Delta t^2 \delta k_f \quad (3.25)$$

Utilizing the expressions of $\boldsymbol{I}_f$ in Equations 3.19 to 3.21, the change in the first AR model coefficient matrix from the undamaged state to the damaged state can be expressed in matrix form in three different cases as following:

1) in case of damaged story nonadjacent to the interface end

$$\Delta \boldsymbol{A}_1 = \begin{bmatrix} 0 & 0 & & & & & & & 0 \\ 0 & 0 & 0 & & & & & & \\ & \ddots & \ddots & \ddots & & & & & \\ & & 0 & \Delta t^2 \delta k_f & -\Delta t^2 \delta k_f & & & & \\ & & & -\Delta t^2 \delta k_f & \Delta t^2 \delta k_f & 0 & & & \\ & & & & \ddots & \ddots & \ddots & & \\ & & & & & 0 & 0 & 0 & \\ 0 & & & & & & 0 & 0 & \end{bmatrix} \quad (3.26)$$

2) in case of damaged story adjacent to the bottom interface end

$$\Delta \boldsymbol{A}_1 = \begin{bmatrix} \Delta t^2 \delta k_f & 0 & & & & & & & 0 \\ 0 & 0 & 0 & & & & & & \\ & \ddots & \ddots & \ddots & & & & & \\ & & 0 & 0 & 0 & & & & \\ & & & 0 & 0 & 0 & & & \\ & & & & \ddots & \ddots & \ddots & & \\ & & & & & 0 & 0 & 0 & \\ 0 & & & & & & 0 & 0 & \end{bmatrix} \quad (3.27)$$

3) in case of damaged story adjacent to the top interface end

$$\Delta \boldsymbol{A}_1 = \begin{bmatrix} 0 & 0 & & & & & & 0 \\ 0 & 0 & 0 & & & & & \\ & \ddots & \ddots & \ddots & & & & \\ & & 0 & 0 & 0 & & & \\ & & & 0 & 0 & 0 & & \\ & & & & \ddots & \ddots & \ddots & \\ & & & & & 0 & 0 & 0 \\ 0 & & & & & & 0 & \Delta t^2 \delta k_f \end{bmatrix} \tag{3.28}$$

Equations 3.26 to 3.28 show that the absolute value of $\Delta \boldsymbol{A}_1$ will be a null matrix with four non-zero terms at element locations corresponding to the output DOFs (f-1, f-1), (f-1, f), (f, f-1) and (f, f) in case of damaged story nonadjacent to the interface end; with one non-zero term at element location corresponding to the output DOF (f, f) in case of damaged story adjacent to the bottom interface end; and with one non-zero term at element location corresponding to the output DOF (f-1, f-1) in case of damaged story adjacent to the top interface end. This information depicts the damage location on the f^{th} story. Additionally, the absolute value of the non-zero term of $\Delta \boldsymbol{A}_1$ is directly proportional to the story stiffness degradation. Thus, the damage can be localized and quantified by identifying these four (or one) high-valued elements in the matrix, $\Delta \boldsymbol{A}_1$. Therefore, the changes in the first AR model coefficient matrix can be used as a damage indicator for the proposed substructural damage identification approach. For the sake of simplicity, the changes in the first AR model coefficient matrix is abbreviated as CFAR hereafter.

3.3 Performance Verification by Simulation

A simulation of a 12-story shear building model was performed to show the feasibility of the proposed scheme for damage identification. The building is simplified into a 12-DOF lumped mass structural system as shown in Figure 3.2.

The mass of every floor and the lateral stiffness were assumed to be 100 kg and 1 MN/m, respectively. The damping ratio of all modes was chosen as 3%. The first three undamaged natural frequencies of the structure were calculated as 2.0, 6.0, and 9.8 Hz for the 1st, 2nd, and 3rd modes, respectively. The 12-DOF system was simulated to be subjected to white noise excitation, and the noise contributing to 5% of the signal RMS value was added to the acceleration responses of the structure. The acceleration responses at different DOFs were recorded for 50 seconds with a sampling frequency of 200 Hz. The story stiffness reduction was regarded to be damage to the structure. Twelve damage cases (damage in each story from the 1st story through the 12th story) with five different damage severities (10%, 20%, 30%, 40%, and 50% lateral stiffness reduction) were studied. Hence, there were 60 different damage scenarios in total.

Firstly, according to the substructure division method described in section 3.2, the whole structure was divided into 3 substructures, as shown in Figure 3.3.

Considering strong flexibility for handling the disturbance modeling, the autoregressive moving average with exogenous inputs (ARMAX) model was adopted to model each substructure and further obtain the AR coefficient matrix for the undamaged and unknown states. According to Equation 3.13 and the expression of the input vector $\boldsymbol{u}_l(t)$, Substructure I can be modeled as a 2-input 3-output ARMAX model. The ground acceleration ($\ddot{z}_g$), and the acceleration of the 4th DOF relative to the ground ($\ddot{y}_4$) were used as the inputs, and the relative acceleration of the 1st, 2nd and 3rd DOF to the 4th DOF ($\ddot{y}_1^r$, $\ddot{y}_2^r$ and $\ddot{y}_3^r$) were used as the outputs.

Similarly, Substructure II can be modeled as a 3-input 4-output ARMAX model. The ground acceleration ($\ddot{z}_g$), the acceleration of the 4th and 9th DOF relative to the ground ($\ddot{y}_4$ and $\ddot{y}_9$) were used as the inputs, and the relative acceleration of the 5th, 6th, 7th and 8th DOF to the 4th DOF ($\ddot{y}_5^r$, $\ddot{y}_6^r$, $\ddot{y}_7^r$, and $\ddot{y}_8^r$) were used as the outputs. Substructure III can be modeled as a 2-input 3-output ARMAX model. The ground

acceleration ($\ddot{z}_g$) and the acceleration of the 9th DOF relative to the ground ($\ddot{y}_9$) were used as the inputs, and the relative acceleration of the 10th, 11th, and 12th DOF to the 9th DOF ($\ddot{y}_{10}^r$, $\ddot{y}_{11}^r$, and $\ddot{y}_{12}^r$) were used as the outputs to construct the ARMAX model.

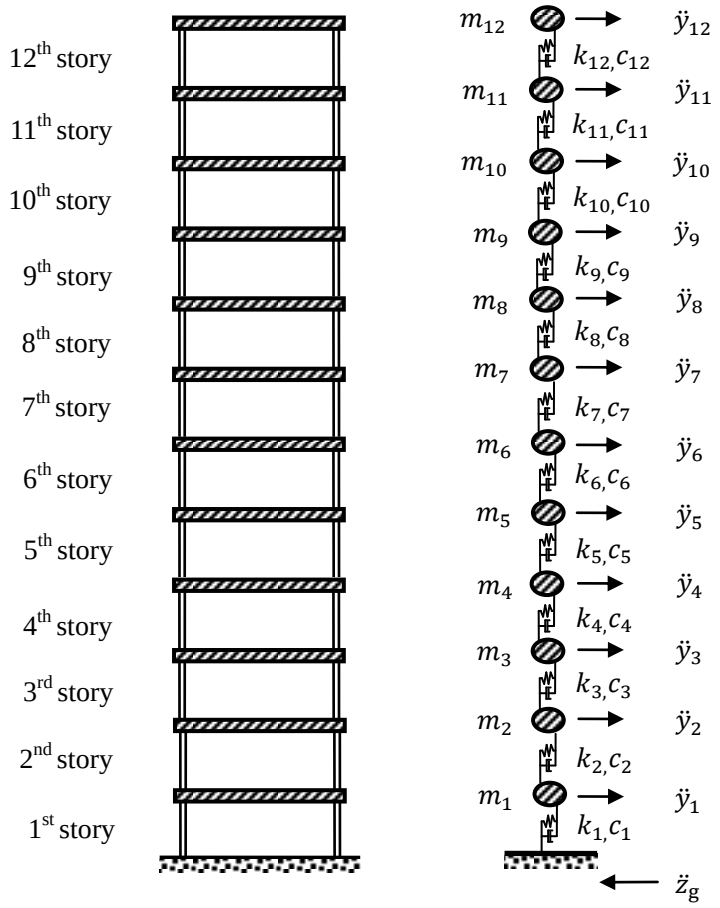

Figure 3.2. 12-story shear building

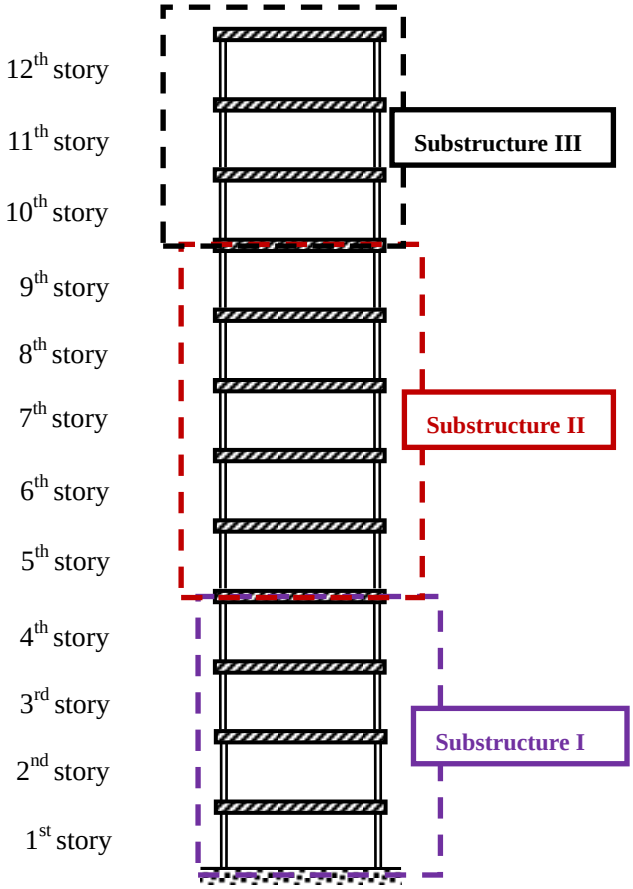

Figure 3.3. Structure division for 12-story shear building

The Burg's (maximum entropy) method (BM) was used to identify the ARMAX model coefficients from input-output data sets for each substructure and each damage scenario. The changes in the first AR model coefficient matrix (CFAR) from the undamaged state to the damaged states were estimated. Figure 3.4 shows a three-dimensional bar plot of the CFAR against output DOFs for Substructure II in the case of 10% damage occurring in 5^{th} story, 6^{th} story, 7^{th} story, 8^{th} story, and 9^{th} story, respectively. The absolute values of CFAR are listed in Table 3.1 for Substructure I in the case of 10% damage occurring in 1^{st} story, 2^{nd} story, 3^{rd} story, and 4^{th} story, respectively. The similar results for Substructure III are also listed in Table 3.2. The

double underlined values in Tables 3.1 and 3.2 mean the large values compared to the rest of the elements of CFAR. It can be observed from Figure 3.4, Tables 3.1 and 3.2 that the CFAR attains large values at the output DOFs next to the damaged location while the values in the rest of the positions are close to zero. Taking Substructure II as an example, the CFAR shows large value at the element (m_8, m_8) when damage taking place in 9^{th} story, and in the case of damage in 8^{th} story, large values of CFAR appear at two diagonal elements (m_8, m_8), (m_7, m_7) and two off-diagonal elements (m_7, m_8), (m_8, m_7). This is in good agreement with the theoretical conclusion that the elements of CFAR corresponding to the output DOFs adjacent to the damaged location are proportional to the stiffness reduction in the structure, as shown in Equations 3.25 to 3.28.

Figure 3.5 shows a three-dimensional bar plot of the CFAR against output DOFs for Substructure II in the case of 10%, 20%, 30%, 40%, and 50% damage occurring in 7^{th} story, respectively. In addition, Figure 3.6 shows a plot of peak value of CFAR with five different damage intensities for all the three substructures. It is revealed from Figures 3.5 and 3.6 that there is a linear relationship between the peak values of CFAR and the damage intensities. This is in perfect accordance with the conclusion drawn from Equations 3.25 to 3.28, which were deduced by ignoring the higher order terms. Thus, it is clearly reasonable that a first order approximation as derived earlier in Equations 3.25 to 3.28 is satisfactory to reveal the linear relationship between the peak values of CFAR and the damage intensities even in the case of a high intensity of damage. Therefore, one can draw a conclusion that the proposed substructural damage identification approach based on changes in the first AR Model coefficient matrix (CFAR) is able to detect both location and severity of damage for shear structure in the simulation.

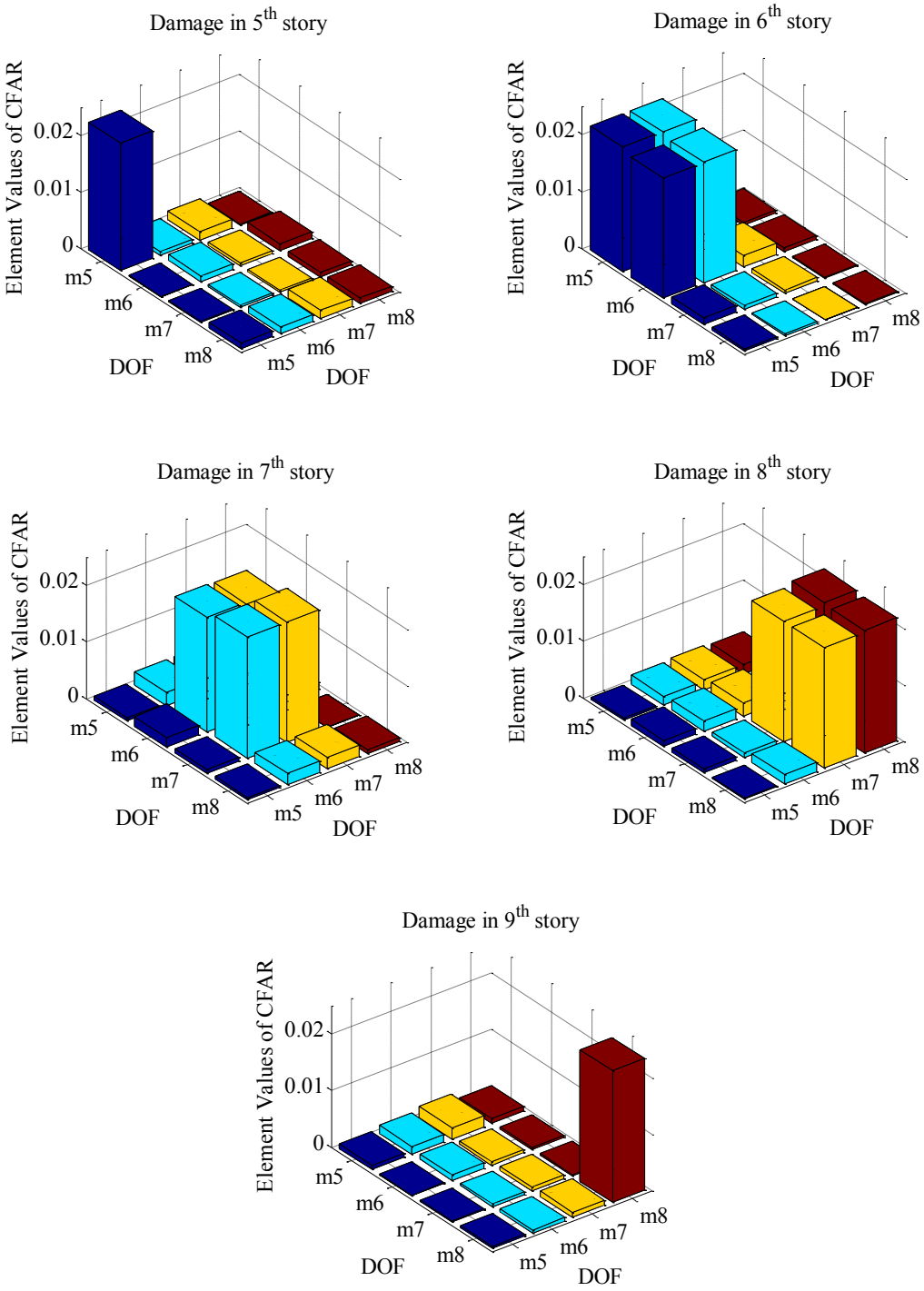

Figure 3.4. Changes in the first AR model coefficient matrix for Substructure II (10% damage)

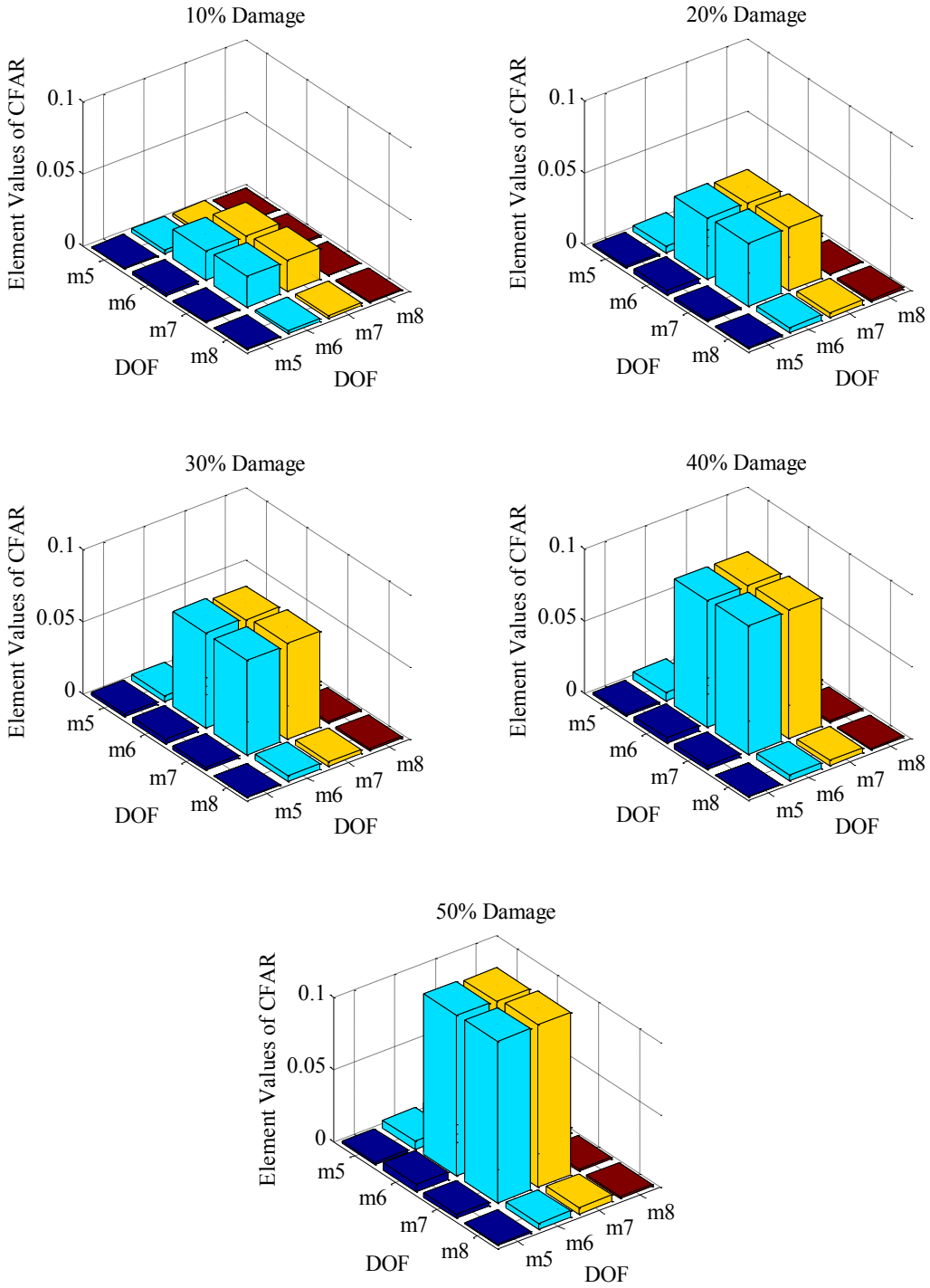

Figure 3.5. Changes in the first AR model coefficient matrix for Substructure II

(damage in 7th story)

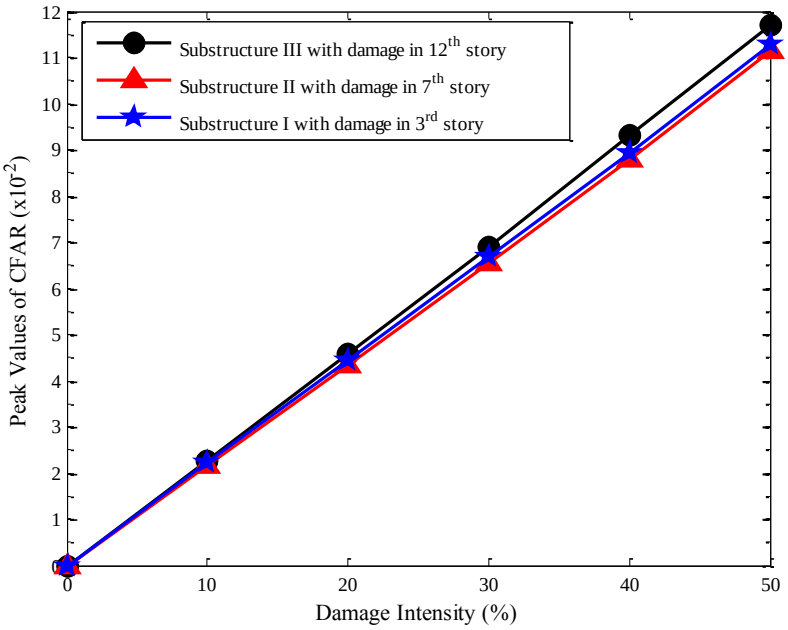

Figure 3.6. Linear relationship between CFAR and damage intensity

Table 3.1. Changes in the first AR model coefficient matrix for Substructure I (10% damage)

DOF	m_1	m_2	m_3
	Damage in 1st story		
m_1	0.0230	0.0004	0.0003
m_2	0.0010	0.0003	0.0001
m_3	0.0006	0.0003	0.0001
	Damage in 2nd story		
m_1	0.0228	0.0227	0.0008
m_2	0.0209	0.0207	0.0013
m_3	0.0004	0.0006	0.0012
	Damage in 3rd story		
m_1	0.0001	0.0004	0.0002
m_2	0.0016	0.0209	0.0210
m_3	0.0007	0.0218	0.0229
	Damage in 4th story		
m_1	0.0007	0.0001	0.0002
m_2	0.0006	0.0004	0.0011
m_3	0.0008	0.0015	0.0235

Table 3.2. Changes in the first AR model coefficient matrix for Substructure III (10% damage)

DOF	m_{10}	m_{11}	m_{12}
	Damage in 10th story		
m_{10}	0.0219	0.0006	0.0013
m_{11}	0.0004	0.0004	0.0005
m_{12}	0.0010	0.0001	0.0003
	Damage in 11th story		
m_{10}	0.0206	0.0209	0.0018
m_{11}	0.0224	0.0227	0.0003
m_{12}	0.0016	0.0015	0.0009
	Damage in 12th story		
m_{10}	0.0011	0.0012	0.0012
m_{11}	0.0003	0.0230	0.0220
m_{12}	0.0014	0.0222	0.0228

3.4 Experimental Verification

In this section, the measured data from a shake table experiment of a five-story frame structure was utilized to verify the performance of our proposed methodology. The experimental setup and procedure are the same as Section 2.6.

Then the similar procedures as the simulation cases were performed on the experimental measured data to detect both location and severity of damages in the test building model. First of all, following the substructure division rules described in section 3.2, the whole structure was divided into 2 substructures, as shown in Figure 3.7.

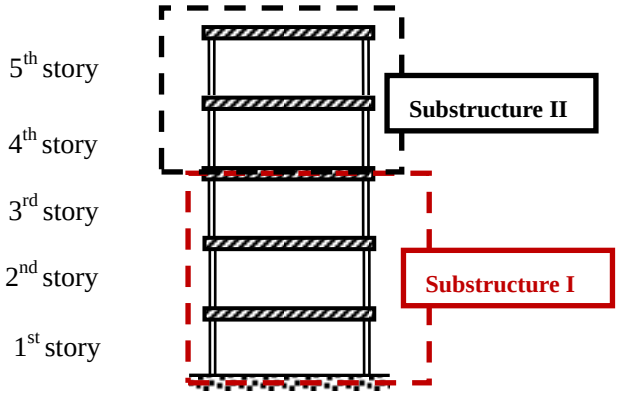

Figure 3.7. Structure division for 5-story experimental building model

According to Equation 3.13, Substructure I was modeled as a 2-input 2-output ARMAX model. The ground acceleration ($\ddot{z}_g$) and the acceleration of the 3rd DOF relative to the ground ($\ddot{y}_3$) were used as the inputs, and the relative acceleration of the 1st and 2nd DOF to the 3rd DOF ($\ddot{y}_1^r$ and $\ddot{y}_2^r$) were used as the outputs.

Similarly, Substructure II was also modeled as a 2-input 2-output ARMAX model. The ground acceleration ($\ddot{z}_g$) and the acceleration of the 3rd DOF relative to the ground ($\ddot{y}_3$) were used as the inputs, and the relative acceleration of the 4th and 5th DOF to the 3rd DOF ($\ddot{y}_4^r$ and $\ddot{y}_5^r$) were used as the outputs to construct the ARMAX model.

Next the changes in the first AR model coefficient matrix (CFAR) from the undamaged state to the damaged states were estimated to depict the damage existing in the experimental building model. As shown in Figure 3.8, the absolute values of CFAR are plotted against output DOFs in the form of a three-dimensional bar chart for Substructure I in the case of 10% damage occurring in 1st story, 2nd story and 3rd story, respectively. Table 3.3 provides the absolute values of CFAR for Substructure II with 10% damage in 4th story and 5th story, respectively, in which the large values are double underlined. From Figure 3.8 and Table 3.3, it can be observed that large CFAR values

are found at the output DOFs next to the damaged location, which is consistent with the previous theoretical derivation and the results of simulation verification.

Figure 3.9 presents the three-dimensional bar plot of the CFAR against output DOFs for Substructure I in the case of 10%, 20%, and 30% damage occurring in 1st story, respectively. And Figure 3.10 shows a plot of peak value of CFAR with three different damage intensities for Substructure I and II. One can also notice from Figures 3.9 and 3.10 that the peak values of CFAR increase linearly with the damage intensities. This is also in good agreement with the previous theoretical derivation and the results of simulation verification.

It is therefore clear that the proposed substructural damage identification approach based on changes in the first AR Model coefficient matrix (CFAR) can still successfully locate and quantify the damage when applied to the experimental data. After experimentally verifying and confirming the feasibility and robustness of the proposed methodology as discussed above, the conclusion can be drawn that it can obtain satisfactory damage identification results in both simulation and laboratory experiment.

Table 3.3. Changes in the first AR model coefficient matrix for Substructure II (10% damage)

DOF	m_4	m_5
	Damage in 4th story	
m_4	0.0162	0.0010
m_5	0.0029	0.0027
	Damage in 5th story	
m_4	0.0201	0.0158
m_5	0.0189	0.0188

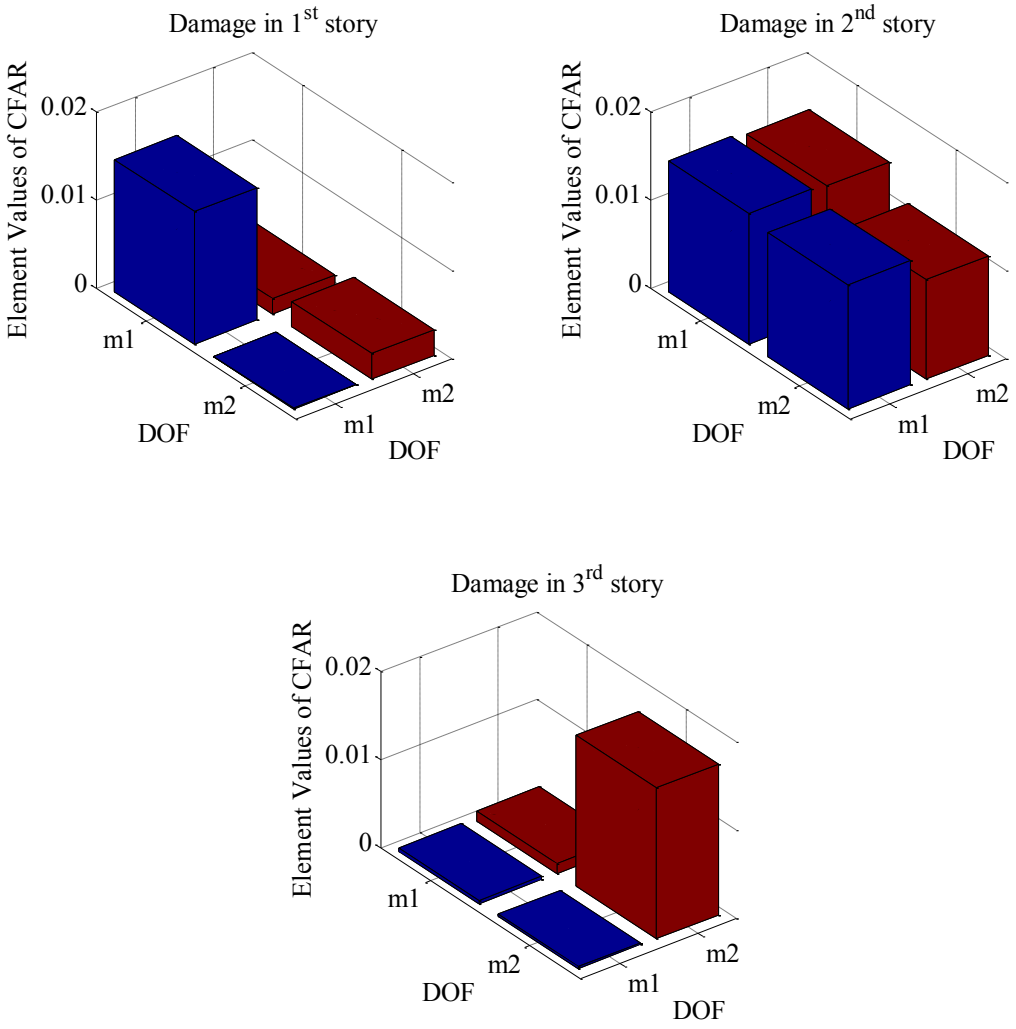

Figure 3.8. Changes in the first AR model coefficient matrix for Substructure I (10% damage)

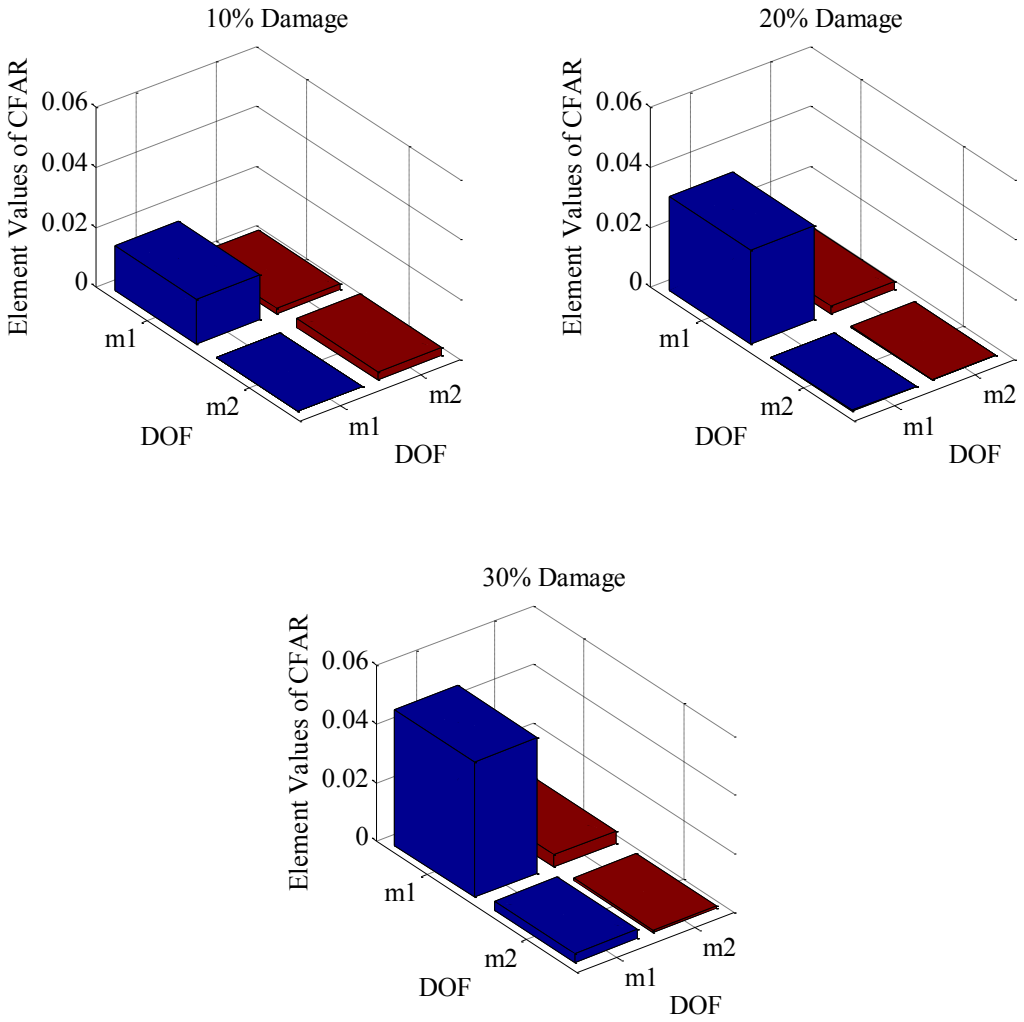

Figure 3.9. Changes in the first AR model coefficient matrix for Substructure I (damage in 1st story)

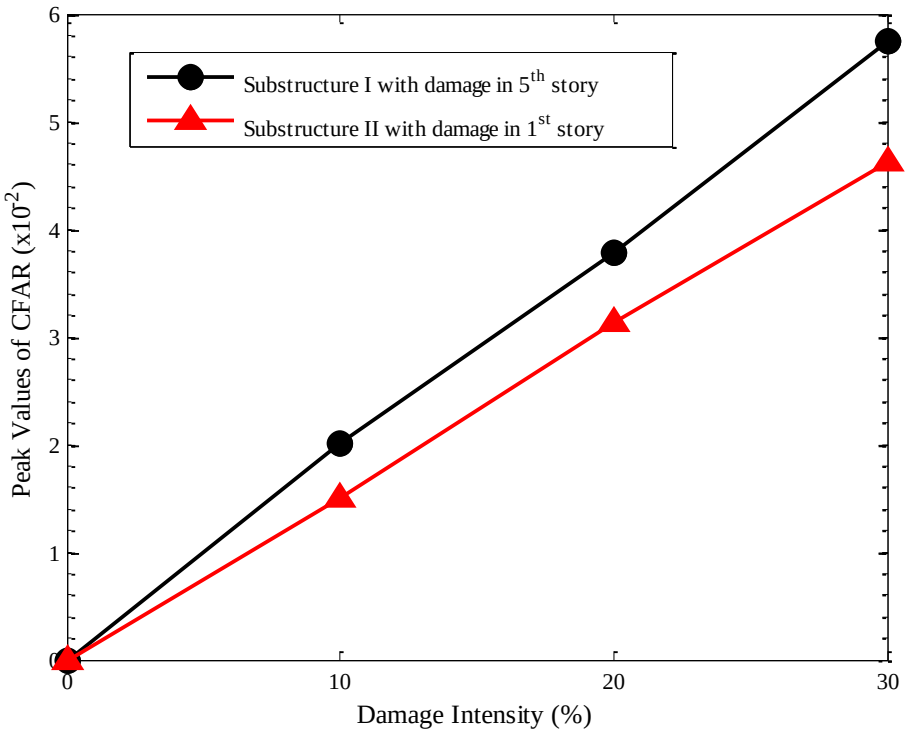

Figure 3.10. Linear relationship between CFAR and damage intensity

3.5 Decentralized Damage Identification Strategy for Shear Structures

Responses from just a few sensors are always deficient to accurately evaluate the structural condition for large scale structures. Because the dynamic property and vibration performance of large scale structures are normally intricate and complicated in both time and spatial scale. In addition, damage/deterioration in structures is intrinsically a local phenomenon. Signals from sensors in the vicinity of the damaged elements are expected to contain more information on damage than those located far from the damage. Therefore, a large number of sensors densely distributed over the entire structure are considered necessary to effectively detect arbitrary

damage/deterioration in a large scale structure. However, centrally acquiring data from a large number of sensors will cause significant limitations for conducting SHM either using wired or wireless sensors. Utility of traditional wired sensors needs to face the challenges such as high equipment costs, long deploying time, difficulties in cabling and the constant maintenance for a large wiring plant. On the other hand, power requirements and bandwidth limitations bring huge difficulty to sending all the measured data to a certain central station using wireless sensors. In both cases of wired and wireless sensors, the SHM measurement system will generate a tremendous amount of data and all of them would need to be transferred to such a central station. It is challenging and time-consuming to manage and deal with this huge amount of data. Thus, in order to raise the efficiency of the SHM network, it is necessary to get rid of the redundant information through data aggregation.

In recent years, smart sensor technology has been rapidly developed, which makes SHM system with a dense array of sensors more feasible and practical. Spencer et al. (2002, 2004) carefully reviewed state of the art of current smart sensing technologies. Usually the five essential feature of a smart sensor are: ① on-board microprocessor, ② sensing capability, ③ wireless communication, ④ battery-powered, and ⑤ low cost.

The most important difference between smart sensors and standard integrated sensors are their ‘smart’ characteristics, which are always achieved through the on-board microprocessors. The sensor’s microprocessors embedded with certain programs grant these sensors the capability of saving data locally, conducting desired computations, making decisions, scanning necessary information, transmitting results promptly, communicating with neighboring sensors, etc. By adopting the substructure concept, the computation necessary for the damage detection of a whole complex structure can be divided into several components and the component part of the computation can then be performed locally at the sensor level for each substructure. So that redundant

information can be eliminated, which will significantly cut down on the information to be sent back to the central station. It is also worthy to note that all the smart sensors to date communicate with each other through a wireless link. However, damage identification algorithms applicable to the decentralized computing environment offered by smart sensor technologies are limited at the present moment. Thus it is urgently needed to develop damage identification algorithms which can take advantage of the decentralized computing environment.

Next step a decentralized damage identification strategy (DDIS) is presented and it is suitable for implementation on a smart sensor network applied on shear structures. In this proposed strategy, the entire structure is divided into several substructures with some overlaps, the smart sensors inside and at the interface of the substructure are grouped together and only the locally measured information is used to evaluate the condition of local substructures; the associated damage identification algorithm is done in a decentralized manner. Damage identification results for these local substructures can then be reported back to the central station. Continuous online monitoring of a structure can be done without relying on central data processing. In the sequel, to simplify the damage indicator (CFAR) proposed previously, the diagonal elements from changes in the first autoregressive coefficient matrix (CFAR) are extracted to construct a vector in their original order and the vector is designated here as damage indicating vector (DIV). In each substructure, DIV can reveal the location and severity of the damage, which forms the basis for the decentralized damage identification strategy. Finally, simulations are conducted to investigate the potential of the DIV algorithm for implementation on wireless smart sensor networks (WSSN), where the issues of scalability of the DIV approach are undertaken by utilizing a decentralized, hierarchical and in-network processing strategy.

3.5.1 Damage Indicating Vector (DIV)

In section 3.2, the relationship between changes in the first AR model coefficient matrix and the stiffness reduction in the substructure is derived theoretically. Recall that, the change in the first AR model coefficient matrix from the undamaged state to the damaged state takes the matrix form in three different cases as shown in Equations 3.26 to 3.28.

By extracting the diagonal elements from the matrix $\Delta \boldsymbol{A}_1$ and arranging their values in the original order, a row vector is constituted as following which is designated here as damage indicating vector (DIV) $\boldsymbol{A}_{\text{div}}$ for the proposed decentralized damage identification strategy (DDIS):

$$\boldsymbol{A}_{\text{div}} = \text{diag}(\Delta \boldsymbol{A}_1) \tag{3.29}$$

where diag( ) signifies the arithmetic operator which formulates a row vector by extracting the diagonal elements from a matrix and arranging them in the row vector as their original order. Utilizing the expressions of $\Delta \boldsymbol{A}_1$ in Equations 3.26 to 3.28, damage indicating vector (DIV) $\boldsymbol{A}_{\text{div}}$ can be expressed in three different cases as following:

1) in case of damaged story nonadjacent to the interface end

$$\boldsymbol{A}_{\text{div}} = \begin{bmatrix} 0 & 0 & \cdots & \Delta t^2 \delta k_f & \Delta t^2 \delta k_f & \cdots & 0 & 0 \end{bmatrix} \tag{3.30}$$

2) in case of damaged story adjacent to the bottom interface end

$$\boldsymbol{A}_{\text{div}} = \begin{bmatrix} \Delta t^2 \delta k_f & 0 & \cdots & 0 & 0 & \cdots & 0 & 0 \end{bmatrix} \tag{3.31}$$

3) in case of damaged story adjacent to the top interface end

$$\boldsymbol{A}_{\text{div}} = \begin{bmatrix} 0 & 0 & \cdots & 0 & 0 & \cdots & 0 & \Delta t^2 \delta k_f \end{bmatrix} \tag{3.32}$$

In the case that the damage occurs on the f^{th} story which is between two adjacent

DOFs, $(f\text{-}1)^{th}$ DOF and f^{th} DOF, Equation 3.30 shows that the damage indicating vector (DIV) $\boldsymbol{A}_{\text{div}}$ will be a null vector with two non-zero terms at element locations corresponding to the $(f\text{-}1)^{th}$ and f^{th} output DOFs; In the case of damage occurring on the f^{th} story between the f^{th} DOF and the bottom interface, it is shown in Equation 3.31 that the damage indicating vector (DIV) $\boldsymbol{A}_{\text{div}}$ will be a null vector with only the first element non-zero which corresponds to the f^{th} output DOF; And if the damage occurs on the f^{th} story which is between the top interface and the $(f\text{-}1)^{th}$ DOF, Equation 3.32 reveals that the damage indicating vector (DIV) $\boldsymbol{A}_{\text{div}}$ will be a null vector with only the last element non-zero corresponding to the $(f\text{-}1)^{th}$ output DOF. This information depicts the damage location on the f^{th} story. Additionally, the value of the non-zero term of the damage indicating vector (DIV) $\boldsymbol{A}_{\text{div}}$ is directly proportional to the story stiffness degradation δk_f. Thus, the damage indicating vector (DIV) $\boldsymbol{A}_{\text{div}}$ can indicate the location and severity of the damage occurring in the substructure by identifying the high-valued elements in it.

3.5.2 Decentralized Damage Identification Strategy (DDIS)

3.5.2.1 Hierarchical Organization

To implement the proposed substructural DIV algorithm on wireless smart sensor networks (WSSN), an appropriate network topology must be considered. Three network topologies and data processing schemes are generally considered for WSSN, i.e. centralized data acquisition, independent data processing on each node, and hierarchical system as shown in Figure 3.11 (Nagayama and Spencer 2007).

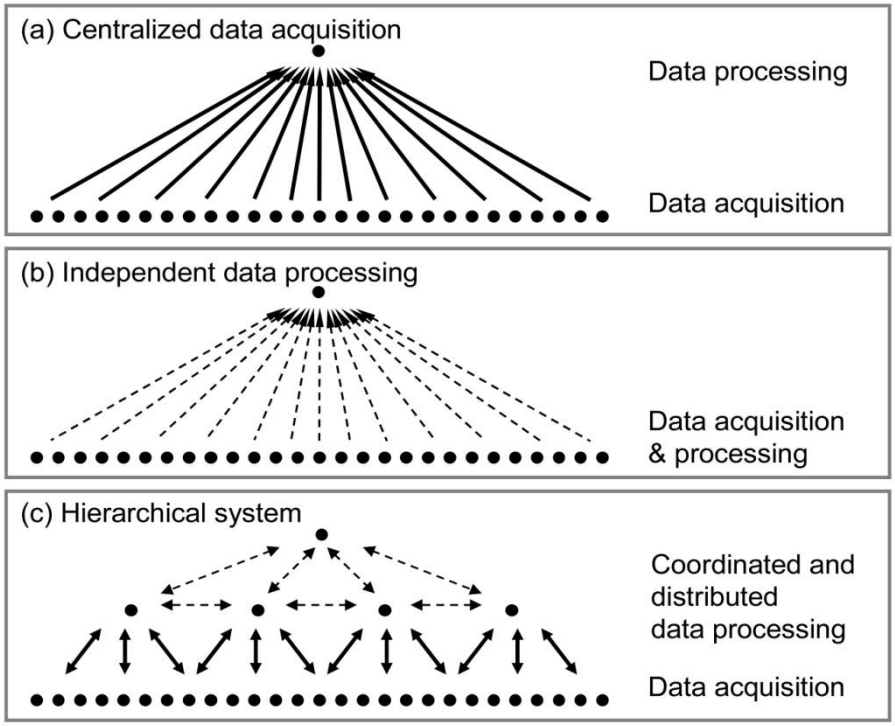

Figure 3.11. Network topologies (Nagayama and Spencer 2007)

Among these topologies, the hierarchical system possesses efficiency in network communication without losing the ability to capture spatial structural response information. By consulting the conceptual hierarchical organization of the decentralized computing strategy approach proposed by Gao et al. (2006), a hierarchical organization suitable for the proposed substructural DIV algorithm is designed as shown in Figure 3.12. Traditional SHM algorithms normally require all the sensors to be connected to a certain central station so that all the measured information to be transferred to it. In marked contrast to the traditional centralized algorithm, the proposed decentralized computing strategy will locally aggregate the measured information by a selected sensor within the substructural sensor group, termed the manager sensor, and redundant information will be discarded so that only limited information is sent back to the central station to provide the condition of the corresponding substructure. In each substructure, small numbers of smart sensors are grouped to form different communities, and each sensor can belong to more than one

community. For each community, the manager sensor collects measured responses and implements the substructural DIV algorithm for this community. Adjacent manager sensors need to communicate with each other to exchange the necessary information.

The manager sensor first locally aggregates the measured response and then decides what kind of information is necessary to be transferred to the central station. In the proposed strategy, each of the communities without damage occurring only sends an 'ok' signal to the central station, which is shown by the dotted line connection in Figure 3.12. The communities in which damage took place need to send the damage information including the damage location and damage intensity about the corresponding substructure, which is shown by the solid line connection in Figure 3.12. In this way, the redundant information is eliminated and only limited information needs to be transferred between sensors throughout the entire structure. This strategy will significantly cut down the communication traffic and the associated power requirement in the sensor network.

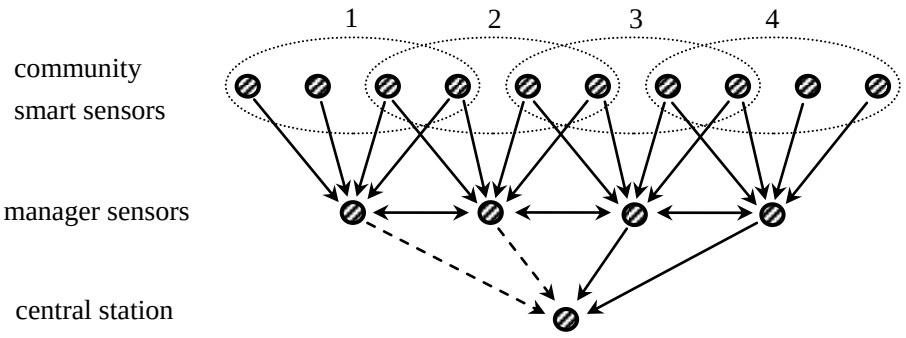

Figure 3.12. Sketch of hierarchical organization

3.5.2.2 Strategy Implementation

The 15-story shear building shown in Figure 3.13 is employed to illustrate the details of the implementation of the proposed SHM strategy.

3.5.2.3 Substructure Division and Community Formation

Firstly, the entire structure is divided into 7 substructures and the corresponding sensor communities are formed. A single community includes a set of adjacent lumped masses, sensors on these masses, and columns between these masses. Figure 3.14 shows an example of how substructures and the corresponding sensor communities can be formed. Different substructures and communities are developed from bottom to up in the shear structure. To facilitate efficient communication among the smart sensors, the masses within the same community should be close to each other, that means the dimension of the substructure should not be large. As an example, substructure 4 in Figure 3.14 includes masses [m_6 m_7 m_8 m_9 m_{10}] and columns [k_7 k_8 k_9 k_{10}].

To allow some computational redundancy, adjacent substructures are recommended to have some overlaps so that each column is monitored by more than a single community.

3.5.2.4 Data Aggregation

To minimize the communication traffic in the sensor network, measured data need to be transferred to the manager sensor for data processing.

Clocks of smart sensors in the same community are first synchronized with each other. After the measured responses are collected, they will be transferred to the manager sensor for data processing and algorithm computation. To make the communication

easier, the manager sensor should be located at the central area to the other sensors in the community. For example, in Figure 3.14, the sensors at mass m_{10} is selected as the manager sensor for substructure 5. As can be seen from the figure, some sensors may need to transfer information to more than one manager sensors. This situation occurs when the smart sensors participate in different communities.

After the data have been sent to the manager sensor, damage identification algorithm can be implemented using the on-board microprocessor to locate and quantify the damage within the community. The proposed substructural DIV algorithm presented in Section 3.5.2 is incorporated in this SHM strategy to identify the location and severity of the damage in each community. The flow chart for damage aggregation in a community is shown in Figure 3.15.

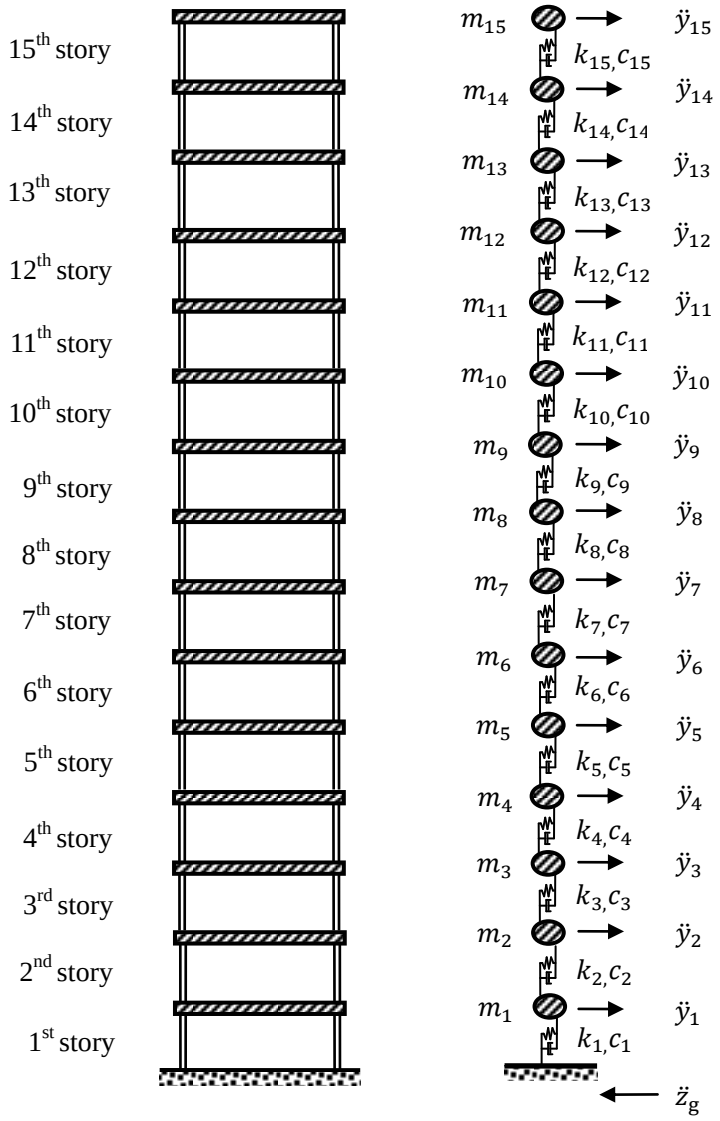

Figure 3.13. 15-story shear building

3.5.2.5 Decision Making

After the data aggregation is done, decision should be made for a community. If there is no damage identified in a community, the manager sensor does not trigger the communication with other manager sensors. Instead, it just transmit a simple 'ok' signal back to the central station. If there is some damage identified in a community,

the manager sensor initiates to send inquiries to its counterpart in adjacent communities. Three possibilities can happen after sending the inquiries:

- The damage candidate in community i does not belong to any adjacent community. The manager sensor in community i transmits the damage information back to the central station.
- The damage candidate in community i belongs to other communities and has already been identified as the potentially damaged location consistently in all of these communities. This damage candidate is then confirmed and reported to the central station by these communities.
- The damage candidate identified by community i belongs to other communities, but there are some conflicts in the damage identification results of the different communities. It is necessary to recollect data for these communities, and then data aggregation and decision making process should be re-conducted until all the communities can obtain the consistent damage identification result.

A flow chart for the decision making is shown in Figure 3.15.

3.5.3 Performance Verification by Simulation

The proposed substructural DIV algorithm is verified using the shear structure shown in Figure 3.13.

The mass of every floor and the lateral stiffness were assumed to be 100 kg and 1 MN/m, respectively. The damping ratio of all modes was chosen as 3%. The first three undamaged natural frequencies of the structure were calculated as 1.6, 4.8, and 8.0 Hz for the 1^{st}, 2^{nd}, and 3^{rd} modes, respectively. The 15-DOF system was simulated to be subjected to white noise excitation, and the noise contributing to 5% of the signal RMS value was added to the acceleration responses of the structure. The acceleration

responses at different DOFs were recorded for 50 seconds with a sampling frequency of 200 Hz. The story stiffness reduction was regarded to be damage to the structure.

Firstly, according to the substructure division method described in section 3.5.2.3, the whole structure was divided into 7 substructures, as shown in Figure 3.14.

Considering strong flexibility for handling the disturbance modeling, the autoregressive moving average with exogenous inputs (ARMAX) model was adopted to model each substructure and further obtain the AR coefficient matrix for the undamaged and unknown states. According to Equation 3.13 and the expression of the input vector $u_{\mathrm{u}}(t)$, Substructures 1 and 7 can be modeled as a 2-input 3-output ARMAX model, Substructures 2~6 can be modeled as a 3-input 3-output ARMAX model.

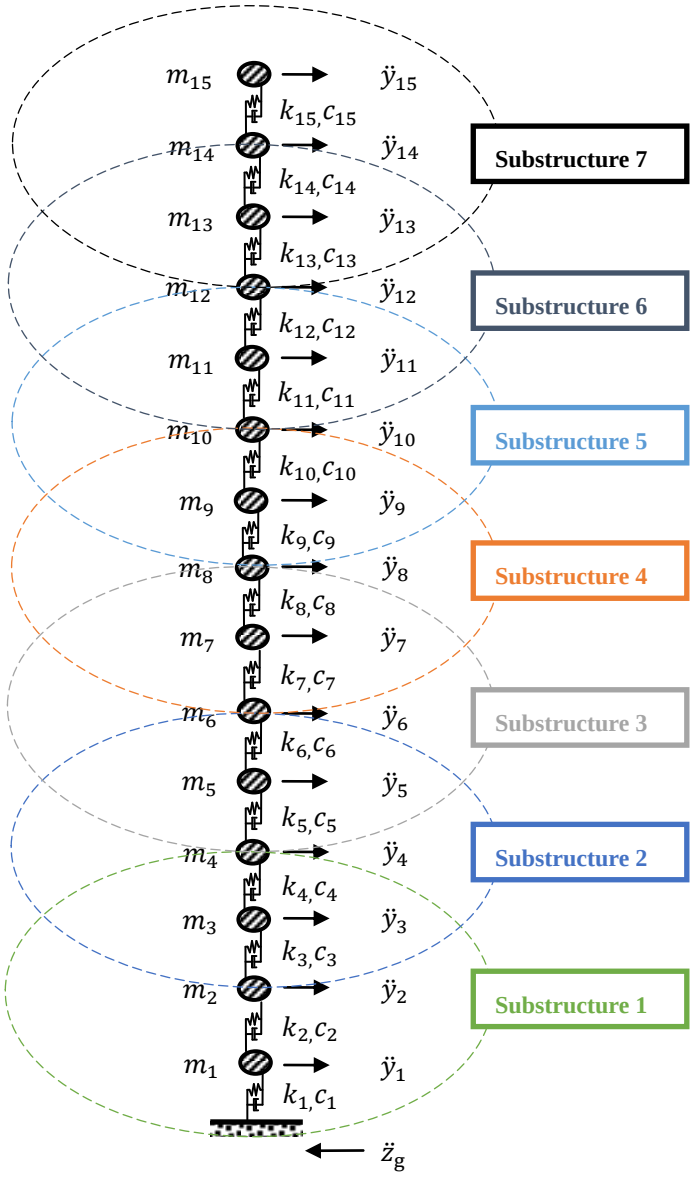

Figure 3.14. Structure division and community formation for 15-story shear building

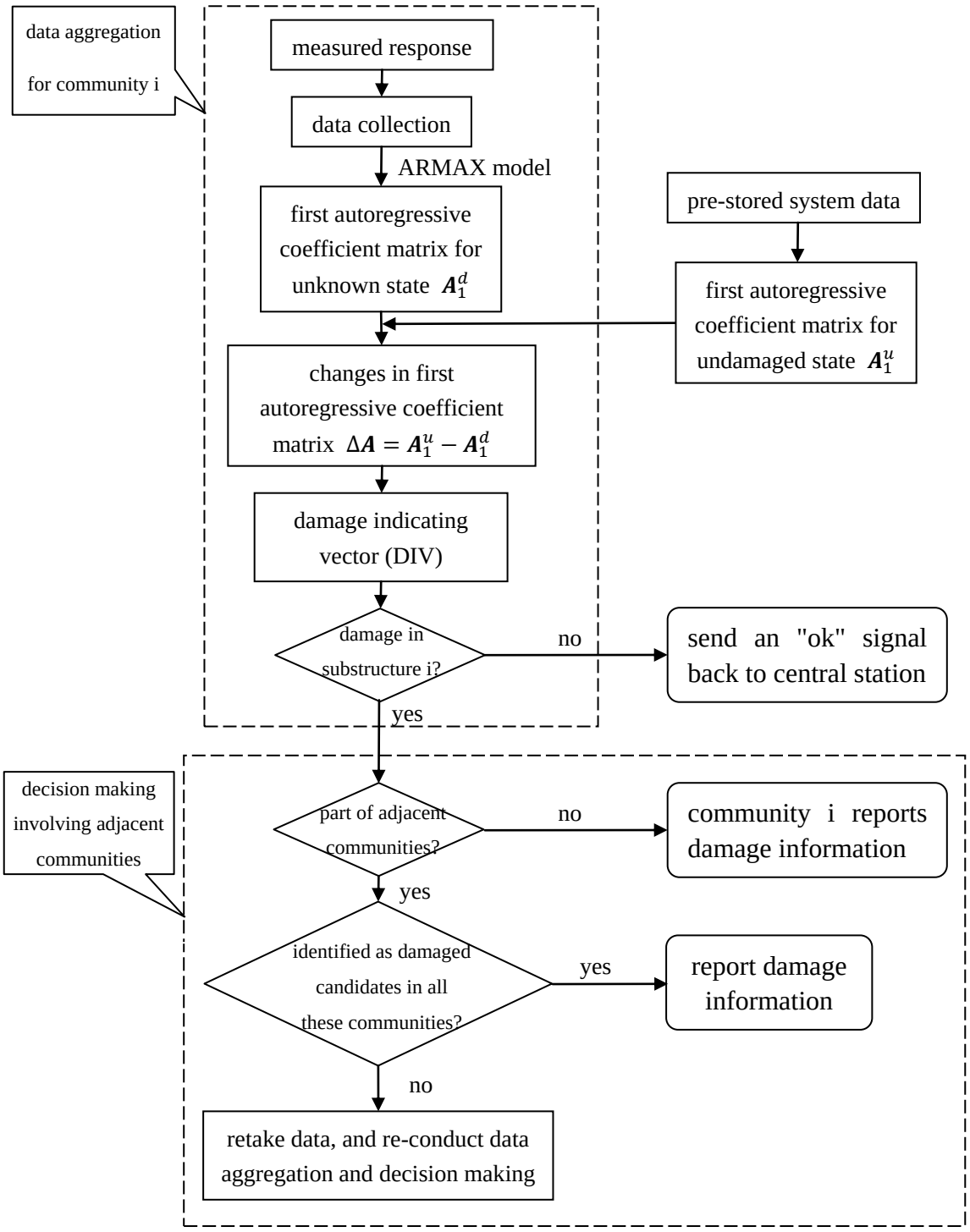

Figure 3.15. Data aggregation and decision making

Two damage cases are considered:

Case 1: single damage scenario--20% stiffness reduction at column 10.

Case 2: multiple damage scenario--20% stiffness reduction in columns 4 and 14.

3.5.3.1 Single Damage Scenario

By applying the proposed substructural DIV algorithm for each community, the damage identification is conducted. The results of the DIV values for substructure 4 and 5 when column 10 has a 20% stiffness reduction is displayed in Figures 3.16 and 3.17. Results from substructure 4 show that the DIV values for column 10 (output DOF No.9) is considerably higher than other elements being monitored. Similarly, results from substructure 5 show that the DIV values for column 10 (output DOF No.s 9 and 10) are also considerably higher than other elements being monitored. Therefore, column 10 is confirmed as a damage location in these substructures. Results from other substructures show no elements having a high DIV values. The manager sensors in communities 4 and 5 send the damage information to the central station, while other communities only send an ‘ok’ signal back to the central station.

3.5.3.2 Multiple Damage Scenario

Figures 3.18 to 3.21 show the results when columns 4 and 14 have a 20% stiffness reduction. Again, substructures 1 and 2 determine column 4 as a possibly damaged element; substructures 6 and 7 identify column 14 as a damage candidate.

In both cases, substructures 1, 2, 6, and 7 report the damage information back to the central station; while other communities having no damage only send back an ‘ok’ signal.

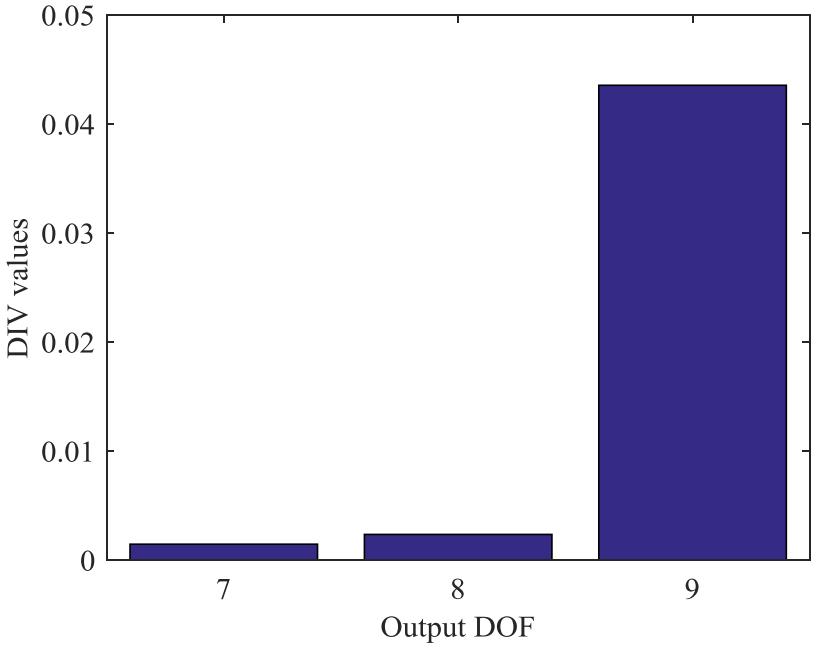

Figure 3.16. DIV values for substructure 4: damage at column 10

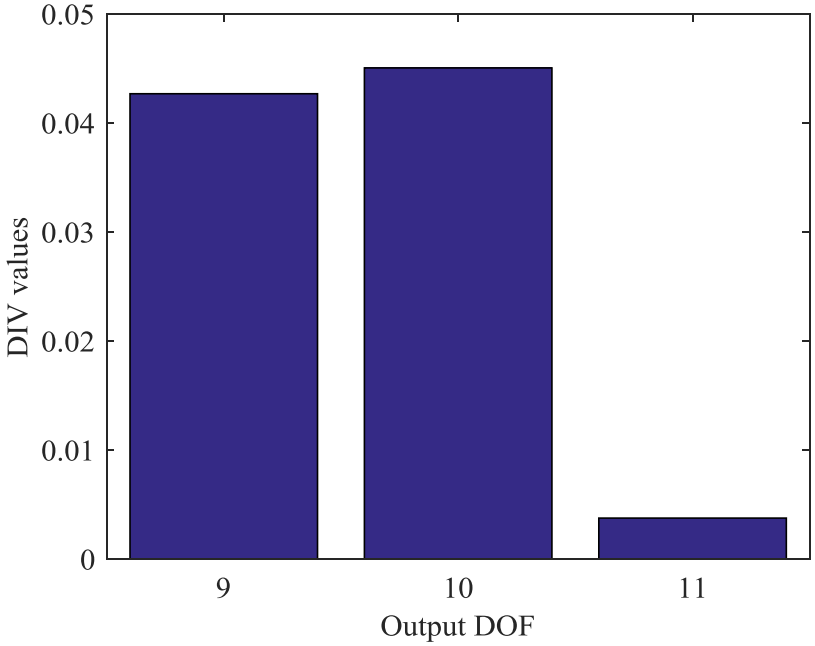

Figure 3.17. DIV values for substructure 5: damage at column 10

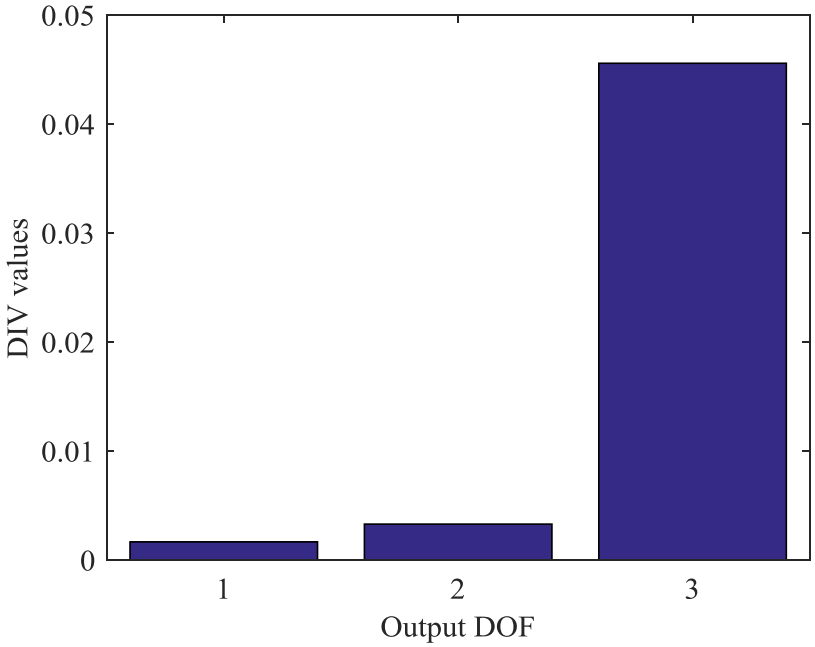

Figure 3.18. DIV values for substructure 1: damage at columns 4 and 14

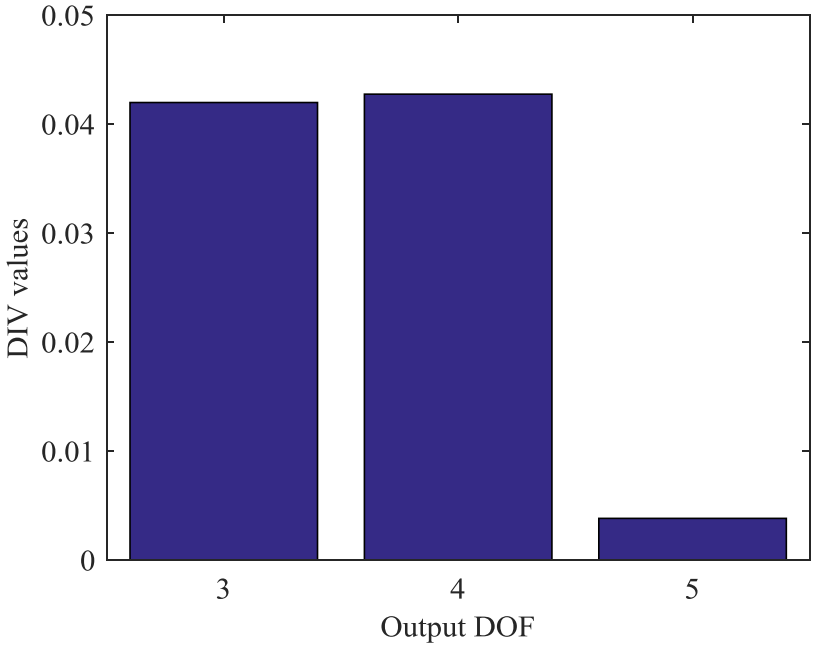

Figure 3.19. DIV values for substructure 2: damage at columns 4 and 14

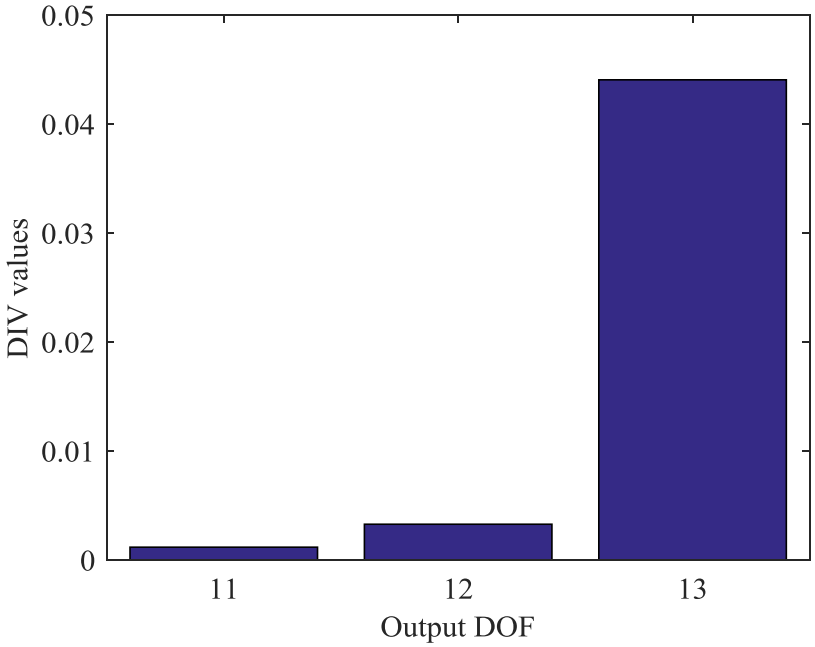

Figure 3.20. DIV values for substructure 6: damage at columns 4 and 14

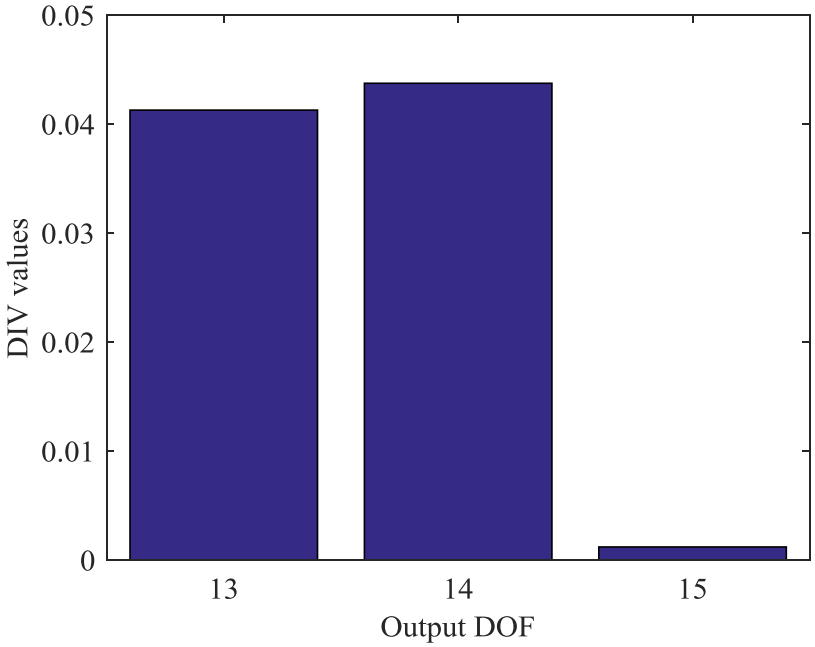

Figure 3.21. DIV values for substructure 7: damage at columns 4 and 14

3.6 Conclusions

In this work, a substructural damage identification approach is presented to locate and quantify damages in a shear structure based on changes in the first AR model coefficient matrix (CFAR). At first, the mathematical derivation draws a conclusion that the elements of CFAR corresponding to the output DOFs adjacent to the damaged location are proportional to the stiffness reduction in the structure, indicating the damage location and severity. After that, a numerical simulation of a 12-story shear building model and an experiment of a five-story metal building model have verified that the proposed approach can satisfactorily locate and quantify the damage in both simulation and laboratory experiment. As the structure is divided into substructures, which have a considerably smaller number of degrees of freedom (DOFs), thus only the structural responses related to the substructure being detected are required in the substructural damage identification procedure, and it is not necessary to monitor the responses of all DOFs of the structure simultaneously, greatly reducing the computation time and cost of SHM systems. It may also be noted that the evaluation of the AR model coefficient matrix involves only very easy and simple computation, without having to take long time to identify the mass, stiffness and damping matrices of the structure. These means that the proposed approach is easy, efficient and robust for local substructural damage identification of shear structures. Moreover, as the damage identification process can be independently conducted on each substructure, this method is promising for application in a parallel and decentralized damage identification system (e.g., using wireless mobile sensor network to perform SHM).

In the following step, a new decentralized damage identification strategy (DDIS) for SHM is proposed that is suitable for implementation on a network of wireless SHM system for shear structures. First, the basic concept of the substructural DIV algorithm was briefly introduced. Then numerical studies using the propose strategy to detect

damage were conducted. The proposed DDIS approach differs from the traditional SHM algorithms because it does not rely on central acquisition and data processing. In the proposed approach, adjacent smart sensors are grouped together to form sensor comminutes to monitor the local substructures. Extraneous information is discarded before damage information is sent to the central station, therefore only limited information needs to be transferred wirelessly. Numerical simulations with noise included in measurements have been conducted. Structural damage has been consistently identified using locally measured data from sensor communities. These results have shown the proposed DDIS approach promising for practical SHM with a densely distributed sensor network.

CHAPTER 4
Conclusions and Future Studies

4.1 Conclusions

The main contributions of this thesis are that it made improvements on the damage assessment based on autoregressive models and substructure approach. This thesis is devoted to overcome the problems such as high equipment costs, long setup time, difficulties in cabling and the long computation time by proposing a decentralized damage identification strategy based on the combination of substructural approach and autoregressive models, which is especially effective and economic for large scale shear structures. The proposed method is suitable for use in a parallel and decentralized damage detection system and can work more efficiently for large scale structures.

Firstly, an improved substructure-based damage detection approach is proposed to locate and quantify damages in a shear structure, which extends from a previously established substructure approach. Similarly as in the previous approach, a substructure approach is adopted in the improved procedure to divide a complete structure into several substructures. To improve the noise immunity and damage

detection robustness under different types of excitations and realistic conditions, this paper proposes an ARMAX model residual-based technique to correct the former damage indicator. The correction coefficient is defined as the normalized Kolmogorov-Smirnov (K-S) test statistical distance between the two distinguished data sets of ARMAX model residual generalized from input-output data process for undamaged and damaged states. To better assess the performance of the improved procedure, simulation and experimental verifications of the proposed approach have been conducted and the results are compared with the previous method. It shows that the improved procedure works much better and more robust than previous method especially when it is applied to realistic problems.

Secondly, to seek the balance between the number of substructures and the computation intensity inside each substructure, a more flexible substructural damage identification approach is proposed in this study to identify structural damage including its location and severity, using changes in the first autoregressive coefficient matrix as the damage indicator. First of all, a more flexible substructure division scheme is adopted in the procedure to divide a complete structure into several substructures in three different types. To establish a relation between changes in autoregressive coefficients and structural damage for each substructure, a theoretical derivation is presented. Thus the accelerations are fed into ARMAX models to determine the autoregressive coefficients for each substructure under undamaged and various damaged conditions, based on which changes in the first autoregressive coefficient matrix (CFAR) are obtained and adopted as the damage indicator for the proposed substructural damage identification approach. In what follows a numerical simulation and an experimental verification of the proposed approach are then carried out and the results show that the proposed procedure can successfully locate and quantify the damage in both simulation and laboratory experiment.

Moreover, to simplify the above studied method, the diagonal elements from changes

in the first autoregressive coefficient matrix (CFAR) are extracted to construct the damage indicating vector (DIV). Then simulations are conducted to investigate the potential of the DIV algorithm for implementation on wireless smart sensor networks (WSSN), where the issues of scalability of the DIV approach are undertaken by utilizing a decentralized, hierarchical and in-network processing strategy.

The proposed substructural damage identification approach can satisfactorily locate and quantify the damage in both simulation and laboratory experiment. As the structure is divided into substructures, which have a considerably smaller number of degrees of freedom (DOFs), thus only the structural responses related to the substructure being detected are required in the procedure, and it is not necessary to monitor the responses of all DOFs of the structure simultaneously, greatly reducing the computation time and cost of SHM systems. It may also be noted that the evaluation of the autoregressive coefficient matrix involves only very easy and simple computation, without having to take long time to identify the mass, stiffness and damping matrices of the structure. These means that the proposed approach is easy, efficient and robust for local substructural damage identification of shear structures. Moreover, as the damage identification process can be independently conducted on each substructure, by utilizing some decentralized and hierarchical processing strategy, this method is promising and efficient for application on wireless smart sensor networks (WSSN) to perform SHM systems for large scale shear structures.

4.2 Future Studies

With the previously mentioned conclusions and contributions, it is considered that the objectives given for the study at the current stage are fulfilled and suitable for applying to large scale shear building structures. Although this research has successfully addressed some of the challenges for application of damage identification

algorithm to large scale buildings based on the combination of substructure approach and autoregressive models, a few directions for further study in the future should be considered.

Firstly, in this study the laboratory experimental data is still from a simplified structure subject to linear damages in a controlled operational and environmental condition. In the further study, more realistic conditions involving operational and environmental variations in the data should be taken into consideration, in order to challenge the damage identification and to test the robustness of the algorithm.

In addition, the decentralized damage identification strategy (DDIS) is proposed that provide robust estimates of damage locations and severities for large scale shear building structures. However, the efficacy of the developed strategy is only verified by simulations, in future study it should also be verified using a real wireless sensor network.

Moreover, the damage identification algorithm and strategy proposed in this thesis is only applicable to shear structures with conventional shape. However, there are a lot of structures in real application, which have more complex shapes and types. Thus it is necessary to extend the algorithm and strategy to structures with more complicated shapes and types.

Finally, the proposed algorithm is only able to identify damage in the story level. If the approach can be extended to identify damage in element level, it will be extremely promising for the structural health monitoring practice.

References

Akaike, H. (1974). "A new look at the statistical model identification." *IEEE Transaction on Automatic Control* **19**: 716-723.

Alvin, K. F., Robertson, A. N., Reich, G. W., and Park, K. C. (2003). "Structural system identification: from reality to models." *Computers and Structures* **81**(12): 1149-1176.

Auweraer, H. V. D. and Peeters, B. (2003). "Sensors and systems for structural health monitoring." *Journal of Structural Control* **10**(2): 117-125.

Basseville, M. (1989). "Distance measures for signal processing and pattern recognition." *Signal processing* **18**(4): 349-369.

Berman, A. and Flannelly, W. (1971). "Theory of incomplete models of dynamic structures." *AIAA Journal* **9**(8): 1481-1487.

Bernal, D. (2002). "Load vectors for damage localization." *Journal of Engineering Mechanics* **128**(1): 7-14.

Cawley, P. and Adams, R. (1979). "The location of defects in structures from measurements of natural frequencies." *The Journal of Strain Analysis for Engineering Design* **14**(2): 49-57.

Cempel, C. (1980). "Diagnostically oriented measures of vibroacoustical processes." *Journal of Sound and Vibration* **73**(4): 547-561.

Chance, J., Tomlinson, G. R., and Worden K. (1994). A Simplified Approach to the Numerical and Experimental Modelling of the Dynamics of a Cracked Beam. *Proceedings of the 12th International Modal Analysis Conference*: 778-785.

de Lautour, O. R. and Omenzetter, P. (2006). Detection of seismic damage in buildings using time series analysis and pattern recognition. *Proceedings of*

the 4th World Conference on Structural Control and Monitoring, San Diego, USA: 1-8.

Dilena, M. and Morassi, A. (2004). "The use of antiresonances for crack detection in beams." *Journal of Sound and Vibration* **276**(1-2): 195-214.

Doebling, S. W. and Farrar, C. (1997). Using statistical analysis to enhance modal-based damage identification. in *Structural Damage Assessment Using Advanced Signal Processing Procedures* Proceedings of DAMS' 97, Univ. of Sheffield, UK: 199-210.

Doebling, S. W., Farrar, C. R., Prime, M. B., and Shevitz, D. W. (1996). *Damage Identification and Health Monitoring of Structural and Mechanical Systems from Changes in Their Vibration Characteristics: A Literature Review*, Los Alamos National Laboratory report LA-13070-MS, Los Alamos, NM, USA.

Fanning, P. and Carden, E. P. (2001). "Auto-regressive and statistical process control techniques applied to damage indication in telecommunication masts." *Key Engineering Materials* **204-205**: 251-260.

Farrar, C. R. and Cone, K. M. (1995). Vibration testing of the I-40 bridge before and after the introduction of damage. *Proceedings of the 13th International Modal Analysis Conference*, Florida, USA: 203-209.

Farrar, C. R. and Worden, K. (2007). "An introduction to structural health monitoring." *Philosophical Transactions of the Royal Society A: Mathematical, Physical and Engineering Sciences* **365**(1851): 303-315.

Fassois, S. D. and Sakellariou, J. S. (2007). "Time-series methods for fault detection and identification in vibration structures." *Philosophical Transactions of the Royal Society* **A**(365): 411-448.

Fugate, M. L., Sohn, H., and Farrar, C. R. (2001). "Vibration-based damage detection using statistical process control." *Mechanical Systems and Signal Processing* **15**(4): 707-721.

Gao, Y. and Spencer, B. F. (2006). "Online damage diagnosis for civil infrastructure employing a flexibility-based approach." *Smart Materials and Structures* **15**(1): 9-19.

Gao, Y., Spencer, B. F., and Ruiz-Sandoval, M. (2006). "Distributed computing strategy for structural health monitoring." *Structural Control and Health Monitoring* **13**(1): 488-507.

Harikrishnan, P., Koushik, R., and Samit, R. C. (2014). Damage characterization in frame structures using output-only modal and feature-based techniques.

Proceedings of the Third International Conference on Advances in Control and Optimization of Dynamical Systems, Kanpur, India: 973-980.

Hayton, P., Utete, S., King, D., King, S., Anuzis, P., and Tarassenko, L. (2007). "Static and dynamic novelty detection methods for jet engine health monitoring." *Philosophical Transactions of the Royal Society A: Mathematical, Physical and Engineering Sciences* **365**(1851): 493-514.

He, K. and Zhu, D. (2011). "Structural Damage Detection Using the Changes in Natural Frequencies: Theory and Applications." *Journal of Physics: Conference Series - The 9th Conference on Damage Assessment of Structures* **305**(1) , Article ID 012054.

Hearn, G. and Testa, R. (1991). "Modal analysis for damage detection in structures." *Journal of Structural Engineering* **117**(10): 3042-3063.

Hoshiya, M. and Saito, E. (1984). "Structural identification by extended Kalman filter." *Journal of Engineering Mechanics* **110**(12): 1757-1770.

Hou, J., Jankowski, L., and Ou, J. (2010) "A substructure isolation method for local structural health monitoring." *Structural Control and Health Monitoring* **18**(6): 601-618.

Hou, J., Jankowski, L., and Ou, J. (2012). "Experimental study of the substructure isolation method for local health monitoring." *Structural Control and Health Monitoring* **19**(4): 491-510.

Hou, Z., Noori, M., and Amand, R. St. (2000). "Wavelet-based approach for structural damage detection." *Journal of Engineering Mechanics* **126**(7): 677-683.

Itakura, F. and Umezaki, T. (1987). Distance measure for speech recognition based on the smoothed group delay spectrum. in *Acoustics, Speech, and Signal Processing* Proceedings of IEEE International Conference on ICASSP '87: 1257-1260.

Kalpakis, K., Gada, D., and Puttagunta, V. (2001). Distance measures for effective clustering of ARIMA time series. *Proceedings of the 2001 IEEE International Conference on Data Mining*, San Jose, CA, USA: 273-280.

Kar, C. and Mohanty, A. R. (2004). "Application of KS test in ball bearing fault diagnosis." *Journal of Sound and Vibration* **269**(1-2): 439-454.

Kessler, S. S., Spearing, S. M., Atalla, M. J., Cesnik, C. E. S., and Soutis, C. (2002). "Damage detection in composite materials using frequency response methods." *Composites Part B: Engineering* **33**(1): 87-95.

Kim, J. T., Ryu, Y. S., Cho, H. M., and Stubbs, N. (2003). "Damage identification in

beam-type structures: frequency-based method vs mode-shape-based method." *Engineering Structures* **25**(1): 57-67.

Koh, C. G., See, L. M., and Balendra, T. (1991). "Estimation of structural parameters in time domain: a substructure approach." *Earthquake Engineering & Structural Dynamics* **20**(8): 787-801.

Koh, C. G., Hong, B., and Liaw, C. Y. (2003). "Substructural and progressive structural identification methods." *Engineering Structures* **25**(12): 1551-1563.

Koh, C. G. and Shankar, K. (2003). "Substructural identification method without interface measurement." *Journal of Engineering Mechanics* **129**(7): 769-776.

Kuwabara, M., Yoshitomi, S., and Takewaki, I. (2013). "A new approach to system identification and damage detection of high-rise buildings." *Structural Control and Health Monitoring* **20**(5): 703-727.

Lee, E. T. and Eun, H. C. (2014). "A Model-Based Substructuring Method for Local Damage Detection of Structure." *Shock and Vibration* **2014**: Article ID 390769, 11 pages. doi:10.1155/2014/390769.

Lee, S. (1997). "A note on the residual empirical process in autoregressive models." *Statistics and Probability Letters* **32**(4): 405-411.

Lieven, N. and Ewins, D. (1988). Spatial correlation of mode shapes, the coordinate modal assurance criterion (COMAC). *Proceedings of the 4th International Modal Analysis Conference*, Bethel: 690-695.

Ljung, L. (1999). *System Identification : Theory for the User*. Prentice Hall PTR: Upper Saddle River, New Jersey.

Ljung, L. (2002). "Asymptotic behavior of the extended Kalman filter as a parameter estimator for linear systems." *Automatic Control, IEEE Transactions on* **24**(1): 36-50.

Ljung, L. and Glad, T. (1994). *Modeling of dynamic systems*. Englewood Cliffs, N.J., PTR Prentice Hall.

Lu, Y. and Gao, F. (2005). "A novel time-domain auto-regressive model for structural damage diagnosis." *Journal of Sound and Vibration* **283**(3-5): 1031-1049.

Marple, S. L. (1987). *Digital Spectral Analysis with Applications*, Prentice Hall: Englewood Cliffs.

Martin, R. (2000). "A metric for ARMA processes." *IEEE Transactions on Signal Processing* **48**(4): 1164-1170.

Mattson, S. G. and Pandit, S. M. (2006). "Statistical moments of autoregressive model

residuals for damage localization." *Mechanical Systems and Signal Processing* **20**(3): 627-645.

Mita, A. (2003). *Structural dynamics for health monitoring*, SANKEISHA Co Ltd: Nagoya, Japan.

Nagayama, T. and Spencer, B. F. (2007). *Structural Health Monitoring Using Smart Sensors*, NSEL Report Series, Report No. NSEL-001, Department of Civil and Environmental Engineering, University of Illinois at Urbana-Champaign, USA.

Nair, K. K. and Kiremidjian, A. S. (2007). "Time series based structural damage detection algorithm using Gaussian Mixtures Modeling." *Journal of Dynamic Systems, Measurement, and Control* **129**: 285-293.

Nair, K. K., Kiremidjian, A., and Law, K. H. (2006). "Time series-based damage detection and localization algorithm with application to the ASCE benchmark structure." *Journal of Sound and Vibration* **291**(1-2): 349-368.

Omenzetter, P. and Brownjohn, J. M. W. (2006). "Application of time series analysis for bridge monitoring." *Smart Materials and Structures* **15**(1): 129-138.

Pandey, A. K., Biswas, M., and Samman, M. M. (1991). "Damage detection from changes in curvature mode shapes." *Journal of Sound and Vibration* **145**(2): 321-332.

Park, K. C., Reich, G. W., and Alvin, K. F. (1998). "Structural damage detection using localized flexibilities." *Journal of Intelligent Material Systems and Structures* **9**(11): 911-919.

Peeters, B., Maeck, J., and Roeck, G. D. (2001). "Vibration-based damage detection in civil engineering: excitation sources and temperature effects." *Smart Materials and Structures* **10**(3): 518-527.

Qian, Y. and Mita, A. (2008). "Acceleration-based damage indicators for building structures using neural network emulators." *Structural Control and Health Monitoring* **15**(6): 901-920.

Qiao, P., Lu, K., Lestari, W., and Wang, J. (2007). "Curvature mode shape-based damage detection in composite laminated plates." *Composite Structures* **80**(3): 409-428.

Rytter, A. (1993). *Vibration based inspection of civil engineering structures*. (Ph.D. dissertation) Department of Building Technology and Structural Engineering, Aalborg University, Denmark.

Rytter, A. and Kirkegaard, P. (1997). "Vibration based inspection using neural

networks." in *Structural Damage Assessment Using Advanced Signal Processing Procedures* Proceedings of DAMS' 97, Univ. of Sheffield, UK: 97-108.

Sara, C. and Lucia, F. (2014). "Quantity vs. quality in the model order reduction (MOR) of a linear system." *Smart Structures and Systems* **13**(1): 099-109.

Salawu, O. S. (1997). " Detection of structural damage through changes in frequency: a review." *Engineering Structures* **19**(9): 718-723.

Salawu, O. S. and Williams, C. (1995). "Bridge assessment using forced-vibration testing." *Journal of Structural Engineering* **121**(2): 161-173.

Shi, Z., Law, S. S., and Zhang, L. M. (1998). "Structural damage localization from modal strain energy change." *Journal of Sound and Vibration* **218**(5): 825-844.

Söderström, T. and Stoica, P. (1988). *System identification*, Prentice-Hall Englewood Cliffs, NJ.

Sohn, H. (2007). "Effects of environmental and operational variability on structural health monitoring." *Philosophical Transactions of the Royal Society A: Mathematical, Physical and Engineering Sciences* **365**(1851): 539-560.

Sohn, H. and Farrar, C. R. (2001). "Damage diagnosis using time series analysis of vibration signals." *Smart Materials and Structures* **10**(3): 446-451.

Sohn, H., Farrar, C. R., Hemez, F. M., Shunk, D. D., Stinemates, D. W., and Nadler, B. R. (2004). *A Review of Structural Health Monitoring Literature: 1996-2001*, Los Alamos National Laboratory Report, LA-13976-MS.

Spencer, B. F., Ruiz-Sandoval, M., and Gao, Y. (2002). Frontiers in structural health monitoring. *Proceedings of China–Japan Workshop on Vibration Control and Health Monitoring of Structures and Third Chinese Symposium on Structural Vibration Control*, Shanghai, China.

Spencer, B. F., Ruiz-Sandoval, M., and Krata, N. (2004). "Smart sensing technology: opportunities and challenges." *Journal of Structural Control and Health Monitoring* **11**(4): 349-368.

Stoffels, N., Sircoulomb, V., Hermand, G., and Hoblos, G. (2012). Toward a monitoring of storage facilities for radioactive waste. *Proceedings of the International Meeting on Clays in Natural and Engineered Barriers for Radioactive Waste Confinement*, Montpelier, France: 355-356.

Stubbs, N. and Kim, J. (1996). "Damage localization in structures without baseline modal parameters." *AIAA Journal* **34**(8): 1644-1649.

Stubbs, N., Kim, J. T., and Topole, K. (1992). An efficient and robust algorithm for damage localization in offshore platforms. *Proceedings of the ASCE 10th Structures Congress*: 543-546.

Tee, K. F., Koh, C. G., and Quek, S. T. (2005). "Substructural first- and second-order model identification for structural damage assessment." *Earthquake Engineering and Structural Dynamics* **34**(15): 1755-1775.

Tohkura, Y. (1987). "A weighted cepstral distance measure for speech recognition." *IEEE Transactions on Acoustics, Speech, and Signal Processing* **35**(10): 1414-1422.

Vestroni, F. and Capecchi, D. (2000). "Damage detection in beam structures based on frequency measurements." *Journal of Engineering Mechanics* **126**(7): 761-768.

Wang, J. Y., Ko, J. M., and Ni, Y. Q. (2000). Modal sensitivity analysis of Tsing Ma Bridge for structural damage detection. *Proc. SPIE 3995* Nondestructive Evaluation of Highways, Utilities, and Pipelines IV, 300 (June 9, 2000); doi:10.1117/12.387822.

Wang, X. and Makis, V. (2009). "Autoregressive model-based gear shaft fault diagnosis using the Kolmogorov–Smirnov test." *Journal of Sound and Vibration* **327**(3-5): 413-423.

West, W. (1986). Illustration of the use of modal assurance criterion to detect structural changes in an orbiter test specimen. *Proceedings of the 4th International Modal Analysis Conference*, Los Angles, CA, USA: 1-6.

Williams, E. and Messina, A. (1999). "Applications of the multiple damage location assurance criterion." *Key Engineering Materials* **167-168**: 256-264.

Wolff, T. and Richardson, M. (1989). Fault detection in structures from changes in their modal parameters. *Proceedings of the 7th International Modal Analysis Conference*, Las Vegas, Nevada, USA: 1-8.

Wong, C., Zhu, W., and Xu, G. (2004). "On a Interative General-Order Perturbation Method for Multiple Structural Damage Detection." *Journal of Sound and Vibration* **273**(1-2): 363-386.

Xing, Z. and Mita, A. (2012). "A substructure approach to local damage detection of shear structure." *Structural Control and Health Monitoring* **19**(2): 309-318.

Yao, R. and Pakzad, S. N. (2011). Data-driven methods for threshold determination in time-series based damage detection. *Proceedings of the Structures Congress 2011*, Las Vegas, Nevada, USA: 77-88.

Yao, R. and Pakzad, S. N. (2012). Structural damage detection using multivariate time series analysis. in *Proceedings of the Society for Experimental Mechanics Series 2012* Topics on the Dynamics of Civil Structures: 299-308.

Yun, C. B. and Lee, H. J. (1997). "Substructural identification for damage estimation of structures." *Structural Safety* **19**(1): 121-140.

Zhang, D., Li, H., and Bao, Y. (2014). Substructure parameter estimation for shear structures with limited measurements and unknown structural mass. *Proc. SPIE 9061* Sensors and Smart Structures Technologies for Civil, Mechanical, and Aerospace Systems 2014, 90612F (8 March 2014); doi: 10.1117/12.2044905.

Zheng, H. and Mita, A. (2007). "Two-stage damage diagnosis based on the distance between ARMA models and pre-whitening filters." *Smart Materials and Structures* **16**(5): 1829-1836.

Zheng, H. and Mita, A. (2008). "Damage indicator defined as the distance between ARMA models for structural health monitoring." *Structural Control and Health Monitoring* **15**(7): 992-1005.

Zheng, H. and Mita, A. (2009). "Localized damage detection of structures subject to multiple ambient excitations using two distance measures for autoregressive models." *Structural Health Monitoring* **8**(3): 207-222.

Author’s biography

Liu Mei was born in Anhui Province of China in 1982. In 2006, Liu Mei received the B.E. degree from Tsinghua University, Beijing, China and majored in structural engineering. He went to Tongji University, Shanghai, China, for the study on wind engineering and disaster reduction. In 2009, he obtained the M.E. degree from Tongji University with the thesis “Study on the seismic behavior of 500kV transformers”. From 2009, he studies in Mita Lab, Keio University, Japan. His research topic is concerning with the damage identification of shear structures based on substructural approach and autoregressive models.

List of publications

Journal Papers:

1. Liu Mei, Akira Mita and Jin Zhou, "An improved substructural damage detection approach of shear structure based on ARMAX model residual", *Journal of Structural Control and Health Monitoring*. DOI: 10.1002/stc.1766, published online: 16 June 2015.
2. Liu Mei, Akira Mita and Jin Zhou, "A substructural damage identification approach for shear structure based on changes in the first AR model coefficient matrix", *Journal of Structures*, Vol. 2015, Article ID 976349, 16 pages, 2015. DOI: 10.1155/2015/976349.

Related Journal Papers:

1. Jin Zhou, Akira Mita and Liu Mei, "Posterior density estimation for structural parameters using improved differential evolution adaptive Metropolis algorithm", *Journal of Smart Structures and Systems*, Vol. 15 (3), pp. 735-749, 2015. DOI: 10.12989/sss.2015.15.3-4.000.
2. Jin Zhou, Akira Mita and Liu Mei, "An improved differential evolution adaptive Metropolis algorithm based Bayesian structural identification using the gradient of likelihood measures", *Journal of Structures*, Vol. 2015, Article ID 236475, 9 pages, 2015. DOI: 10.1155/2015/236475.
3. Jin Zhou, Akira Mita and Liu Mei, "Multi-objective differential evolution strategy for stochastic system identification considering uncertainties", *Journal of Mechanical Systems and Signal Processing*, under review.

International Conference Papers:

1. Liu Mei, Akira Mita and Zhenhua Xing, "Substructure damage detection method for shear structure using sub-time series and ARMAX", *Structural Health Monitoring: Research and Applications*, Trans Tech Publications Ltd, Peer reviewed papers from the 4th Asia-Pacific Workshop on Structural Health Monitoring, Melbourne, Australia, pp. 149-159, December 5-7, 2012.
2. Liu Mei, Akira Mita and Zhenhua Xing, "Experimental verification of substructure damage detection method using ARX and ARMAX", *Proc. of the 8th International Workshop on Structural Health Monitoring*, Stanford University, USA, pp. 2319-2326, September 13-15, 2011.
3. Liu Mei and Akira Mita, "Correlation between damage detection and observed damage for a full-scale four-story steel building during the collapse test", *Proc. of SPIE Smart Structures/NDE 2011*, Vol. 7984, San Diego, USA, 79842N, March 6-10, 2011. DOI: 10.1117/12.880211.